ALLUVIAL FANS IN THE MCMURDO DRY VALLEYS: A PROXY FOR MELTING ALONG TERRESTRIAL MARGINS OF THE EAST ANTARCTIC ICE SHEET

A Thesis
Submitted to the Graduate Faculty
of the
North Dakota State University
of Agriculture and Applied Science

By

Felix Jacob Zamora

In Partial Fulfillment of the Requirements
for the Degree of
MASTER OF SCIENCE

Major Program:
Environmental and Conservation Science

June 2013

Fargo, North Dakota

North Dakota State University
Graduate School

Title

Alluvial fans in the McMurdo Dry Valleys: A proxy for melting along terrestrial margins of the East Antarctic Ice Sheet

By

Felix Jacob Zamora

The Supervisory Committee certifies that this ***disquisition*** complies with North Dakota State University's regulations and meets the accepted standards for the degree of

MASTER OF SCIENCE

SUPERVISORY COMMITTEE:

Dr. Adam Lewis
Chair

Dr. Kenneth Lepper

Dr. Stephanie Day

Dr. Jack Norland

Approved:

June 30th, 2013
Date

Dr. Craig Stockwell
Department Chair

ABSTRACT

Surface melting along Antarctic ice sheet margins is the most poorly understood input in models of future sea level rise. Alluvial fans in the McMurdo Dry Valleys originate from meltwater produced from high-elevation glaciers and snowbanks along these margins but many show no evidence for recent melting. These fans could serve as a record of past melting along terrestrial ice sheet margins, which would help quantify inputs to sea-level rise.

To describe how melting has taken place in the past, five representative fans were examined. Fans are composed of thin, planar-bedded gravelly sands deposited by sheetflooding. Geospatial analsysis suggests the distance of the meltwater source from the Ross Sea is the predominant control on fan activity, and that aggradation results when regional climatic gradients shift inland. Geomorphic observations suggest centuries to millennia pass between periods of aggradation. OSL dating indicates that fans are no older than Holocene in age.

ACKNOWLEDGEMENTS

I would like to acknowledge several people for their assistance in my graduate school endeavors. Most importantly, I would like to thank my advisor, Dr. Adam Lewis. His knowledge and guidance provided me the means to become a successful student. Next, I would like to thank my committee members, Dr. Kenneth Lepper, Dr. Stephanie Day, and Dr. Jack Norland for their guidance throughout this process. Also, I would like to thank Ashley Steffen, Marcie Occhi, Dr. Jane Willenbring, Deidra Lies, and Marianne Okal for their assistance with fieldwork and laboratory work. Lastly, I would like to thank my family for their encouragement and teaching me the importance of a good work ethic.

DEDICATION

This work is dedicated to my grandfather, Felix Joseph Zamora, who exemplifies what is achievable with hard work and persistence.

TABLE OF CONTENTS

ABSTRACT iii

ACKNOWLEDGEMENTS iv

DEDICATION v

LIST OF TABLES vii

LIST OF FIGURES viii

LIST OF APPENDIX TABLES x

LIST OF APPENDIX FIGURES xi

CHAPTER 1. INTRODUCTION 1

CHAPTER 2. DEPOSITIONAL SETTING 17

CHAPTER 3. GEOSPATIAL ANALYSIS 39

CHAPTER 4. TIMING OF FAN DEPOSITION 52

CHAPTER 5. CONCLUSIONS 71

REFERENCES 74

APPENDIX A. EXCAVATION LOCATIONS 82

APPENDIX B. EXCAVATION DIAGRAMS 87

APPENDIX C. GRAIN SIZE ANALYSIS 102

APPENDIX D. RESULTS OF PALEOHYDRAULIC RECONSTRUCTION 110

APPENDIX E. GEOGRAPHIC ATTRIBUTES OF FANS USED IN GEOSPATIAL ANALYSIS 112

LIST OF TABLES

Table		Page
3.1.	Results of linear regression analysis of fan area and geographic attributes	47
3.2.	Highest correlated results of multiple linear regression analysis	49
4.1.	Concentration of dosimetrically relevant elements From INAA	66
4.2.	Results of OSL analysis	66
4.3.	Ages of the most recent alluvial fan deposits on the sampled fans	67
4.4.	Ages of recent deposits on the Jason Fan	67
4.5.	Summary of age constraints based on stratigraphic and geomorphic observations and OSL dating of the youngest deposits	70

LIST OF FIGURES

Figure		Page
1.1.	Aeolus Fan	3
1.2.	Sponsors Central Fan	4
1.3.	Satellite image of the McMurdo Dry Valleys, Antarctica	7
1.4.	High-elevation alpine glaciers along the Asgard Range	8
1.5.	Jason Fan	12
1.6.	Northern Bull Pass Fan	14
1.7.	Southern Bull Pass Fan	15
1.8.	Upper Wright Fan	16
2.1.	Image of pit FZE-11-01	23
2.2.	Sand-gravel couplets of Jason Fan alluvium	24
2.3.	Image of pit FZE-11-02	25
2.4.	Stacked melt-packages along the northern margins of the Aeolus Fan	26
2.5.	Channels at the head of the Aeolus Fan	27
2.6.	Planar-bedded sand at the head of the Aeolus Fan	28
2.7.	Set of three stacked melt-packages at the head of the Aeolus Fan	29
2.8.	Image of pit FZE-11-48	31
2.9.	Image of pit FZE-11-30	31
2.10.	Image of pit FZE-11-58	33
2.11.	Image of pit FZE-11-62	34
3.1.	ELA position as illustrated by the source glacier of the Mt. Harker Fan	47
3.2.	Comparison of distance from the Ross Sea and fan area	49
4.1.	Domed polygons on the Jason Fan	58

4.2. Differing polygonal ground maturity on the Southern Bull Pass Fan 58

4.3. Relict sand wedge cross-cutting alluvium on the Aeolus Fan 59

4.4. Image showing evidence of minor flow within polygon troughs 60

4.5. Image of a large sand wedge underlying till pavements on the Jason Fan 61

4.6. Image of OSL sampled sand wedge on Jason Fan.....68

LIST OF APPENDIX TABLES

Table		Page
C.1.	Cumulative percentage values of grain size distribution of sediment samples	102

LIST OF APPENDIX FIGURES

Figure Page

A.1. Jason Fan excavation locations 82

A.2. Aeolus Fan excavation locations 83

A.3. Northern Bull Pass Fan excavation locations 84

A.4. Southern Bull Pass Fan excavation locations 85

A.5. Upper Wright Fan excavation locations 86

B.1. Diagram of excavation FZE-11-01 87

B.2. Diagram of excavation FZE-11-02 87

B.3. Diagram of excavation FZE-11-03 87

B.4. Diagram of excavation FZE-11-04 88

B.5. Diagram of excavation FZE-11-05 88

B.6. Diagram of excavation FZE-11-06 88

B.7. Diagram of excavation FZE-11-07 89

B.8. Diagram of excavation FZE-11-11 89

B.9. Diagram of excavation FZE-11-15 89

B.10. Diagram of excavation FZE-11-16 90

B.11. Diagram of excavation FZE-11-18 90

B.12. Diagram of excavation FZE-11-26 90

B.13. Diagram of excavation FZE-11-27 91

B.14. Diagram of excavation FZE-11-28 91

B.15. Diagram of excavation FZE-11-29 91

B.16. Diagram of excavation FZE-11-33 92

B.17. Diagram of excavation FZE-11-34 92

B.18. Diagram of excavation FZE-11-35 92
B.19. Diagram of excavation FZE-11-36 93
B.20. Diagram of excavation FZE-11-37 93
B.21. Diagram of excavation FZE-11-38 93
B.22. Diagram of excavation FZE-11-39 94
B.23. Diagram of excavation FZE-11-40 94
B.24. Diagram of excavation FZE-11-41 94
B.25. Diagram of excavation FZE-11-42 95
B.26. Diagram of excavation FZE-11-43 95
B.27. Diagram of excavation FZE-11-44 95
B.28. Diagram of excavation FZE-11-49 96
B.29. Diagram of excavation FZE-11-30 96
B.30. Diagram of excavation FZE-11-31 96
B.31. Diagram of excavation FZE-11-32 97
B.32. Diagram of excavation FZE-11-46 97
B.33. Diagram of excavation FZE-11-47 97
B.34. Diagram of excavation FZE-11-48 98
B.35. Diagram of excavation FZE-11-50 98
B.36. Diagram of excavation FZE-11-52 98
B.37. Diagram of excavation FZE-11-56 99
B.38. Diagram of excavation FZE-11-58 99
B.39. Diagram of excavation FZE-11-59 99
B.40. Diagram of excavation FZE-11-60 100

B.41. Diagram of excavation FZE-11-61 100

B.42. Diagram of excavation FZE-11-62 100

B.43. Diagram of excavation FZE-11-63 101

B.44. Diagram of excavation FZE-11-64 101

B.45. Diagram of excavation FZE-11-65 101

C.1. Cumulative percentage curves of grain size distribution of Jason Fan sediment samples 105

C.2. Cumulative percentage curves of grain size distribution of Aeolus Fan sediment samples 106

C.3. Cumulative percentage curves of grain size distribution of Northern Bull Pass Fan sediment samples 107

C.4. Cumulative percentage curves of grain size distribution of Southern Bull Pass Fan sediment samples 108

C.5. Cumulative percentage curves of grain size distribution of Upper Wright Fan sediment samples 109

CHAPTER 1. INTRODUCTION

Antarctica is a key component of the global climate system. Its vast surface of snow and ice reflects solar radiation back into space, cooling global climate; it supplies cold, dense water that sinks along ice sheet margins to help drive global thermohaline circulation (e.g. Broecker, 1991); and it imposes a sharp thermal gradient on the Southern Hemisphere that enhances atmospheric circulation (e.g. Parish and Bromwich, 1987). Two ice sheets, the marine-based West Antarctic Ice Sheet (WAIS) and the continental-based East Antarctic Ice Sheet (EAIS), cover over 99% of the continent. Melting of the WAIS would raise global sea level by about 8 m, whereas melting of the EAIS would account for nearly 65 m of sea-level rise (Williams & Hall, 1993). Over the past two decades, satellite mapping of ice sheet gravity and perimeter retreat indicate extensive loss of ice from Antarctica, which is contributing to global sea-level rise, but many uncertainties regarding the nature of the mass loss remain (Rignot et al., 2011). Surface melting on the EAIS is at present only estimated and remains the most poorly understood input in models of future sea-level rise (IPCC, 2007).

Records that specifically gauge melting along terrestrial margins of the EAIS are lacking. Numerous paleoclimate records exist that record fluctuations of the ice sheet. For example, marine sediments drilled just offshore of the McMurdo Dry Valleys region record obliquity-driven oscillations of the EAIS-fed Ross Ice Shelf during Pliocene and Pleistocene time (Naish et al., 2009) and retreat of the shelf throughout Holocene time beginning just after the Last Glacial Maximum (LGM) (Dunbar et al., 2007; McKay et al., 2008). However, these records register no details related to melting, only the absence of an ice shelf, which may relate more to water temperature than to other forcing mechanisms such as increased air temperature.

Fluctuations of regional temperature are known from ice core studies. Oxygen isotopes measured in ice-cores collected across coastal and central regions of the EAIS register an early Holocene optimum followed by less pronounced optima since then (Masson et al., 2000) but these records are not directly correlated to melting along ice sheet margins. These records only register conditions on the high-elevation polar-plateau, whereas margins of the EAIS are hundreds to thousands of km removed and thousands of m lower.

This lack of records registering melting along ice sheet margins arises from the fact that most of the EAIS terminates in the ocean, leaving few easily accessible geologic deposits. The longest terrestrial margins are in the McMurdo Dry Valleys region. Along this margin, however, the most active meltwater systems originate from low-elevation glaciers along the coast and flow inland toward closed-basin lakes on valley floors. Fluctuations of these closed-basin lakes due to glacial melting have been used as a record of millennial scale climate patterns since the LGM (Hall et al., 2000; Hall et al., 2010). However, the majority of meltwater feeding into these lakes is thought to have originated from the Ross Ice Sheet when it blocked low-elevation valley mouths in the eastern Dry Valleys. Given its low-elevation and close connection to ocean temperatures, climatic processes that would control melting of the Ross Ice Sheet are not directly analogous to those that would induce melting along the margins of the EAIS. In order to build an accurate record of past surface melting along margins of the EAIS, a proxy closer to the margins and at appropriate elevations must be used.

Alluvial fans found throughout the Dry Valleys are evidence of past meltwater generation. These fans are among the youngest features in this ancient landscape and in most cases directly overlie dated tills that range in age from Pliocene to middle Miocene (Marchant et al., 1993; Hall et al., 1993; Lewis et al., 2006, 2007, 2008). They record meltwater flowing from

high-elevation glaciers in a landscape where liquid water is exceptionally rare. Unlike valley-floor records, they register melting at elevations equal to those of modern ice sheet margins (**Figure 1.1. and 1.2.**). Moreover, since fans can only be created from flows of water large enough to carry sediment, they are an archive of only relatively large melting events. Climate conditions conducive to generate this volume of meltwater represent a drastic departure from

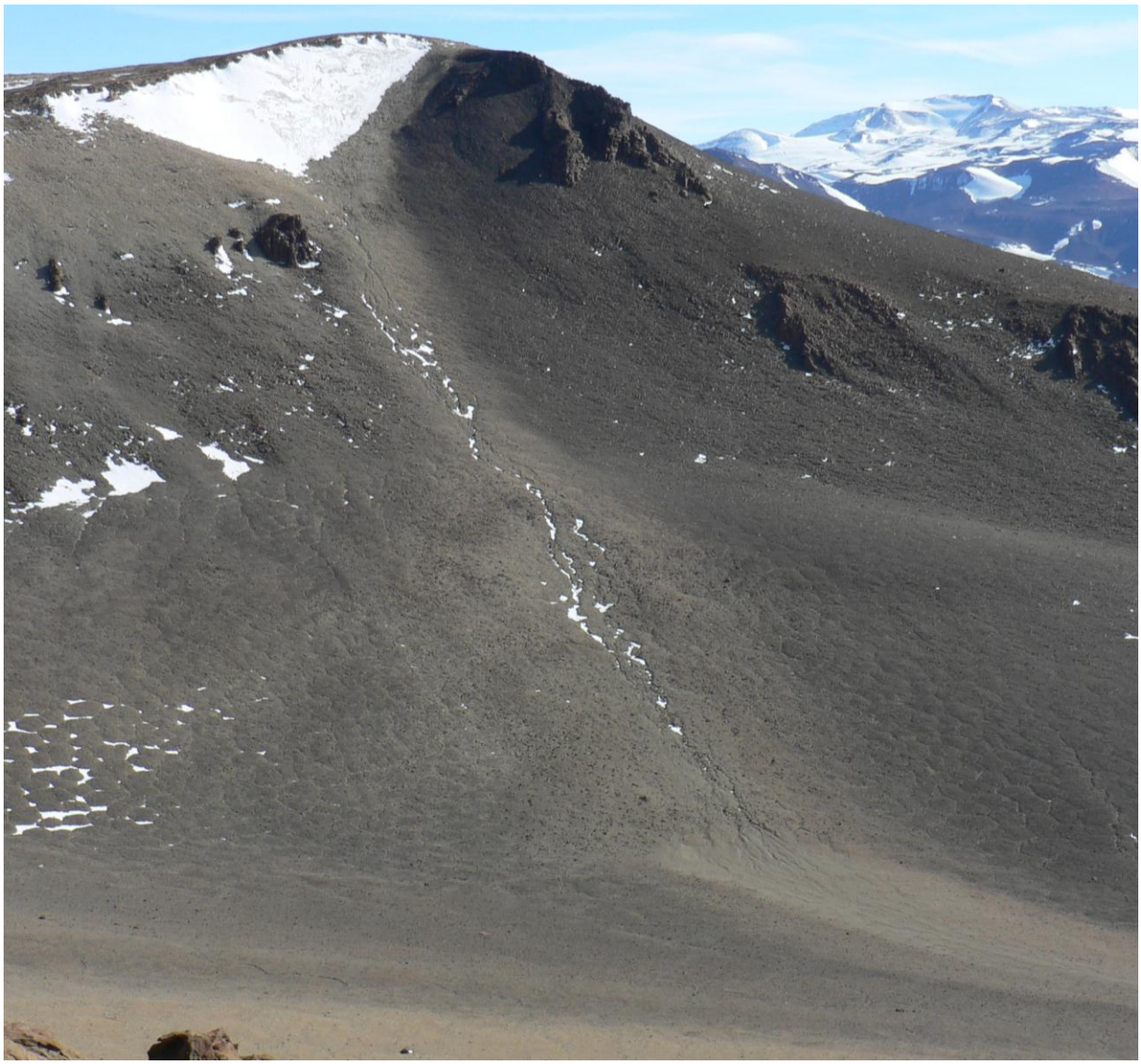

Figure 1.1. Aeolus Fan. The margin of the East Antarctic Ice Sheet can be seen in the upper right portion of the image. View is to the west. Scale varies in the image; the snowbank is approximately 100 m wide.

Figure 1.2. Sponsors Central Fan. The snow patch at the fan head lies at an elevation of 1350 m. View is to the southwest. Scale varies in the image; the fan margin is approximately 250 m wide.

those of the perennially cold and dry region today. This thesis represents a first attempt to use alluvial fans as a proxy for meltwater generation along terrestrial margins of the EAIS.

1.1. Goals and objectives

The diffuse distribution of alluvial fans could afford a widespread proxy record of meltwater generation at variable distances from the coast and at different elevations in the Dry Valleys. The goal of this thesis is to determine if alluvial fans, that today appear inactive, accurately capture past melting events along terrestrial margins of the EAIS. Multiple objectives were crafted to accomplish this. The first is to use fan sedimentology and stratigraphy to help understand fan-forming depositional processes including the paleohydrology of meltwater flows from fan catchments. A second objective is to use GIS analyses of spatial data to identify the geographic attributes of meltwater sources that are most relevant to fan area, which is used as a proxy for overall fan activity. Properties examined include distance from the coast, elevation, insolation and coverage of snow and ice in fan catchments. The final objective is to use surface geomorphology and optically stimulated luminescence (OSL) dating to develop a preliminary chronology of fan aggradation and determine when these seemingly relict fans were last active. Results from this study will enhance understanding of melting along terrestrial margins of the EAIS by 1) describing how melting takes place, 2) identifying geomorphic and climatic controls governing melt processes, and 3) providing an initial estimate of the frequency of past melting events. A second thesis, currently underway at NDSU, will focus on producing a detailed chronologic record of melting for these same fans.

1.2. Physical setting and climate conditions

The McMurdo Dry Valleys are the largest ice-free region in Antarctica. The region lies within the Transantarctic Mountains (TAM), which are bound to the west by the margin of the EAIS and to the east by the seasonally open Ross Sea. McKay Glacier to the north and Ferrar

Glacier to the south extend from the EAIS to the Ross Sea, partitioning the Dry Valleys from the rest of the TAM. The main physical features of the Dry Valleys, and the derivation of the name, are three east-west trending valleys that extend across the region, each being approximately 80 km long and 15 km across (**Figure 1.3.**). All three valleys head to the west at steep scarps as much as 2,500 m high, and all three open to the east at the Ross Sea coast. The three valleys are separated from each other by east-west trending mountain ranges that reach elevations as high as 2,800 m. Steep, rectilinear slopes lead down from the mountain ranges to the broad valleys floors.

The local bedrock consists of a basement of Precambrian to Paleozoic-aged granites and gneisses, which crop out at elevations below 800 m. Overlying these are generally flat-lying sedimentary rocks of the Beacon Supergroup, which are Devonian- to Triassic-aged siltstones, sandstones, and conglomerates. Jurassic-aged dolerite sills, up to 300 m thick, intrude the Beacon Supergroup along formational contacts and other major stratigraphic boundaries (Isaac et al., 1996; Elliot and Flemming, 2004).

The Dry Valleys are a polar desert. High-elevation plateaus along the ice sheet margin have mean annual temperatures (MAT) as low as –27.4°C, increasing to –19.6°C on valley floors near the Ross Sea coast (Doran et al., 2002). Average summer temperatures at high-elevations plateaus are about –10°C (Marchant & Head, 2007). The warmest average summer temperatures occur along the coast and are as high as 1.4°C (Clow et al., 1988). Surface temperature generally decreases with elevation and distance from the Ross Sea (Doran et al., 2002).

Annual precipitation in the Dry Valleys does not exceed 5 cm water equivalent with virtually all precipitation falling as snow (Keys, 1980). Precipitation is greatest along the coast at the eastern margin of the Dry Valleys and rapidly decreases inland (Fountain et al., 2009).

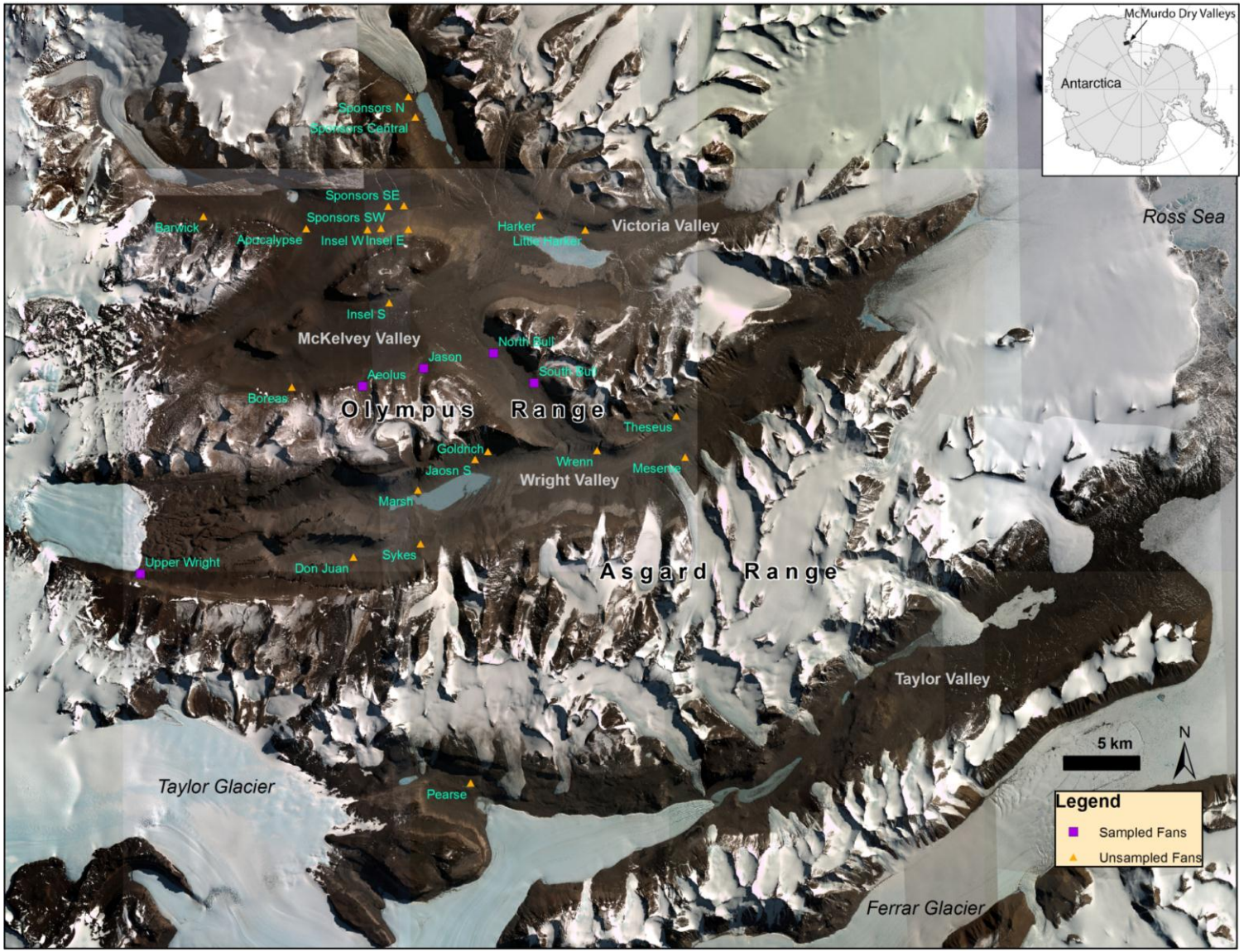

Figure 1.3. Satellite image of McMurdo Dry Valleys, Antarctica. Image shows visited fans, and fans integrated in the geospatial analysis. Base image provided courtesy of the Polar Geospatial Center.

The majority of snowfall sublimates before melting (Chinn, 1981). Snowfall only accumulates in the lee of topographic obstacles or on protected slopes where it often sustains alpine glaciers. All alpine glaciers in the Dry Valleys are cold-based, meaning that ice throughout the glacier is below the pressure-melting point. They originate at elevations between 2,500 and 1,500 m and most terminate on high-elevation slopes (**Figure 1.4.**) where they ablate primarily by sublimation. The largest extend to valley floors where melting accounts for a portion of ablation (Chinn, 1987; Lewis et al., 1998; Lewis et al., 1999). Glacial geologic studies indicate that alpine glaciers have been very stable since the Pliocene at low elevations (Fountain et al., 1998) and since the Miocene at elevations above about 1,200 m (Lewis et al., 2007). Till sheets and moraines indicate farthest extents of no more than several hundred meters from their current positions (Lewis et al., 2007).

Figure 1.4. High-elevation alpine glaciers along the Asgard Range. Glaciers originate along the crest of the mountain range and flow towards the floor of Wright Valley. View is to the south. Mt Odin is the peak at left, Brunhilde Peak is at right; View is 5 km wide at mountain front.

Melting along margins of alpine glaciers and perennial snowbanks is the only significant source of meltwater contributing to surface hydrologic processes in the Dry Valleys (Fountain et al., 1998). Meltwater flows originating from these sources are enhanced by melt from snow in shallow nivation hollows along the flanks of the mountain ranges and within proglacial stream channels (Head et al., 2007; Morgan et al., 2007). Meltwater production depends on positive energy balance at the ice and snow surface. The energy balance is only positive between the late spring and summer months of November and February when incoming solar radiation is highest. Melting during this period is highly variable, however, because of a complex arrangement of factors. The low zenith of the sun and the mountainous topography create diurnal changes of incident solar radiation on glaciers and snowbanks. Melt variability is further complicated by changes in local cloud cover, which occur frequently in this coastal setting, and by fresh snow cover that can radically increase albedo. Apart from the insolation characteristics of meltwater sources, the ambient air temperature changes with the geographic locations in the Dry Valleys, making meltwater generation more common at some locations than others. These effects are reflected in the unusual mass balance of glaciers in Taylor Valley, for example, which become increases with lower elevation and with decreased distance from the Ross Sea (Fountain et al., 1994).

Fan aggradation depends on meltwater flows competent enough to carry sand- and gravel-sized sediment. In the Dry Valleys, however, meltwater generation is complicated by the amount of sublimation taking place. Generally, sublimation predominates over melting due to the cold, dry, windy conditions that characterize much of the Dry Valleys (Chinn, 1987). The proportion of sublimation versus melting changes relative to geomorphic position along glaciers and snowbanks. Specifically, areas that have lower albedo, greater exposure to both incoming

and reflected long-wave radiation, and are sheltered from wind experience a greater proportion of ablation due to melt. This difference is highlighted at Canada Glacier in Taylor Valley, where 40-80% of ablation at the horizontal glacial surface is due to sublimation, whereas ablation at the terminus is almost entirely due to melting (Lewis et al. 1999).

1.3. Alluvial fans as indicators of climate and meltwater production in the Dry Valleys

Much research has focused on the correlation of alluvial fan processes with a specific climate regime (Bull, 1964; Church and Ryder, 1972; Williams, 1969, 1973; Wasson, 1977; Hartley et al., 2005; Owen et al., 2006; Suresh et al., 2007; Bacon et al., 2010; Steffen et al., 2010). These studies associate fan evolution to climate trends at decadal (e.g. El Nino) to millennial (e.g. Milankovitch) timescales. Climate trends are inferred from the frequency of deposition, hiatuses in deposition, and the type of depositional regime. Most studies associate periods of gravity-flow dominated deposition with warm, wet climates. Depositional hiatuses or periods of intense erosion are associated with colder, dryer climates that either produce small volumes of sandy alluvium (e.g. Hartley et al., 2005) or flows that cut down into the fan (e.g. Steffen et al., 2010).

The rareness of fan-forming flows, even on the most active alluvial fans, has led some researchers to question their value as paleoclimate records. Blair and McPherson (1994) argued that fan aggradation is inherent to the piedmont environment on which fans are found, and that any fluid gravity flow or sediment gravity flow will contribute to construction, regardless of climate. The difficulties in using fans as climate proxies were summarized by Dorn (1996) who asked if it is "even possible to correlate, in time, climatic changes with fan aggradation or with hiatuses in deposition."

Advances in geochronology have alleviated many of the concerns regarding accurate correlation of alluvial deposits over time. Specifically, optically stimulated luminescence (OSL)

has emerged as a robust method to establish accurate geochronologies for alluvial deposits (Delong and Arnold, 2007; Fuchs and Lang, 2009; Fuchs et al., 2010; Lepper et al., 2011). OSL dating is advantageous when studying alluvial deposits because of the ease of stratigraphic interpretation of the sample, abundance of material, and easy comparison with other techniques (Delong and Arnold, 2007). This technique has been successfully applied to studies correlating alluvial deposition to climate changes with confirmation from additional independent age controls (Robinson et al., 2005; Roberts et al., 2009).

Along with a wide variety of geomorphic features, numerous alluvial fans lie between the coast of the McMurdo Dry Valleys and the margin of the EAIS. Marchant & Head (2007) recognized the geographic dependence of landforms and related geomorphic processes taking place in the Dry Valleys. They argued that specific equilibrium landforms develop in conjunction with the environmental conditions of fixed microclimate zones, with landforms not associated with the predominant climate conditions serving as evidence for periods of disequilibrium. Most alluvial fans in the Dry Valleys would be counted among landforms that are in disequilibrium given the relative stability of the Dry Valleys landscape since the mid-Miocene (Marchant et al., 1993; Summerfield et al., 1999; Sugden et al., 1999; Lewis et al., 2006, 2007). These features standout as clear evidence of flowing meltwater and climatic warmth in an otherwise stable landscape paralyzed under cold and dry polar-desert conditions.

1.4. Studied fans

This study focused on five fans in the Olympus and Asgard Ranges in the western McMurdo Dry Valleys (**Figure 1.3.**). These fans were selected because each is fed by a single meltwater source, has clearly defined margins, and because their differences in size, catchment area, aspect, and distance from the Ross Sea provide a range of possible controls on meltwater production. Fans were visited between November and December of 2011. The following is a

brief description of the geomorphology of each individual fan. Sedimentological analyses for each are given in chapter 2 and a chronology of near-surface sediments is given in chapter 4.

1.4.1. Jason Fan

The Jason Fan lies at the mouth of Bratina Valley, northeast of Mt. Jason in the Olympus Range (-77.45509°, 161.51737°; **Figure 1.5.**). The fan lies on a north-facing structural bench

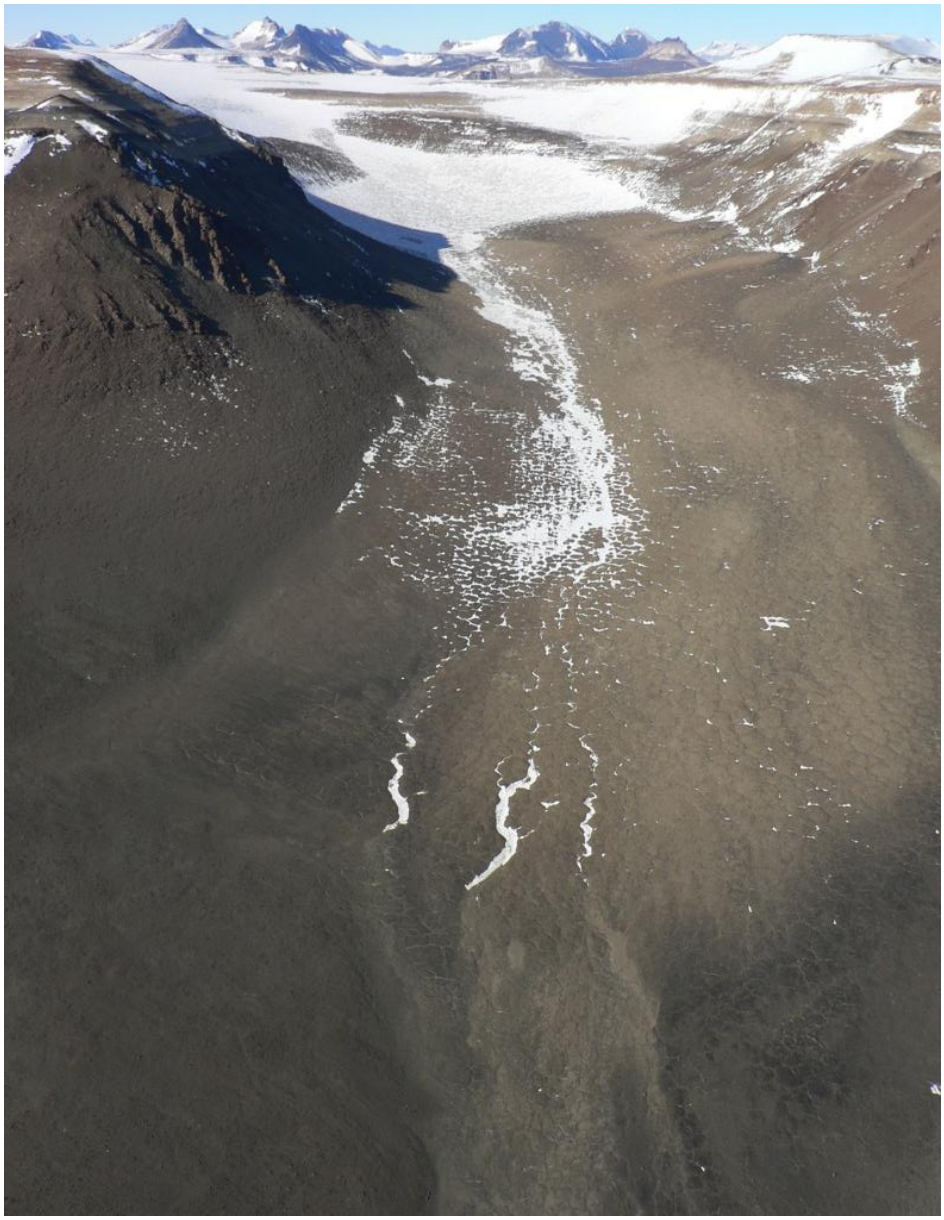

Figure 1.5. Jason Fan. View is to the south. Mt. Hercules is the flat-topped peak at right of image; peaks of the Asgard Range are visible in the background. Scale varies in this image; valley is approximately 1.3 km wide.

that flanks the Olympus Range at an elevation of about 1,100 m. The Jason Fan has a long, narrow profile with a low slope. The fan measures 410 m along its central axis and is 160 m wide. Meltwater originates from a north-facing niche glacier that lies between 1,350 and 1,450 m elevation. The meltwater channel is approximately 1.95 km in length with an average gradient of 6%. Ice and snow filled the majority of the channel cross-section in 2011 and during previous years based on air photos and satellite images. A network of partially wind-eroded and obscured overflow channels extends from the edge of the fan to the lip of the structural bench. There they merge to form a single channel that extends to the floor of McKelvey Valley, evidently carrying water during periods of greatest flow. Relative to the channels leading from the glacier to the fan head, this overflow channel is highly degraded, suggesting flows reach it less frequently. A meteorological station deployed at the terminus of the glacier from November 26, 2011 through February 29, 2012 recorded an average temperature of -11.0°C in Bratina Valley.

1.4.2. Aeolus Fan

The Aeolus Fan is situated along the western slope of Cartwright Valley, east of Mt. Aeolus in the Olympus Range (-77.46451°, 161.34735°; **Figure 1.1.**). The fan lies at an elevation of 1,200 m along the same structural platform as the Jason Fan. The fan is 370 m long along its central axis. At its widest, the fan is 55 m across and gradually tapers to a point at its toe. At the head of the fan, the axis is oriented east, shifting northeast as it meets the valley floor and becomes parallel to the valley thalweg. Meltwater originates from a northeast-facing niche glacier, which is perched in an alcove below a structural bench at an elevation between 1,400 m and 1,350 m elevation. Meltwater then follows a steep, narrow meltwater channel to the fan head. The channel is 0.7 km long and has an average gradient of 23%. A series of abandoned, degraded meltwater channels are directly adjacent to the modern channel at the fan head,

indicating multiple episodes of fan aggradation. From November 26, 2011 through February 29, 2012 a meteorological station deployed near the terminus of the glacier recorded an average temperature of -10.0°C.

1.4.3. Northern Bull Pass Fan

The Northern Bull Pass Fan lies at the northern end of Bull Pass in the Olympus Range, southwest of Mt. Booth, at an elevation of 700 m (-77.44869°, 161.70721°; **Figure 1.6.**). The fan extends 100 m along its main axis and is 85 m wide at the toe. The fan's surface is relatively undisturbed by periglacial processes compared to the other study fans, suggesting this fan has aggraded relatively recently. Meltwater is generated from a southwest-facing glacier south of Mt. Booth. This glacier lies between 1,450 m and 1,300 m elevation. A narrow channel, 1.8 km long with an average gradient of 15.7%, routes water from the glacier to the fan.

Figure 1.6. Northern Bull Pass Fan. View is looking up-slope to the east. The fan is approximately 85 m wide. Till pavements surround the fan and extend beneath fan deposits, clearly marking the contact between alluvium and till.

1.4.4. Southern Bull Pass Fan

The Southern Bull Pass Fan is situated at the mouth of Orestes Valley, on the southern end of Bull Pass at an elevation of 650 m (-77.47279°, 161.78718°; **Figure 1.7.**). The fan extends 1,200 m along its main axis and is 1,100 m wide at the toe. The fan has a steep upper portion that quickly changes to a broad, flat surface halfway down its profile. Meltwater originates from a south-facing alpine glacier that occupies a cirque on the northern slopes of Orestes Valley. The glacier lies between 1,500 m and 1,150 m elevation. Meltwater is fed to the fan by a channel 4.7 km long with an average gradient of 7.5%. Long reaches of the channel contain perennial snow and ice cover, as seen in aerial and satellite images taken over multiple

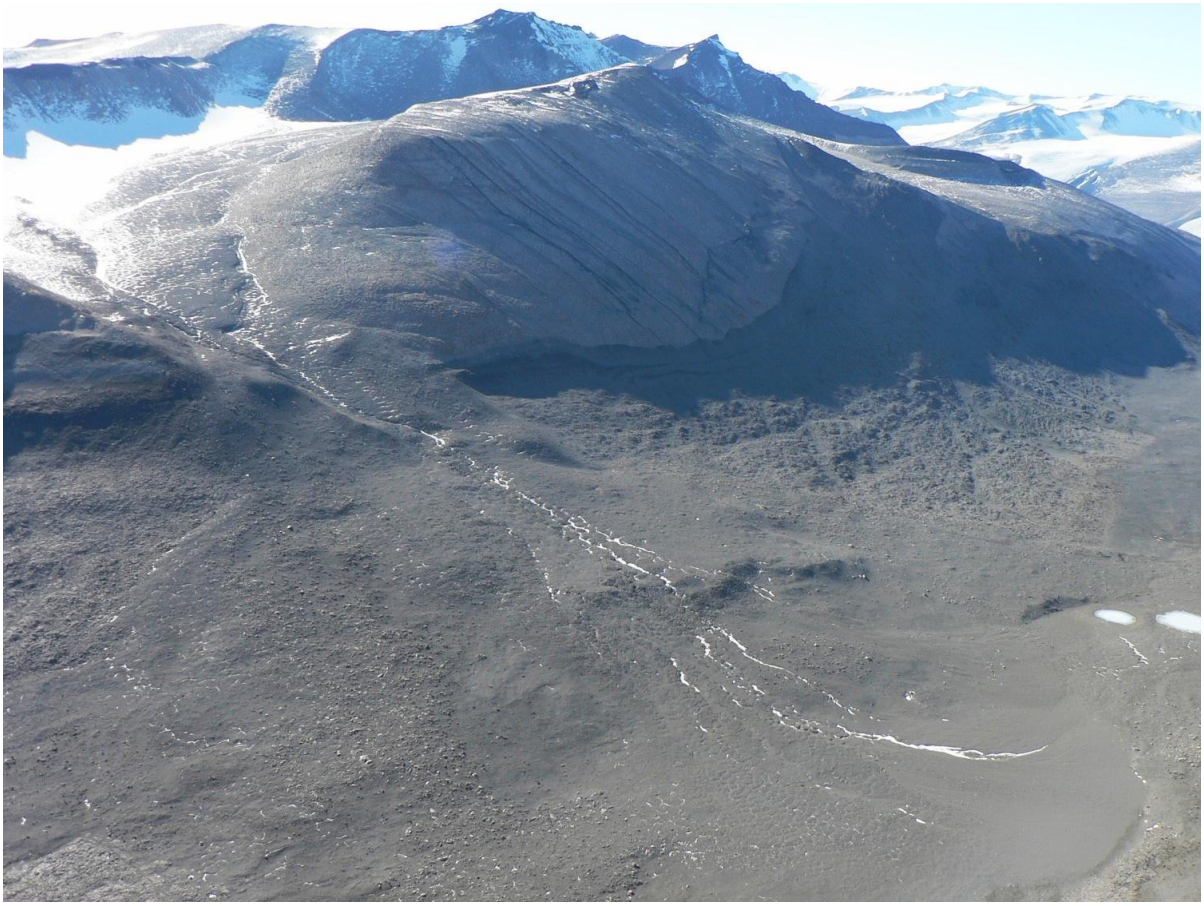

Figure 1.7. Southern Bull Pass Fan. The source glacier lies in Orestes Valley, with meltwater flowing down the channel, depositing the fan at the southern end of Bull Pass. View is to the southeast; Mt Orestes is the peak in the middle distance. Scale varies in this image; the snow-filled channel is approximately 2.9 km long.

years. The Southern Bull Pass Fan is the largest of the five study fans as is the glacier that feeds it. The size and topography of the fan suggest multiple episodes of aggradation and degradation.

1.4.5. Upper Wright Fan

The Upper Wright Fan lies northwest of Mt. Thor at the head of Wright Valley, along the northern slopes of the Asgard Range at an elevation of 900 m (-77.57006°, 160.69669°; **Figure 1.8.**). The fan creates a broad, gently sloped surface that extends 85 m along its main axis and is 70 m wide at the toe. The toe of the fan forms the shore of a small pond that is perennially ice-covered and frozen to its base. Similar to the Northern Bull Pass Fan, the surface is relatively undisturbed by periglacial processes, suggesting it has aggraded relatively recently. Meltwater originates from a north-facing niche glacier that sits just beneath the lip of a structural platform. The glacier lies between 1,125 m and 1,000 m elevation. Meltwater is routed to the fan by a short channel 0.6 km long with an average gradient of 16.7%.

Figure 1.8. Upper Wright Fan. The snowbank is perched along the northern slopes of the Asgard Range, below Mt. Thor. The person in red provides scale.

CHAPTER 2. DEPOSITIONAL SETTING

2.1. Purpose

Alluvial fans are a sedimentary archive that registers streamflow from high-elevation glaciers and snowbanks in the Dry Valleys. However, volumes of meltwater sufficient to produce overland flow, let alone cause fan aggradation, have never been observed in modern times in any of these fan catchments. Moreover, stable desert pavements and well-developed polygonal patterned ground on fan surfaces indicate that most have been inactive for significant periods. Fans in the Dry Valleys must be evidence of past climatic warmth when streamflow from fan catchments was sufficient for fan aggradation.

Within the accumulated sediments that form a fan, individual sedimentary sequences can be differentiated that are associated with discrete periods of melting. Each sedimentary sequence can be comprised of several or a single sedimentary bed. For the remainder of this thesis a sedimentary sequence that corresponds to a distinct period of melting will be referred to as a *melt-package*. Buried desert pavements, contrasts in sediment color, and bedding contacts mark stratigraphic boundaries between melt-packages. The identification of these individual melt-packages is critical for development of an accurate chronology.

The sedimentological characteristics of beds in each melt-package will be used to describe the depositional setting present during these discrete periods of fan aggradation. An accurate understanding of the depositional environment is essential to characterize how melting takes place. Sedimentary structures, bedding, grain-size distribution, and the maximum clast size of each bed provide information about depositional environment such as flow regime, competence, velocity, and depth. The information presented here provides a window on past

melting events that occurred at high-elevations in the Dry Valleys. The goal is to provide a more complete portrait of past melting events that took place along terrestrial margins of the EAIS.

2.2. Methods

2.2.1. Field methods

From 19 November through 19 December 2011, I dug 65 pits to expose sediments in five fans in the Olympus Range and the Asgard Range in the western McMurdo Dry Valleys. Pits were sited to expose specific sections of fans, particularly thick stratigraphic sequences containing multiple melt-packages, or basal contacts between alluvial deposits and underlying Miocene-aged tills. The location of each pit was recorded using hand-held GPS units and the characteristics of local topography were noted (all pit locations used in this study are recorded in Appendix A). The upper portions of pits were excavated using hand tools until ice-cemented sediments prevented further digging, typically at depths ranging from 15 to 30 cm. An electrical jackhammer and portable generator were used when necessary to extend excavations below the level of ice-cemented permafrost. Most pits were dug as deep as necessary to expose the contact between alluvial deposits and underlying till. Maximum depths were typically 0.5 to 1 m. Pits were kept to a minimum size, usually less than 1 m^2, to reduce environmental impacts.

Once pits were completed, stratigraphic sections were cleaned and photographed. Individual melt-packages were identified on the basis of texture, sorting, graded beds, sediment color, and buried desert pavements with special attention paid to the identification of contacts between melt-packages. Other physical characteristics pertaining to depositional setting, such as sedimentary structures and clast fabric, were identified and recorded.

I collected representative sediment samples from each melt package or, if possible, each bed identified in the exposed sections. Unfrozen samples were sieved in the field through a -4ϕ

screen to separate cobbles and boulders from finer-grained matrix. Matrix samples were placed in labeled Whirl-pack plastic bags for transport to NDSU. Clasts larger than -4ϕ were counted relative to their abundance in each sieve pan. A representative sample was then placed in labeled canvas bags; a minimum of 40 clasts was collected where possible. Where strata were ice-cemented, samples were collected as frozen blocks that included both matrix and clasts. This unsorted material was placed in labeled Whirl-pack plastic bags for transport to NDSU. Ice-cemented samples were transported to NDSU alongside dry samples, arriving as thawed, wet sediments in sealed plastic bags.

2.2.2. Laboratory methods

Sedimentological analyses were conducted at NDSU in the Department of Geosciences Sedimentology Laboratory. All analyses were done following the procedures of Folk (1974). Before sedimentological analyses took place, water was removed from the sediment samples. Dry samples were transferred to aluminum pans and placed in an oven at 50°C for 12 hours to remove any possible moisture. The same procedure was applied to thawed samples because the interstitial ice content, having thawed in transit, was so low that none produced any water that could be poured off.

Gravel was separated from a 1.0 to 1.5 kg split of matrix samples using standard dry sieving techniques and an automated Ro-tap shaker. The gravel was sieved at 1ϕ intervals between -1ϕ and -4ϕ with the sand- and mud-sized material collected in a pan below. Weights of gravel retained at each interval were recorded to the nearest 0.01 g using an Ohaus Adventure Pro scale. The weighed gravel samples were then placed in labeled plastic bags for storage and potential future use.

Sand analysis was completed by splitting a 50 to 100 g subsample from matrix that passed through the gravel sieves. Subsample splits were weighed to the nearest 0.01 g. They were then placed in 250 ml beakers, filled with ~100 ml of a 2.55 g/L Calgon solution, and placed in a Branson 3510 sonicator for 20 minutes to disaggregate and disperse flocculated sediments. The entire subsample was then wet sieved using a 4ϕ screen, which allowed the mud fraction and solution to pass through. The mud was collected in a 1 L Nalgene bottle and set aside for later pipette analysis. The sand fraction collected on the 4ϕ screen was then rewashed using tap water and dried overnight in an oven at 50°C for 12 hours. The dried sand fraction was then weighed. Finally, the sand was sieved and weighed at 1ϕ intervals between 0ϕ and 4ϕ. The weighed sand samples were then placed in labeled plastic bags and stored.

Pipette analysis was used to determine the grain-size distribution of the silt fractions at 1ϕ intervals and the total mass of the clay fraction, which included all sediment below 8ϕ. To begin the pipette analysis the mud and Calgon solution was transferred from the Nalgene bottle into a 1 L graduated cylinder. When necessary, additional Calgon solution was added to bring the total volume to 1 L. Using a stir rod, the solution was vigorously stirred to develop a uniform distribution of grain sizes throughout the cylinder. Once the rod was removed, 20 ml subsamples were extracted using a glass pipette at the depth and time intervals specified by Folk (1974). Each subsample was placed in a beaker and dried at 100°C for 20 hours. The subsamples were then left in the open to equilibrate with atmospheric moisture content before being weighed to the nearest 0.01 g. The samples were discarded after being weighed. The percentage of each grain size interval was calculated and cumulative percentage graphs were developed for each sample. Equation 2.1 was used to calculate the inclusive graphic standard deviation (σ_I) as a measure of sorting using the verbal classification scale of Folk (1974).

$$\sigma_I = \frac{\Phi 84 + \Phi 16}{4} + \frac{\Phi 95 + \Phi 5}{6.6} \quad (2.1.)$$

The graphic mean grain size (M_Z) was calculated using equation 2.2.

$$M_Z = \frac{\Phi 84 + \Phi 50 + \Phi 16}{3} \quad (2.2.)$$

All sedimentological results are reported in Appendix C.

2.2.3. Methods of paleohydraulic reconstruction

I applied the methods of Costa (1983) that utilize the maximum clast size along the intermediate axis (d_I) as a proxy for the mean channel velocity and the depth of paleo-flows. He applied this approach to flood events in nine watersheds with steep, bedrock channels in the Front Range of Colorado. This method assumes that flow takes place under a fluvial regime, as opposed to debris flows or gravity flows, and that the largest clasts deposited are indicative of the hydrologic competence of the flows. This method has become a common paleohydraulic technique (e.g. Maizels, 1987; Lewis et al., 2006; Cummings et al., 2011) and has been utilized to reconstruct flow events on alluvial fans (Blair, 1987; Haug et al., 2010).

In this original calculation Costa utilized 123 clasts 50 mm or larger and the associated velocities of the streams. A least-squares regression curve of his observations yields equation 2.3:

$$\bar{v} = 0.20 d_I^{0.455} \quad (2.3.)$$

Costa (1983) also utilized an equation developed by Strand (1973) to estimate the limiting clast size needed for riprap stability given a specific bed velocity. This equation

$$v_b = 5.9\sqrt{d_I} \quad (2.4.)$$

was developed using clasts between 10 mm and 600 mm in size. The depth averaged stream velocity, equation 2.5, could then be derived from the equation of Strand (1973).

$$\bar{v} = \sim 1.2 v_b \quad (2.5.)$$

The final method of Costa (1983) is a least-squares regression curve derived from the arithmetic average of velocities estimated from four methods, two of which are discussed above, yielding equation 2.6.

$$\bar{v} = 0.18 d_I^{0.487} \quad (2.6.)$$

Depth was estimated using a form of Manning's equation (eq. 2.7).

$$D = \left[\frac{v \times n}{\sqrt{S}} \right]^{1.5} \quad (2.7.)$$

The average velocity used is the arithmetic average of the three methods presented above; I determined the average slope of channels from a 30 m DEM in ArcGIS. A Manning's coefficient of n = 0.05 was used, which corresponds to steep channels composed of gravels, cobbles, and boulders.

For paleohydraulic reconstruction of fan flows I used clasts larger than -4ϕ that were separated from matrix in the field. Not all pits yielded clasts larger than -4ϕ, which reduced the sample size of this reconstruction compared to the grain size analysis. A General Ultratech caliper was used to measure d_I to the nearest 0.01 mm. The five largest clasts from each sample were used to calculate an average d_I for that deposit. Full results of the paleohydraulic reconstruction are presented in Appendix D.

2.3. Sedimentology, stratigraphy, and paleohydrology of the study fans

2.3.1. Jason Fan

The Jason Fan is comprised of bedded alluvium 70 cm thick at maximum. Deposits overlie a hummocky till surface, causing the thickness of fan deposits to vary over short distances. Alluvial sediments of the Jason Fan are comprised of sandstone and dolerite. Fan sediments are poorly sorted and have an overall grain size of coarse sand. On average, sediments are 13% gravel, 85% sand, and 2% silt and clay. The gravel fraction is subangular to subrounded

clasts of sandstone, dolerite, and siltstone from the catchment bedrock. Fan sediments weather to a light reddish brown color (2.5YR 7/3). At the ground surface, sediments are capped by a gravel pavement one clast thick. Pavement clast lithology is identical to that found within the alluvium. Pavement clasts show limited signs of ventifaction and have developed a light orange varnish on their northern faces. Fan sediments directly overlie a till sheet above a sharp basal contact. This till consists of boulders, cobbles, and gravel set within a pale red (2.5YR 7/2) to grey (7.5YR 7/0), muddy sand matrix. The boundary between alluvium and till is sharply marked by a buried pavement that extends unbroken to tills surrounding the fan (**Figure 2.1.**). This pavement is composed primarily of siltstone cobbles and dolerite boulders. Clasts marking this contact have undergone extensive ventifaction and have a thick, well-developed orange varnish.

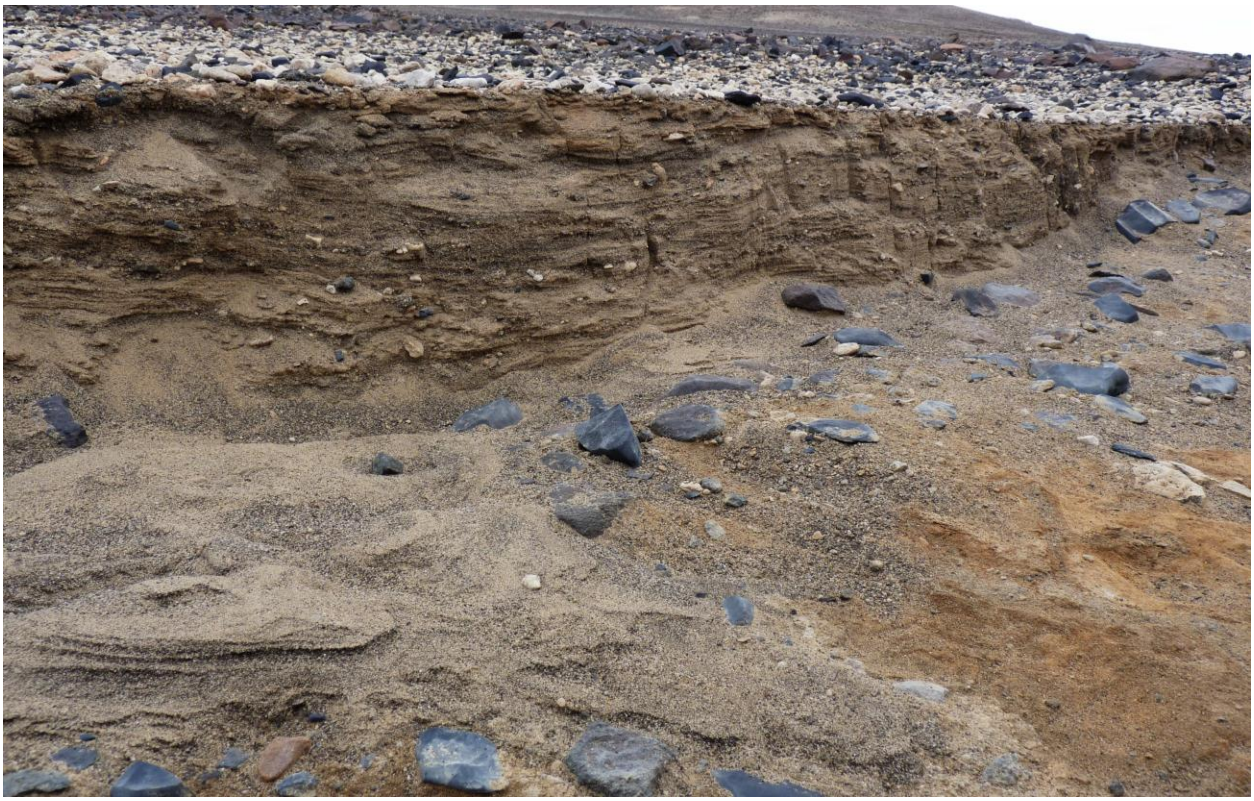

Figure 2.1. Image of pit FZE-11-01. Planar-bedded, sands overly Miocene-aged tills, with a buried pavement sharply marking the contact. The alluvium overlying pavement is 50 cm thick at image center.

Individual melt-packages in the Jason Fan are 10 to 40 cm thick and are made up of 1 to 3 beds. Each bed is 10 to 15 cm thick and is composed of evenly graded, planar-bedded gravelly sand. Some beds included a 2- to 4-cm-thick basal gravel layer, which when repeated forms sand-gravel couplets within melt-packages (**Figure 2.2.**). Pavements marked the tops and bottoms of individual melt-packages. The hummocky surface over which melt-packages were deposited limits their lateral extent and inhibits placing them in a stratigraphic order that extends over the entire fan. Modern and relict sand wedges, less than 15 cm wide, frequently crosscut the planar bedding of alluvial deposits and extend down through the till (**Figures 2.2. and 2.3.**). These sand wedges and their implications will be discussed in more detail in Chapter 4.

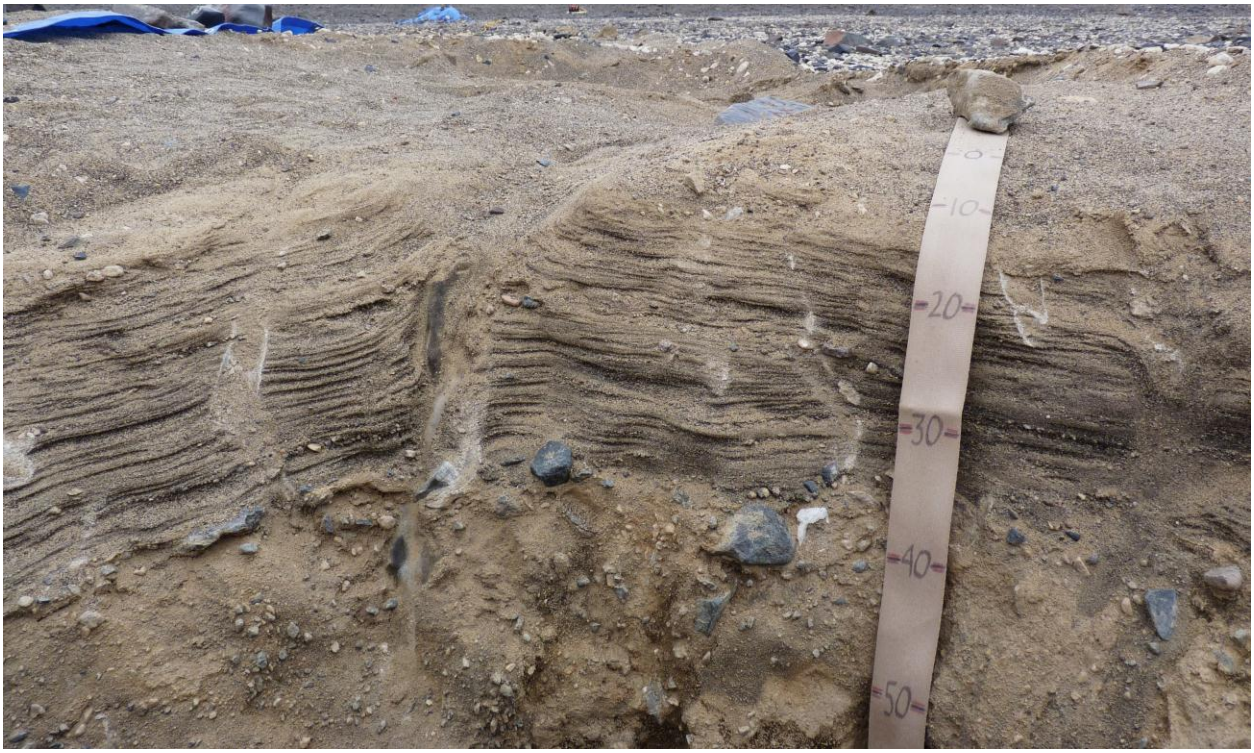

Figure 2.2. Sand-gravel couplets of Jason Fan alluvium. Planar-bedded sands (ice-cemented) overlying Miocene-aged tills, with a buried pavement sharply marking the contact. An active sand-wedge is seen in the center of the photo (3 cm wide, just to right of dark percussion mark), crosscutting alluvial deposits.

Paleohydraulic reconstruction estimates based on maximum clast size indicates flow velocities as fast as 1.46 m/s and as slow as 1.14 m/s during deposition of the Jason Fan. Based on four samples, velocity generally decreases from the head of the fan toward the toe. Estimates of flow depth range from 10.7 cm at the deepest, to 7.4 cm at the shallowest. Since these depth estimates are based on the velocities from above, they follow the same pattern of decreasing values from the head of the fan towards the toe.

Figure 2.3. Image of pit FZE-11-02. A relict sand wedge cross-cuts alluvial deposits and till.

2.3.2. Aeolus Fan

The thickest deposits of the Aeolus Fan are at its head where they reach a depth of 50 cm. Deposits thin laterally until they sharply terminate at the fan's edge. Along the length of the fan they quickly thin below the head, maintaining a thickness of about 5 cm over the lower 200 m of the 370-m-long fan, until feathering out at the toe.

Sediments of the Aeolus Fan are derived from sandstone with a small portion of dolerite intermixed. Fan sediments are poorly sorted, gravelly sand, being on average 20% gravel, 77.5%

sand, and 2.5% silt and clay. The overall mean grain size of fan sediment is coarse sand. Gravel clasts are subangular to subrounded sandstone and dolerite derived from the catchment bedrock. The sediments weather to a very pale brown color (10YR 8/3). The alluvium is capped by a gravel pavement one clast thick. Pavement clasts match those found within the alluvium and have developed a light orange varnish on their northern faces. There is slight evidence of ventifaction on some of the larger pavement clasts. A well-preserved buried pavement identical to that found on the fan surface was found separating two melt-packages along the northern edge of the fan (**Figure 2.4.**). Fan sediments directly overlie a till. The till consists of boulders,

Figure 2.4. Stacked melt-packages along the northern margins of the Aeolus Fan. Upper melt-package is approximately 4 cm thick; lower melt-package is 12 cm thick. A buried pavement marking the upper surface of till is visible at lower right; it includes the buried sandstone cobble. Sediments are wet where ice cement has begun to melt with exposure to sun.

cobbles and gravel of sandstone and dolerite set within a yellow (10YR 7/6), muddy sand matrix. A buried pavement overlying the till sharply marks the boundary between alluvium and till. This till pavement is laterally continuous and covers the ground surface around the fan. The pavement is composed of boulders, cobbles and gravel of sandstone and dolerite that have a well-developed orange varnish and have been intensely ventifacted.

Alluvial beds on the Aeolus Fan accreted as the main channel migrated laterally from south to north at the head of the fan over a distance of 30 m. This trend is also evident in the relative ages of channels at the fan head: abandoned southern channels appear more weathered and subdued than the younger northern ones (**Figure 2.5.**). In total, 4 melt-packages were identified at the head of the fan. Melt-packages ranged in thickness from 5 to 15 cm with each

Figure 2.5. Channels at the head of the Aeolus Fan. Degraded channels on the southern (left) margins indicate that channel migration has proceeded from south to north, causing beds and melt-packages to accrete laterally. Field of view is approximately 65 m across image center. Mature polygonal ground developed on till adjacent to younger polygonal ground on the Aeolus fan. Polygonal ground on the Aeolus fan has less relief and is inconsistently shaped in comparison. The polygons at right are 6-8 m in diameter.

extending laterally as much as 20 m. Beds within melt-packages are thickest near the head of the fan, averaging 5 to 15 cm thick and thinning to 5 cm thick. Beds are made up of poorly sorted, planar-bedded gravelly sand and are evenly graded (**Figure 2.6.**). One bed in the Aeolus Fan was composed of a layer of imbricated cobbles overlying a 15-cm-thick, massively bedded assortment of cobbles and gravel in a sandy matrix (**Figure 2.7.**). This was the only deposit of this nature seen on all of the five study fans. Scattered sand wedges crosscut these alluvial deposits and extend down through the till.

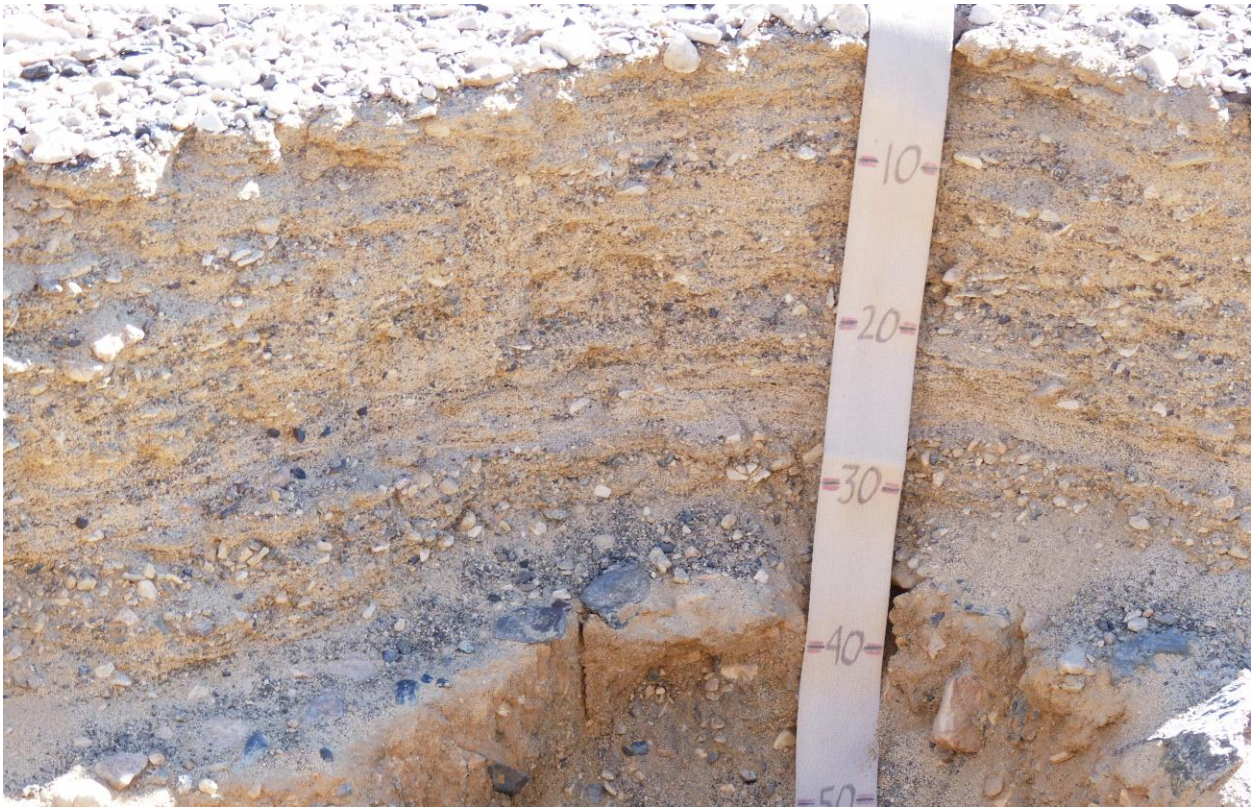

Figure 2.6. Planar-bedded sand at the head of the Aeolus Fan. The underlying till pavement is exposed along the base of the alluvium.

Calculated flow velocities were between 1.35 m/s and 1.02 m/s, based on the maximum clast sizes found within the alluvium. Velocity estimates decrease from the head of the fan toward the toe. Estimates of flow depth range between 3.4 cm and 2.2 cm and also decrease from the head of the fan toward the toe.

Figure 2.7. Set of three stacked melt-packages at the head of the Aeolus Fan. Planar sands overlie a bed of matrix-supported gravel and cobbles (between yellow and brown lines), which overlies planar-bedded sand and fine gravel. These deposits overlie a till (below the orange line). The metal cylinders are 10-cm-wide cores drilled into beds for OSL sampling.

2.3.3. Northern Bull Pass Fan

Deposits of the Northern Bull Pass Fan are a maximum of 40 cm thick, maintaining a similar thickness laterally until abruptly thinning at the fan's edges. Deposits are only 5 to 10 cm thick at the fan toe.

Fan sediments are composed of poorly sorted, gravelly sand made up of granite, dolerite and siltstone. Sediments are, on average, 13% gravel, 85% sand, and 2% silt and clay. The gravel fraction consists of subangular granite with minor amounts of dolerite and siltstone intermixed. Fan sediments weather to a grayish brown (10YR 5/2). A pebble-gravel pavement that is only one-clast thick caps the alluvial sediments. Pavement clasts are identical to those found within the alluvium and show no signs of staining, varnishing or ventifaction. Fans sediments lie directly over till deposits that consist of cobbles and gravel set within a pale olive (5Y 6/4), muddy sand matrix. The boundary between alluvium and till is sharply marked by a buried pavement that is laterally continuous and caps the ground surface surrounding the fan (**Figure 1.6.**). This pavement consists of boulders, cobbles and gravel of granite, dolerite and siltstone that have developed a light orange varnish on their northern faces and have undergone intense ventifaction. Many of the upstanding granite boulders are cavernously weathered.

No buried fan pavements, contrasts in sediment color, or erosional surfaces were identified in any of the excavations, suggesting that only one melt-package was observed. In the upper portion of the fan beds in this single melt-package are between 10 and 15 cm thick. Beds thin to 5 cm, on average, toward the toe of the fan. These beds are composed of poorly sorted, planar-bedded sands with a 1-3 cm thin gravel layer along the base (**Figure 2.8.**). These sand-over-gravel couplets were repeated in 4 individual beds. Beds become coarser and more poorly bedded with distance down the fan. One sand wedge, 2 cm wide, was observed at the base of the fan crosscutting all of these alluvial deposits and extending down into the till (**Figure 2.9.**).

Paleohydraulic reconstruction indicates flow velocities of 1.1 m/s and flow depths of 3.3 cm. These estimates are based off of only two samples that came from adjacent locations on the upper portion of the fan.

Figure 2.8. Image of pit FZE-11-48. Planar-bedded sands with thin gravel couplets (ice-cemented) in the central portion of the Northern Bull Pass Fan. Hammer is 20 cm wide for scale.

Figure 2.9. Image of pit FZE-11-30. A thin sand wedge crosscuts alluvial deposits near the toe of the Northern Bull Pass Fan. Canvas sign is 30 cm wide for scale.

2.3.4. Southern Bull Pass Fan

Excavations in the Southern Bull Pass Fan were limited to the toe of the fan. During a single site visit depth measurements or observations of basal contacts were not undertaken.

Southern Bull Pass Fan sediments are composed of granite, dolerite, and siltstone. Fan sediments are poorly sorted, gravelly sands. On average, sediments are 9% gravel, 88% sand, and 3% silt and clay. The gravel fraction is composed of subangular to subrounded clasts of granite, dolerite, and siltstone. Sediments weather to a brown color (10YR 5/3). Fan sediments are capped by a gravel pavement that is one clast thick, which is composed of clasts identical to those found within the alluvium. Fan pavement clasts show only limited varnish development and minimal ventifaction. An identical buried fan pavement was found at a depth of 10 cm separating planar-bedded, moderately sorted sands from poorly bedded, gravely sand below. The till surrounding the fan is capped by a pavement composed of boulders, cobbles and gravel of granite, dolerite, and siltstone. Granite and dolerite clasts have developed a light orange varnish on their northern faces and all clasts have been intensely ventifacted with some granite boulders being hollowed from cavernous weathering. It is assumed this pavement extends beneath the fan.

Individual beds within the single observed near-surface melt-package are made up of planar-bedded, gravelly sands. Beds are comprised of a 2 to 4 cm thick basal gravel layer overlain by planar-bedded sands 5 to 15 cm thick (**Figure 2.10.**). Excluding the buried pavement observed in one pit, no contrasts in color or erosional surfaces were found to suggest that a sequence of melt-packages had been revealed.

Figure 2.10. Image of pit FZE-11-58. Bedded alluvium near the toe of the Southern Bull Pass Fan. Planar-bedded sands overlie thin basal gravel layers, forming three couplets. The canvas sign is 30 cm wide for scale.

Estimates of flow velocities range between 1.4 m/s and 1.1 m/s. Flow depth estimates range from 8.6 cm at the deepest, to 5.8 cm at the shallowest. These estimates all come from clasts sampled near the toe of the fan.

2.3.5. Upper Wright Fan

The Upper Wright Fan was only visited on one occasion. Measurement of fan thickness and observations of basal contacts were not undertaken. Samples come from four pits located across the fan. Samples from these four pits show that the Upper Wright Fan is comprised of sandstone with smaller portions of dolerite intermixed. Fan sediments are, on average, 21% gravel, 77% sand, and 2% silt and clay. Sediments are poorly sorted, with an overall mean grain size of coarse sand. The gravel fraction consists of subangular to subrounded clasts of sandstone and dolerite derived from the catchment bedrock. Fan sediments weather to a very pale brown

color (10YR 7/3). A gravel pavement, one clast thick, caps fan sediments. Pavements clasts are identical to those found within the alluvium. Fan pavement clasts have developed a light orange varnish on their northern faces and show signs of slight ventifaction. A pavement of boulders, cobbles and gravel comprised of sandstone and dolerite surrounds the fan (**Figure 1.8.**). These pavement clasts have a well-developed orange varnish and have undergone intense ventifaction. This pavement overlies a glacial erosional surface previously described by Lewis et al. (2006). The border between the fan pavement and the pavement of the erosional surface is sharp.

The shallow ice-cement table prevented excavating deep enough to expose the full thickness of a melt-package or any possible contacts between them. With no horizons visible in the shallow excavations, it is likely that only a single, near-surface melt-package was exposed. Individual beds in the package are composed of planar-bedded gravelly sands (**Figure 2.11.**). The beds consist of layers of planar sands with interbeds of gravel 1 to 2 cm thick.

Figure 2.11. Image of pit FZE-11-62. Planar-bedded sands near the toe of the Upper Wright fan. The rough surface in foreground is a shallow ice-cement table at the time of the excavation. Field of view is 20 cm across image center.

Paleohydraulic reconstruction estimates flow velocities between 1.2 m/s and 1.0 m/s. Flow depth estimates range between 3.4 cm and 2.7 cm. Estimates of flow velocity and flow depth decrease from the head of the fan toward the toe.

2.4. Discussion

2.4.1. Sedimentology and stratigraphy

Based on observations from the five study fans, high-elevation alluvial fan deposits in the McMurdo Dry Valleys consist primarily of poorly sorted, planar-bedded gravelly sand. The average grain size of fan deposits is medium- to coarse-grained sand. This bedding and grain size distribution is characteristic of sheetflooding over fan surfaces (Bull, 1962; Wells & Harvey, 1984; Blair, 1987; Blair & McPherson, 1994). The thin gravel layers seen between planar-bedded sands correspond to brief surges in streamflow (Blair & Harvey, 1984). Given that they always rest at the base of the bed, below the typically thicker sequences of planar-bedded sand, these surges must happen during the initial stages of a melt event. The one instance of massive gravelly sand overlain by imbricated cobbles at the head of the Aeolus Fan suggests deposition from a dilute debris flow (Blair & Harvey, 1984). It should be noted that this fan has the steepest channel of the five studied probably making debris flows more likely. The prevalence of deposits corresponding to sheetflooding suggests this is the dominant depositional process on these alluvial fans.

The sedimentary structures observed in these deposits can be directly related to the channel morphology at the fan surface. As channels emerge onto the fan surface they transform from a single, deep channel to a network of shallow, braided channels often partially directed down the surface troughs of thermal contraction polygons (**Figure 2.5.**). These channels are only centimeters deep, quickly allowing flows to become unconfined and deposit the observed

sheets of sand and gravel. On all the study fans the average grain size generally decreased from the head toward the toe, reflecting loss of hydrologic competence as flows progressed down the fan. No lobate, mud-rich or clast supported deposits that might indicate debris flows were observed on any of the five study fans other than the one instance on the Aeolus Fan.

Stratigraphic relationships between alluvial deposits on a given fan were often difficult to interpret. Only melt-packages near the head of the Aeolus Fan were easily placed in stratigraphic order since these accreted laterally from south to north. Elsewhere, aggradation followed the random avulsion patterns characteristic of alluvial fans, producing a more erratic distribution of deposits (e.g. Blair and McPherson, 1994). The prevalence of planar-bedded sands and the resultant topographic smoothness inhibited visual identification of stratigraphic contacts on the fan surface. This made it difficult to efficiently site excavations containing multiple melt-packages and place them in stratigraphic order based on their geographic arrangement. However, stratigraphic contacts might still exist in the regions between individual excavations. With this possibility in mind, samples were collected for future absolute age dating, the results of which will allow placing melt-packages in their proper stratigraphic order. Despite the difficulties of determining stratigraphic order of individual melt-packages, excavations frequently revealed a series of individual beds in a single melt package. In this case, each bed indicates a single melt-event within the range of time represented by that particular package, serving as evidence for multiple meltwater flows during a period of climatic warmth.

The Jason and Aeolus Fans directly overlie wet-based glacial till from the mid-Miocene (Lewis et al., 2007). The Upper Wright Fan is deposited on the southern edge of a glacial erosion surface at least 12.4 Ma old (Lewis et al., 2006). Although no excavations on the Southern Bull Fan extended beneath fan deposits, it can be assumed that wet-based glacial tills

would also underlie them given their presence surrounding the fans and the glacial history of the Bull Pass region (Calkin, 1964).

2.4.2. Paleohydrology

Velocity reconstructions show that, on average, fan-forming flows travel between 1.1 and 1.3 m/s as they emerge from the channel at the fan head. Velocity estimates are higher near the head of the fan and decrease toward the toe of the fan. This reaffirms the loss of hydrologic competence inferred from the down-fan decrease of grain size discussed above. As the flow moves over the shallower slopes of the fan, velocity decreases depositing the largest clasts first followed by progressively smaller clasts as it nears the toe.

Flow velocity estimates on any given fan fall within a narrow range. This suggests that all flows behaved similarly as they reached the fan head. Velocity estimates across all the fans are between 1.0 m/s to 1.4 m/s, suggesting that fan-forming flows are consistently slow.

All flows during fan activation were relatively shallow. Depth estimates across all the fans ranged from 2 cm deep to 10 cm deep. Like velocity, depth estimates on a given fan fall within a narrow range that suggests all flows were of similar discharges. The difference between fans with slower, deeper flows and those with faster, shallower flows can be explained by the differences in their catchments. Fans with gently sloped catchments require deeper flows to reach the velocities necessary to carry similarly sized clasts transported in steeper catchments. The fans that have shallower slopes have larger meltwater sources that allow them to produce larger volumes of meltwater and deeper flows necessary to transport the observed clast sizes.

Paleohydraulic reconstruction suggests that fans form from slow, shallow flows. The narrow range of estimates of velocity and depth across the five study fans suggests that all fan-forming flow occur under this low discharge hydrologic regime. Discharge measurements of

comparable-sized, active meltwater streams in the Fryxell Basin display similarly low discharges (von Guerard et al., 1994; Conovitz et al., 1998).

2.5. Summary

High-elevation alluvial fan deposits in the Dry Valleys are made up almost entirely of planar beds of poorly sorted gravelly sand only tens of centimeters to centimeters thick. Deposits of this type are associated with sheetflooding as flows emerge from the main channel onto the fan surface. Fan aggradation results from consistently slow, shallow discharges of meltwater similar to modern streams near the coast. There is little evidence to suggest that high-discharge flows are the dominant mode of fan aggradation in the Dry Valleys, which is in sharp contrast to fan-building processes in regions in temperate latitudes. These deposits lie directly over regionally extensive surfaces that date back to the Miocene, making alluvial fan deposits some of the youngest in the Dry Valleys.

CHAPTER 3. GEOSPATIAL ANALYSIS

3.1. Purpose

Alluvial fans are found throughout the Dry Valleys. Each fan catchment has a unique morphology that, along with geographic location, influences how and when meltwater is produced, leading to fan aggradation. An understanding of relationships between these geographic attributes and fan activity provides a more detailed portrayal of past meltwater generation, which in turn leads to a better understanding of melting along margins of the EAIS. This chapter will examine how differences in location and catchment morphology affect fan activity. First, previous work detailing the spatial variability of meltwater generation in the Dry Valleys, as it pertains to fan activity, is reviewed. Following that, geographic information systems (GIS) are used to develop a detailed summary of geographic attributes for each fan system. Statistical analysis is then used to identify which relationships between these attributes and fan activity are most important.

3.2. Previous work addressing spatial variability of geomorphic processes

Much work has been done to describe the spatial variability of geomorphic processes in the Dry Valleys. Most studies conclude that the availability of water is the main control. Marchant and Head (2007), for example, identified three microclimate zones in the Dry Valleys based on observations of summertime atmospheric temperature, soil moisture, and relative humidity. Their coastal zone shows the greatest water availability and therefore the highest level geomorphic activity including fluvial erosion, gullying on slopes, growth of polygonal patterned ground, and evidence for in-situ rock weathering. Inland and at increased elevations water availability decreases in parallel with evidence for geomorphic activity, defining an intermediate zone. Their upland zone, at high elevations adjacent to the EAIS, shows the least water

availability and therefore the least geomorphic activity. This general trend of geomorphic activity decreasing with reduced water availability, and how this is in turn related to increasing elevation and distance from the coast, provides the background of how meltwater generation and fan aggradation takes place in the Dry Valleys.

3.3. Meltwater sources

Soil temperature measurements indicate that melting at the ice-cement table is uncommon and does not contribute significantly to surface water. At high elevations adjacent to the ice sheet, soil temperatures remain below -10° C throughout the year at depths of 50 cm and below 0° C at depths down to about 10 cm (Kowalewski et al., 2006). Given typical ice-cement table depths of 30 to 100 cm, sublimation is the only process by which water leaves the soil.

Precipitation does not directly contribute to runoff from watersheds in the Dry Valleys. Almost all precipitation falls as snow. It typically sublimates away without any significant contribution to surface meltwater (Chinn, 1981). Where meltwater does form after snowfalls, it infiltrates the soil to shallow depths and then later evaporates or sublimates. Salt-encrusted rocks, salt efflorescence in soil layers, and distinct salt pans as much as 15 cm thick indicate that evaporation and sublimation exceed infiltration in almost all regions of the Dry Valleys (Campbell et al., 1998; Campbell and Claridge, 2006; Bockheim, 1997). The lack of runoff means that the direct relationship of watershed area to fan area (e.g. Bull, 1977; Silva et al., 1992), as is typical in mid- and low latitude watersheds, does not apply in the Dry Valleys.

The vast majority of surface meltwater in Dry Valleys hydrologic systems originates from alpine glaciers and perennial snowbanks (Conovitz et al., 1998). Alpine glaciers are situated sporadically along the high-elevation crests of the mountain ranges that divide the Dry Valleys. Since meltwater originates from spatially limited glaciers and snowbanks, a direct

relationship between watershed area and fan area does not apply to these catchments. Moreover, meltwater is not generated at all from some regions of a glacier. Rather, meltwater is only generated in the lower region of a glacier, known as the ablation zone. The boundary between the ablation zone and the accumulation zone (the region of the glacier where precipitation exceeds sublimation and melting) is known as the equilibrium line altitude (ELA). In order to examine how effectively the size of the ablation zone explains meltwater generation in Dry Valleys streams, Bomblies (1998) compared glacier area beneath the ELA to the net meltwater generated over a given melt-season across several glacier-fed streams in Taylor Valley. His results showed that some correlation exists between the ablative area of glaciers and net stream discharge, which is related to fan area. However, his relatively weak correlations (R^2=0.6) suggest that there are still unaccounted variables affecting flow.

In addition to melt from scattered glaciers, meltwater contributing to fan formation also originates from permanent snowbanks and snow collected in topographic lows such as bedrock alcoves, stream channels, and polygon troughs (Dickson et al., 2007; Head et al., 2007). The size of these water sources is highly variable. Snow collected in alcoves ranges in surface area from thousands to less than one hundred m^2. For channels, the amount of water stored varies with width, which can range from 1 m to 20 m, and with length, which can be from several kilometers to only several hundred meters (Fountain et al., 1999c). For several fans in this study perennial snowbanks and snow collected in topographic lows represents the only source of meltwater. In catchments with other meltwater sources, snow in channels is critically important because it primes the dry streambed by saturating the hyporheic zone in order for channel flow to take place (Dickson et al., 2007). Intermittent flows can occur throughout the melt-season so long as snow continues to accumulate in these sheltered topographic lows (Morgan et al., 2007).

An important control on meltwater production from glaciers and snowbanks is the balance between melting and sublimation in the glacier ablation zone. In the Dry Valleys, sublimation typically accounts for 70-90% of total glacier ablation compared to only 15-30% from melting (Bull & Carnein, 1970; Lewis et al, 1995). The balance between melting and sublimation, however, changes from year to year. At Canada Glacier in Taylor Valley, the portion of ablation due to sublimation fluctuated from 80% during the summer of 1994-1995 to only 40% during the summer of 1995-1996 (Lewis et al., 1998). The balance between melting and sublimation also varies significantly across the profile of the glacier. In the Dry Valleys most glaciers terminate at vertical cliffs as much as 130 m high. These vertical ice cliffs are exposed to more direct incidence of solar radiation because of the high latitude. They also gather reflected long wave radiation from surrounding surfaces, and are sheltered from local winds, which subdues sublimation (Lewis et al., 1999). This unusual geometry means that ablation from melting is 5-10 times greater at the glacier terminus than the horizontal surface of the glacier (Fountain et al., 1998a; Lewis et al., 1999). Because of this, glacier termini are responsible for a disproportionately large portion of streamflow, despite their small area relative to the total area of the glacier ablation zone (Lewis et al., 1999).

The balance between melting and sublimation varies with geographic location in the Dry Valleys. Katabatic wind patterns are a major control. These winds are density-driven flows that fall off of the ice sheet and are funneled through valleys toward the coast. Speeds are highest in the western Dry Valleys where winds leave the smooth ice sheet and enter the east-west troughs (Bromley, 1985). Katabatic winds warm adiabatically as they flow down slope. This means that temperatures along valley floors can be higher near the EAIS than at the Ross Sea coast (Bromley, 1985; Doran et al., 2002). The rise in temperatures lowers relative humidity making

the air more evaporative, which, along with increased sublimation from higher wind speeds, results in a significant increase in sublimation up-valley (Lewis et al., 1998). This produces increasingly small glaciers (and in turn, smaller ablation zones) and more scattered glaciers up-valley. Many catchments in the western portions of the Dry Valleys hold only permanent snow patches. The glaciers that do exist terminate on high-elevation slopes rather than valley floors. At high elevation summer temperatures are usually far below the melting point (Doran et al., 2002) meaning that almost all ablation of these glaciers is by sublimation. Melting takes place on these high-elevation glaciers and snow banks but only along margins where the low albedo of rocky surfaces aids melting. As it pertains to fan aggradation, these climatic trends affect the volume of meltwater produced by limiting the size of melt sources and affecting the balance between ablation due to melting versus sublimation. This east-to-west climatic gradient must be accounted for when considering meltwater generation and alluvial fans in the Dry Valleys.

Incoming solar radiation is another important control of meltwater production in the Dry Valleys (Dana et al., 1998). Discharge measurements from alpine glaciers coincide with periods of high solar radiation on weekly, daily and hourly time scales (Moorhead & McKnight, 1998; Conovitz et al., 1998). Ebnet et al. (2005) showed that aspect of glacial surfaces relative to incoming solar radiation is a contributing variable. Aspect enhances glacier streamflow models in Taylor Valley, with north-facing glaciers receiving higher amounts of solar radiation resulting in larger volumes of meltwater.

No single variable completely explains the generation of meltwater in the Dry Valleys. Multiple variables must be accounted for in order to accurately portray the complex processes governing melting, and by extension fan aggradation, in the Dry Valleys.

3.4. GIS analysis

Geographic attributes were identified and delineated in ArcMap 10.1 with the Spatial Analyst 10.1 extension. Features were created using the Lambert Conformal Conic projection and the WGS 1984 USGS Transantarctic Mountains coordinate system. Statistical analyses were done in SAS Enterprise Guide 4.3.

3.4.1. Fan identification and digitization

I identified 27 alluvial fans scattered throughout Dry Valleys, between the coast and the margins of the EAIS (**Figure 1.3.**). These features were identified using 0.5 m resolution panchromatic imagery from the Worldview 1 satellite and 2.4 m resolution multiband imagery from the Quickbird 2 satellite collected between October 2008 and February 2011. I digitized the alluvial fans, the glaciers and snowbanks in their catchment that could contribute meltwater, and the stream channels that connect them. Glacier and stream channel shapefiles were joined with preexisting shapefiles developed by the McMurdo Dry Valleys Long Term Ecological Research (MCMLTER) group and from the GPS data gathered during the field season. Geometric attributes of the digitized shapefiles were created using the area and length calculators in ArcGIS.

3.4.2. Attribute selection and delineation

Because stream flow on these fans has never been measured, and in most cases never been observed, I used fan area as a measure of the overall activity. As previously discussed, fan area is frequently compared to the size of the watershed due to its dependence on hydrologic inputs (e.g. Bull, 1977; Silva et al., 1992). Fans were identified by their distinctive shapes, and by the color of their fresh sediments and smooth surfaces relative to surrounding till and bedrock.

Attributes for integration in the GIS analysis were selected based on factors that control meltwater generation in the Dry Valleys as discussed above in section 3.2. Glacier area beneath the ELA, large snow patches accumulated in topographic lows and alcoves, and the length of stream channels were selected as the variables encompassing the physical watershed. The geographic attributes of each fan used in the GIS analysis are reported in Appendix E.

The ELA of each glacier, where applicable, was determined by carefully examining the shape of elevation contours across the surface of the source glacier. The contour shapefile was digitized by MCMLTER from a series of 1977 USGS quadrangles with 50m contour intervals. In the accumulation zone, elevation contours are concave downslope, whereas contours in the ablation zone are convex downslope. The transition from concave to convex contours is the approximate position of the ELA (Porter, 1975; Lenoard et al., 1998) (**Figure 3.1.**). This boundary was used to calculate the area of the glacier below the ELA, where meltwater production is most significant.

The maximum and mean slopes of meltwater channels were calculated to account for their affect on hydrologic competence and channel migration, which would influence the areal extent of the fan. A slope raster was created from a 30 m DEM developed by MCMLTER from 1977 USGS quadrangles of the region. Maximum and mean slope were calculated using the "Zonal Statistics" tool in ArcGIS Spatial Analyst along the length of each fan's meltwater channel.

Distance of the meltwater source from the ocean was determined to capture the geographic changes of ablative processes as made evident by the ELA gradient. This was done using the "Near" tool, which calculated the Euclidean distance between the geographic center of each meltwater source and nearest edge of the Ross Sea.

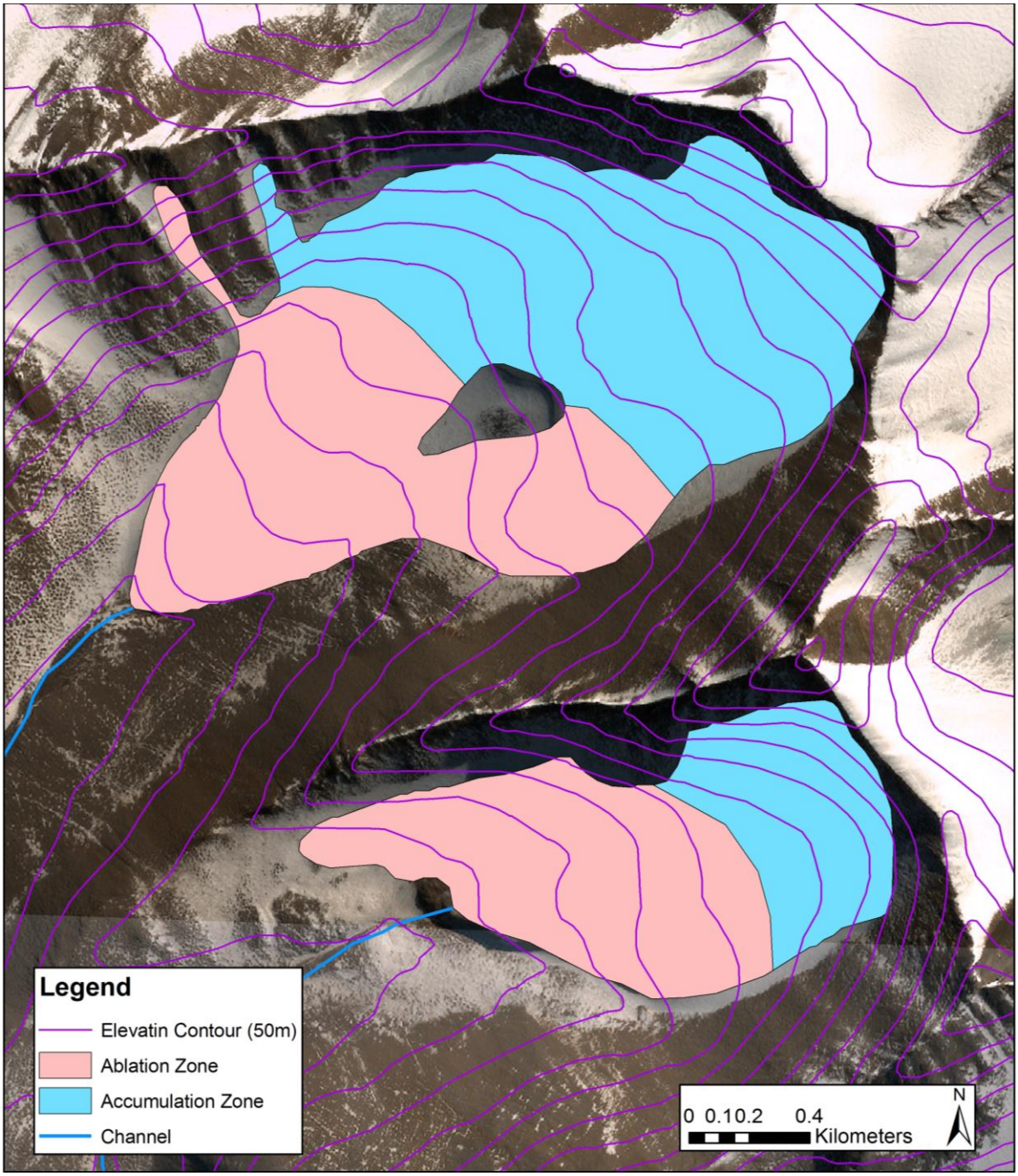

Figure 3.1. ELA position as illustrated by the source glacier of the Mt. Harker Fan. Changes in the shape of the elevation contours mark the boundary between the ablation zone (which is the region of the glacier that does contribute meltwater and the accumulation zone (which does not contribute meltwater).

To account for adiabatic temperature changes that would influence melting, the minimum and mean elevation of each fan's respective meltwater source were calculated. This was done

using the 30 m DEM and the "Zonal Statistics" tool. The defined zones were glacier area below ELA and snowbanks present in each fan catchment.

The same DEM was used to model the direct solar radiation over each respective meltwater source using the "Solar Radiation" tool in ArcGIS Spatial Analyst. Direct solar radiation was calculated in 1-hour intervals using sky sector maps that were recalculated at 1-day intervals. Solar radiation was calculated between December 1st and January 30th, which corresponds to the time of peak discharge in the Dry Valleys (Moorhead & McKnight, 1998). For this time span, the mean direct solar radiation per unit area and the net direct solar radiation were calculated for each fan's respective meltwater source using the "Zonal Statistics" tool.

3.5. Results

Linear regression analyses reveal generally weak correlations, as expressed in R^2 values, between fan area and geographic attributes of the catchment (**Table 3.1.**).

Table 3.1. Results of linear regression analysis of fan area and geographic attributes

Attribute	**R^2**	**R^2 (excluding Mt. Harker)**	**R^2 (Glaciers)[1]**	**R^2(Snow)[2]**
Source Area	0.13	0.01	0.09	0.01
Channel Length	0.36	0.10	0.63	0.00
Channel Slope (Max.)	0.02	0.08	0.04	0.03
Channel Slope (Mean)	0.08	0.00	0.17	0.09
Distance from Sea	0.19	0.34	0.15	0.31
Elevation (Min.)	0.11	0.01	0.20	0.06
Elevation (Mean)	0.09	0.01	0.28	0.08
Mean Direct Rad. per unit area	0.04	0.06	0.05	0.00
Net Direct Radiation	0.09	0.01	0.05	0.01

[1]The dataset used in this iteration was limited to those fans that have glaciers as part of their meltwater source.

[2]The dataset used in this iteration was limited to those fans with meltwater sources that are entirely made up of snow.

Linear regression analysis of all 27 study fans suggest that the variables that explain the variance of fan area best are channel length, followed by distance from the ocean. In an effort to improve correlation, the Mt. Harker Fan was removed from the data set and the linear regression analysis was rerun. In this iteration, fan area and distance from the Ross Sea were best correlated, with a considerably higher R^2 value, but the correlation between fan area and channel length decreased dramatically (**Table 3.1.**). There was little or no change in the correlation of the other attributes. It is worth noting that the Mt. Harker Fan is over an order of magnitude larger than many of the smaller fans and is over three times bigger than the next largest fan. This fan also coalesces with fans fed by other source glaciers to form an extensive bajada that is unique in the Dry Valleys. More detailed study of these fans may reveal unique meteorological processes at this location that result in more frequent fan aggradation.

Observing the change in the primary meltwater source with distance from the sea reveals an interesting trend. From the sea towards the margin of the EAIS, the primary meltwater source of fans shifts from being predominantly glacial, to entirely snow (**Figure 3.2.**). In order to test whether or not geographic attributes affect these types of meltwater sources differently, linear regression analysis were performed on fans based on the type of meltwater source in the catchment.

The linear regression analysis of fans fed by glacial meltwater indicates fan area is best explained by channel length, followed by the mean elevation of the glacier (**Table 3.1.**). With the exclusion of the Mt. Harker Fan, distance from the Ross Sea became the most relevant variable (R^2=0.37) followed by channel length (R^2=0.27). For fans fed entirely by snowmelt, the distance from the Ross Sea is the only relevant variable explaining the variance of fan area (**Table 3.1.**).

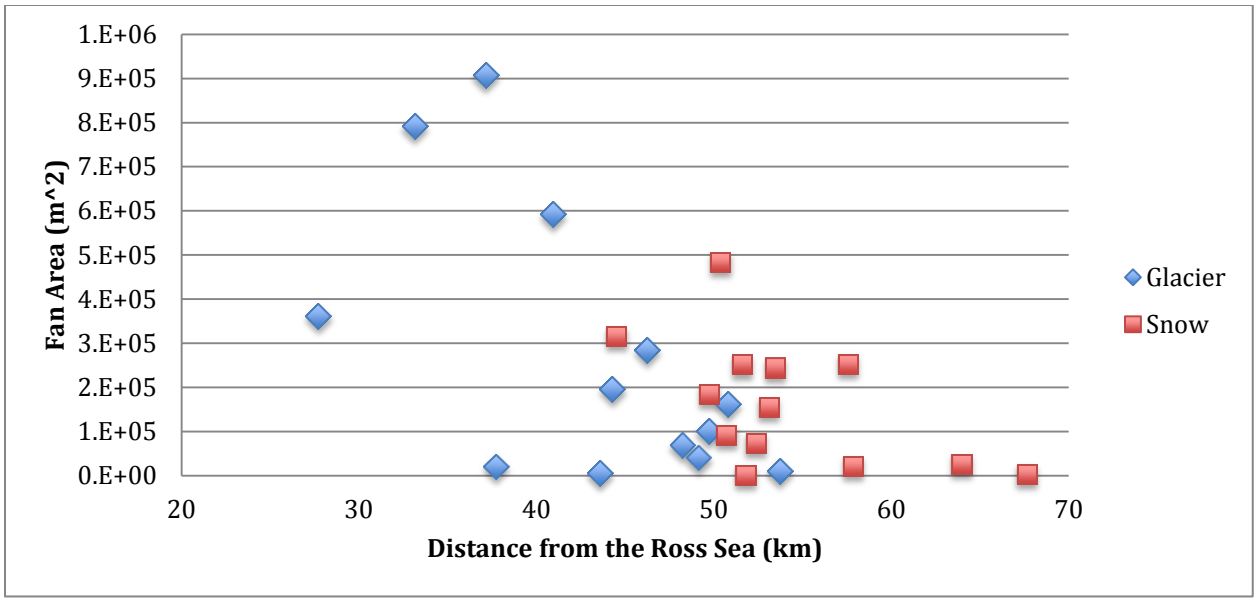

Figure 3.2. Comparison of distance from the Ross Sea and fan area. The type of the meltwater source changes with distance from the Ross Sea. The graph does not include the Mt. Harker Fan.

Multiple linear regression analyses utilizing the entire dataset revealed that no combination of catchment attributes is strongly correlated to fan area, with R^2 values never exceeding 0.36. The three combinations with the highest correlations all include channel length as a variable (the three combinations with highest R^2 are given in **Table 3.2.**). The strongest combination was channel length and the distance of the meltwater source from the Ross Sea. Given the limited sample size, multiple linear regression analyses were not rerun on the basis of the type of meltwater source.

Table 3.2. Highest correlated results of multiple linear regression analysis.

Attributes	**R^2**	**VIF**
Channel Length + Dist. Ross Sea	0.36	1.16
Channel Length + Mean Source Elevation	0.33	1.09
Channel Length + Mean Channel Slope	0.33	1.68

3.6. Discussion

Results of linear regression analyses suggest that the length of the meltwater channel and the distance of the meltwater source from the Ross Sea are the most significant variables

controlling fan area. However, the correlation of channel length is drastically diminished when the Mt. Harker Fan is excluded from the data set, whereas the correlation of distance from the Ross Sea is considerably improved. Results of multiple linear regression models of the entire data set reaffirm the importance of both channel length and the distance of the meltwater source from the Ross Sea in controlling fan area. Multiple linear regression models also suggest mean elevation of the meltwater source or the mean channel slope could also influence fan area.

There are several explanations for the poor correlations drawn from the regression analyses. Primarily, fans are three-dimensional features. Fan area does not necessarily capture the volume of material deposited nor does it capture the total of volume of meltwater generated since its initial deposition. Some fans are deposited on steep surfaces that may cause greater channel migration and produce a more extensive fan relative to fans with similar catchments deposited on gently sloped surfaces. Also, sources of meltwater vary across the fans. While some fans have stable alpine glaciers as the dominant meltwater source, other fans depend entirely on snow cover that changes from year to year. The different melting properties of these sources would affect how melting takes place in a catchment. In a catchment characterized by snow, even when melting conditions are optimal the volume of snow in the catchment may be insufficient to support aggradation. Finally, when the climate warms sufficiently for fan aggradation, the ELA position could shift to higher elevations, expanding the area of ablation zone and, in turn, the physical watershed for fans deposited by glacial meltwater. These complexities weaken the correlations drawn between fan activity and geographic attributes relevant to meltwater generation.

The consistent relationship between fan area and distance from the Ross Sea suggests that climatic gradients along this longitudinal path significantly influence meltwater generation from

high-elevation glaciers and snowbanks. As discussed above in section 3.2.2, these gradients, moving from the Ross Sea up-valley toward the EAIS, include decreased precipitation, increased wind speeds, and increased air temperatures on valley floors. These interact to produce decreased snow accumulation and increased ablation due to sublimation, which restricts regular meltwater production in the western portion of the Dry Valleys compared to the more hydrologically active eastern parts of the region. It has been noted that melting during extremely high-flow years, including some melt at high-elevation sources, was caused by periods of intense, prolonged katabatic winds that pushed air temperature far above freezing, producing large but short-lived pulses of meltwater (Doran et al., 2008). In the western portions of the Dry Valleys, the warming produced from these katabatic wind events could produce pulses of meltwater sufficient for fan aggradation regardless of sublimation. Fan sedimentology, however, suggest that katabatic wind events are not the main control on fan aggradation. Katabatic wind events are frequent occurrences in the Dry Valleys, whereas fan sediments show that fans are constructed from only a few, and possibly only one, melt event.

Based on this analysis, distance from the Ross Sea is the most significant factor controlling fan area, which is used as a proxy for fan activity. This means that a westward (inland) shifting of climatic gradients could explain past aggradation of fans that are today inactive. Climate modeling could show which climate forcing mechanisms and what magnitude of forcing is required to shift these gradients. Estimates for the timing of aggradation, which is addressed in the following chapter, would help correlate these climatic shifts to known changes in regional Antarctic climate forcing. Examples could include changes to heat supplied from surrounding oceans (Volkov et al., 2010) or changes in insolation received at high latitudes from orbital cycles (Huybers and Denton, 2008).

CHAPTER 4. TIMING OF FAN DEPOSITION

4.1. Purpose

In order to identify climate mechanisms responsible for meltwater generation at high elevations in the Dry Valleys, it is necessary to identify when and how frequently fans aggraded. Based on local geologic evidence, the range of possible fan ages is extremely broad. The Dry Valleys have been characterized as a relict landscape, with little geomorphic modification since the climate became cold and dry during the mid-Miocene climate transition (MMCT) 14 Ma ago (Sugden et al., 1999; Lewis et al., 2007). Estimates of erosion rates are extremely low, ranging from 1.0 m Ma^{-1} at relatively wet and warm low-elevation sites to 0.03 m Ma^{-1} at cold and dry high-elevation sites (Schafer et al., 1999; Summerfield et al., 1999; Margerison et al., 2005). Moreover, fragile, unconsolidated ashfall deposits have been preserved at the ground surface for millions of years (Marchant et al., 1993; Lewis et al., 2006, 2007). This stability means that some fans could be relict features millions of years old.

Regardless of their age, compared to the majority of the landscape fans stand out as one of the few landscape features indicative of geomorphic change. Their presence indicates that significant volumes of meltwater have been generated in high-elevation catchments. Fans represent one or multiple departures from the dominant, cold climate regime that has characterized the region since the MMCT. Are these fans relict features, nearly as old as the Miocene-aged tills they rest on, or are they relatively young? Have fans aggraded sporadically since the mid-Miocene? Or, have they aggraded at consistent intervals, corresponding to a cyclical pattern of climate warming? Or, was fan aggradation limited to a single climate-warming event? To answer these questions the timing of fan aggradation must be determined.

This could allow correlation to specific climate-forcing mechanisms and help better characterize the causes of melting along margins of the EAIS.

This study uses stratigraphic relationships, geomorphic observations, and absolute dating of fans to develop a mixed chronologic framework of fan aggradation. Stratigraphic relationships come from field analyses of fan sediments reported in chapter two. This provides maximum age constraints for fans in the Dry Valleys. Geomorphic indicators of age come from rates at which fan surfaces change following alluvial deposition. Lastly, a preliminary numerical chronology is presented for the timing of the most recent depositional events using optically stimulated luminescence (OSL) dating.

4.2. Stratigraphic relationships

As previously discussed in Chapter 2, the Jason and Aeolus Fans overlie mapped wet-based tills (Lewis et al., 2007, 2008). The contact between fan alluvium and till is identified by a buried pavement of varnished and wind-eroded boulders and cobbles. The age of the till is 13.85 Ma based on Ar-Ar dating of ash deposits (Lewis et al., 2007). The Upper Wright Fan rests on the southern edge of a glacial erosion surface that is at least 12.4 Ma old based on Ar-Ar dating of ash deposits on the surface (Lewis et al., 2006). In both of these cases fans overlie, and are therefore younger than, the dated till and erosion surface. Based on these simple stratigraphic relationships, the Jason and Aeolus Fans can be no older than 13.85 Ma; the Upper Wright Fan has a maximum possible age of 12.4 Ma.

4.3. Relative age based on geomorphic observations

4.3.1. Desert pavements

Desert pavements are characterized as a continuous mantle of flat-lying, densely packed clasts overlying a layer of silt or sand filled with gas vesicles (Quade, 2001; Bockheim, 2010).

Pavements are common features of arid environments and characterize most non-ice surfaces in the Dry Valleys. Five hypotheses have been advanced explaining their formation: (i) deflation, (ii) overland flow, (iii) upward migration of clasts, (iv) *in situ* formation from dust deposition, and (v) physical and/or chemical weathering (Bockheim, 2010). Excluding overland flow each of these, alone or in combination, could be responsible for pavement formation in the Dry Valleys. Pavements indicate prolonged periods of surface stability, making them useful in assigning relative ages to surfaces (Cooke, 1970; Quade, 2001).

Desert pavements are present on all of the study fans and on the surrounding landscape as reported in Chapter 2. Fan surface pavements were likely created by an initial deflationary period, during which unprotected sand and silt was winnowed away leaving a gravel lag. This may have been followed by later modification from either freeze-thaw cycles or from *in situ* deposition of eolian dust, as suggested by the interlocking of fan pavement clasts. Similarly, the till pavement also experienced an initial deflationary period. However, boulder-sized material of the till pavement has remained as a lag, while cobble and gravel-sized clasts were further modified into an interlocking arrangement by freeze-thaw cycles or *in situ* by the addition of eolian dust.

Buried pavements on till surfaces represent a long period of surface stability prior to fan deposition (Bockheim, 2010). Some pavements encountered in excavations were relatively sturdy and could be easily exposed by gently bushing aside overlying layers of alluvium. Tracing this pavement laterally reveals that it is the buried continuation of the surrounding till pavement (**Figures 2.1.**). The identical appearances of pavements on till surfaces and those that are buried beneath alluvium suggest that fans have been constructed recently relative to the age of underlying tills. On the Aeolus Fan, a buried pavement identical in physical appearance to the

modern fan pavement was exposed at 5 cm depth (**Figure 2.4.**). This surface also represents a long period of surface stability. The buried fan pavement formed after an episode of deposition, then was itself buried during a subsequent depositional event.

Pavement formational rates permit minimum age estimates to be made for the length of time between till and fan deposition. Pavements form on time scales of 10^2 to 10^3 years (Elvidge & Iverson, 1983) and can remain stable at the surface over scales of 10^4 years (Wells et al., 1995). The prevalence of buried till pavements between till and fan alluvium indicates that centuries to millennia passed between till deposition and the initial deposition of alluvial sediments. Pavement development at the surface of all five study-fans suggests that each is centuries to millennia old. On the Aeolus Fan, the cumulative age of the buried fan pavement and the modern surface pavement suggest an age several centuries or millennia older than those without. Preferential varnishing of the northern face of pavement clasts indicates that fan pavements have been stable. This means that fan deposits are both centuries to millennia in age and that deposition has not taken place for at least as long.

4.3.2. Polygonal patterned ground

Extensive networks of polygonal patterned ground are found in regions of continuous permafrost and are especially common in the Dry Valleys. These polygons develop from fracture of frozen ground brought on by annual temperature fluctuations that cause the ground to expand and contract. (Black & Berg, 1963; McKay et al., 1998; Marchant et al., 2002; Marchant & Head, 2007). Windblown debris and slumped material fill the void created by the fracture, creating an expanding, wedge-shaped deposit of sand with a vertical fabric that extends downward from the ground surface (Marchant et al., 2002; Sletten et al., 2003). The material added at depth results in deformation at the ground surface, usually in the form of two parallel

ridges raised on either side of a central trough. In plan view, sand wedges create a network of linear troughs and ridges that intersect at regular angles, forming polygonal patterned ground. The continued growth of wedges in the subsurface causes increased surface deformation, making polygonal patterned ground appear rougher over time.

Given the continuous annual temperature fluctuations and resulting opening of fractures, wedges are thought to grow at relatively steady rates. In the Dry Valleys Sletten et al. (2003) used the morphology of polygonal ground at different developmental phases in deposits of known ages to estimate developmental timescales. Specifically, polygon maturity is based on diameter, trough depth (which marks the surface expression of the fracture), and the roughness of the ground within polygons. According to their methodology, polygons are relatively large, have shallow troughs, and have a smooth surface throughout the polygon during the *initiation*-phase. In the *developmental* phase, new fractures create smaller and more regularly shaped polygons, troughs are deeper and are bordered by raised edges. Polygon surfaces that have reached the developmental phase also begin to show extensive reworking and abandoned sand-wedges, with only the central portion of the polygon surface remaining undisturbed. The oldest polygons, in the *mature* phase, are the smallest at only 10 to 20 m wide. Polygons become more regular in this phase as the bounding troughs now form triple-junctions at consistent angles. Mature polygons have the deepest troughs and the entire polygon surface has been reworked by the repeated rearrangement of fractures.

Polygonal ground in the initiation phase takes decades to centuries to develop, the developmental phase takes thousands of years to develop, and the mature polygon phase takes as many as a million years to develop (Sletten et al., 2003). Using these criteria, the maturity of polygonal ground overlying fans affords age estimates for the fan deposits. However, it is

important to note that these are minimum age constraints. Polygon development might be retarded due to lack of crack-filling material, insufficient soil-water content to provide cohesive strength to the substrate, or seasonal thermal fluctuations that are insufficient to cause the tensile stresses necessary for fracture.

Sletten et al. (2003) also derived growth rates of sand wedges based on the displacement between stakes on opposite sides of polygon troughs that have been measured over a period of 39 years. According to their work, sand wedges in the initiation phase have an average growth rate of 0.5 to 1 mm/yr while sand wedges in the developmental phase have an average growth rate of 0.2 to 0.3 mm/yr. Sand wedges in the mature phase grew at an average rate of only 0.01 mm/yr.

Polygonal patterned ground is present on all of the study fans. Descriptions of patterned ground are based on direct observation and on visual analysis of air photos and satellite imagery. The diameter and relief of polygons varies from fan to fan. Polygons extend unbroken from fan surfaces to surrounding till. Compared to adjacent till surfaces, polygons developing on alluvial fans have larger diameters and less relief (**Figure 2.5.**). This is consistent with the work of Sletten et al. (2003) as polygons on alluvium should be in an earlier phase compared to those developed on adjacent, older till surfaces.

Polygons on the Northern Bull and Upper Wright Fans were the largest of the study fans and had the least relief. On these fans, polygon diameters range between 20 and 35 m with roughly planar interior surfaces. In contrast, polygons are smaller and show greater relief on the Jason and Aeolus Fans. On these fans, polygons are between 6 and 10 m in diameter with uneven, domed interiors (**Figures 2.5. and 4.1.**). The Southern Bull Fan contains regions of large, low-relief polygons similar to those of the North Bull and Upper Wright Fans, and regions of smaller, high-relief polygons similar to those of the Jason and Aeolus Fans (**Figure 4.2.**).

Figure 4.1. Domed polygons on the Jason Fan. Well-sorted sands in in foreground have been moved by meltwater running down the polygon trough. The canvas sign is 30 cm wide for scale.

Figure 4.2. Differing polygonal ground maturity on the Southern Bull Pass Fan. Recent fan aggradation has buried well-developed polygons in upper and lower left portions of image; older polygons are still visible in the foreground and at upper right. Melt water flows from the lower right to the upper left in the image. Older polygons average 10 m in diameter.

Polygon troughs measured at the Jason and Aeolus Fans range between 10 cm to 20 cm wide and average 5 cm deep. Troughs are filled with sand and fine gravel. In cross-section, these troughs overlie sand wedges that crosscut alluvial and till deposits. Sand wedges were not present in every pit, and none were exposed in excavations of the Southern Bull or Upper Wright Fans. A single, 2 cm wide sand wedge was observed on the Northern Bull Fan (**Figure 2.9.**). Sand wedges observed on the Jason and Aeolus Fans are between 5 cm and 15 cm in width (**Figures 2.2., 2.3., and 4.3.**). Sand wedges on the Jason Fan commonly contained interstitial ice (**Figure 2.2.**). Ripples and small channels can be found within some segments of the polygon troughs of the Jason and Aeolus Fans suggesting that small volumes of meltwater have recently flowed down troughs (**Figure 4.4.**). The interstitial ice found in some sand-wedges likely results from meltwater entering open cracks. On the Jason and Aeolus Fans, relict sand wedges were observed in cross-section where there was no modern expression of a polygon at the surface (**Figures 2.3. and 4.3.**). On the Jason Fan, a relict sand wedge was observed extending downward from the buried till surface, penetrating the buried till, but it did not extend upward into the alluvial deposits (**Figure 4.5.**).

Figure 4.3. Relict sand wedge cross-cutting alluvium on the Aeolus Fan. Sign is 30 cm wide for scale.

Figure 4.4. Image showing evidence of minor flows within polygon troughs. Narrow channel formed in polygon troughs on the Jason Fan suggest small volumes of meltwater have recently flowed down troughs. Sands falling into an open contraction crack have left a faintly visible trace in sands in foreground. Canvas sign is 30 cm wide for scale.

With the visual observations of polygon diameter and relief and the measured width of sand wedges, the developmental phase of polygons on each fan and a rough age of the surface can be assigned. The large polygon size and low relief observed on the Northern Bull and Upper Wright Fans, along with the thin sand wedge observed in cross-section on Northern Bull, suggest that these fans are in the initiation phase of development. The planar surface of both fans indicates minimal reworking of the surface from prolonged deformation. Given the small size and higher relief of polygons on the Jason and Aeolus Fans, along with the width of wedges, polygonal ground on these fans is in its developmental phase. This is reaffirmed by the uneven surface between polygons and the presence of relict sand wedges, indicating prolonged deformation as older polygons are abandoned and new ones develop. The polygonal ground on

the Southern Bull Fan can be separated into distinct regions in the initiation phase and the developmental phase. The presence of both polygon ground types on the Southern Bull Fan implies the surface has two separate ages.

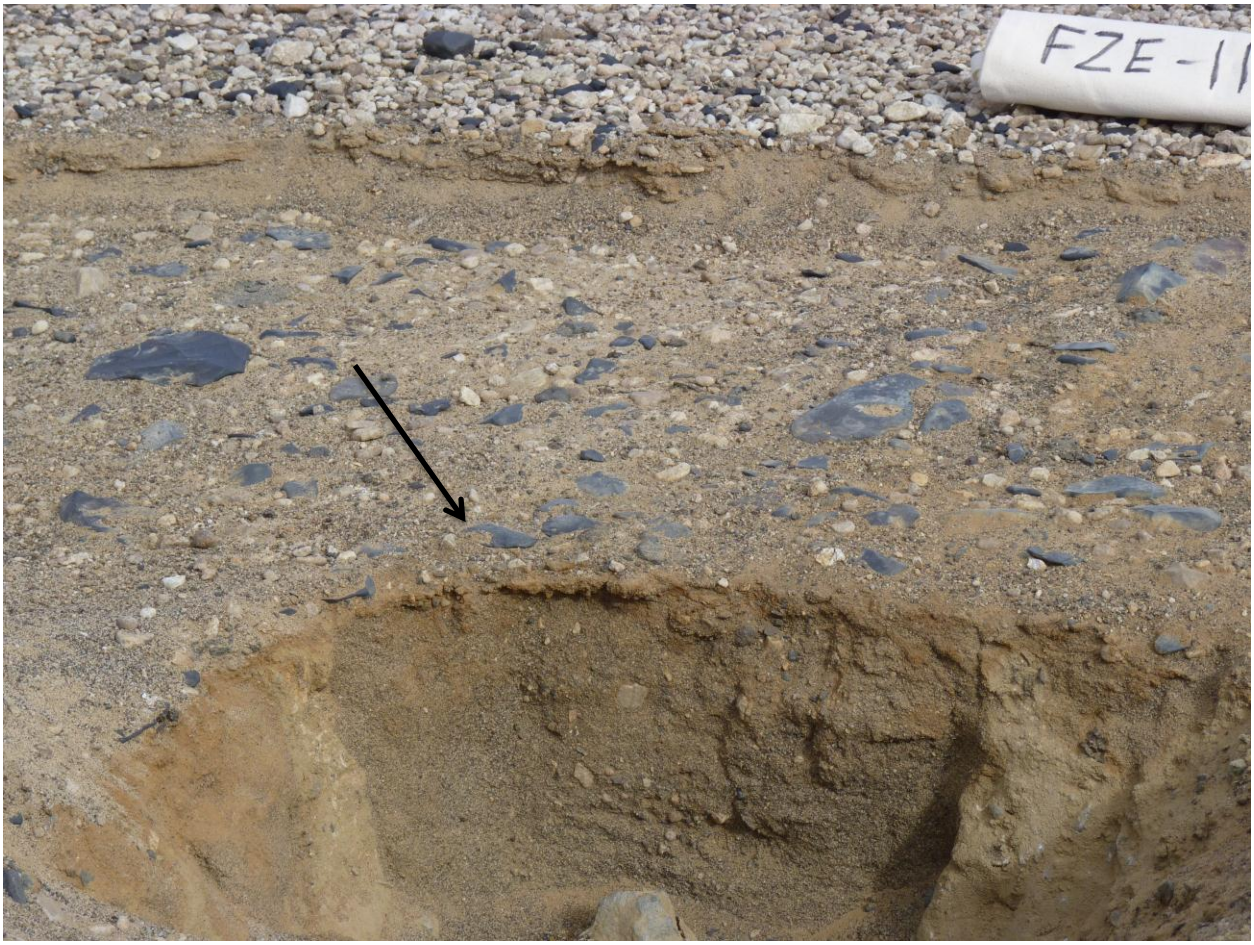

Figure 4.5. Image of a large sand wedge underlying till pavements on the Jason Fan. Note that the wedge does not extend up into alluvium indicating the wedge is a relict feature formed before deposition of alluvium. Field of view is approximately 70 cm at image center.

Based on the developmental phases of polygonal ground across each of the five study fans, the Northern Bull and Upper Wright Fans were deposited as recently as decades to centuries ago while the Jason and Aeolus Fans were deposited as recently as a thousand years ago. Since polygonal ground of both ages is present on the Southern Bull Fan, it can be inferred that deposition has occurred thousands of years ago (possibly in conjunction with the Jason and

Aeolus Fans), and again decades to centuries ago (possibly in conjunction with the Northern Bull and Upper Wright Fans).

Based on the width of sand wedges and a growth rate of 0.5 mm/yr to 1 mm/yr (Sletten et al., 2003), polygons began developing on the Northern Bull Fan at least 10 to 50 years ago and began developing on the Jason and Aeolus Fans at least 50 to 300 years ago. Vertically oriented clasts frequently crosscut alluvial deposits where there is no modern surface expression of a polygon, suggesting multiple phases of polygon development have occurred since deposition. Because fractures may not expand every year and fractures may not fill every year, these are considered to be minimum age estimates.

4.4. Optically stimulated luminescence dating

OSL dating is associated with the family of dosimetric dating methods. OSL measures the number of electrons accumulated in lattice defects of geologic materials. These electrons are derived from naturally occurring ionizing radiation. This radiation causes electrons to build up in lattice defects at predictable rates over geologic timescales. In nature, exposure to light rapidly purges these accumulated electrons, essentially resetting the clock. In a laboratory setting luminescence emitted from sediment samples is calibrated to known doses of radiation that allows the naturally accumulated radiation dose to be measured. The quantity of stored electrons is proportional to the accumulated radiation dose, which is proportional to the time that has elapsed since deposition, permitting calculation of a depositional age (Lepper, 2007).

4.4.1. OSL methods

4.4.1.1. OSL sampling

Samples for OSL dating were collected from freshly exposed faces in excavations at or near the mouth of the most recently active meltwater channel of each fan. Closed-end metal

cylinders and sealed pipes were inserted horizontally into the strata, removed from the profile, and capped in the field. This method allowed sediments captured within cylinders to be transported from the field without being exposed to light. The geographic coordinates and the sample location within the profile were recorded for each sample.

4.4.1.2. Sample processing

OSL analyses were conducted at the NDSU Optical Dating and Dosimetry Laboratory. All OSL samples were processed and measured under controlled lighting conditions. After disposing of the contaminated ends of the sample, ~200 cm^3 of sediment was sieved to obtain grains within the 150 – 250 μm size range. Clean quartz sand was acquired by subjecting the grains to standard luminescence dating sample preparation procedures (Lepper et al., 2007). These include digestion of organic matter by H_2O_2, treatment with HF acid to etch quartz grains surfaces and breakdown feldspars, and HCl and Na-pyrophosphate rinses to remove precipitates and particulates. Following drying, the clean grains were attached to aliquots using a non-luminescent medical adhesive.

4.4.1.3. Data collection

Environmental dose rates for the samples were determined from elemental concentrations of K, Rb, U, and Th. Elemental analyses were obtained via instrumental neutron activation (INAA) performed at the Ohio State University Research Reactor. Joe Talnagi at the Ohio State University performed INAA data reduction. Elemental concentrations of K, Rb, U, and Th are reported in **Table 4.1**.

All measurements and irradiations were conducted using a Risø DA-15 automated TL/OSL reader system housed in the Optically Stimulated Luminescence and Dosimetry lab at NDSU. The system is equipped with a 40 mCi $^{90}Sr/^{90}Y$ β-source for dose calibrations, which

irradiates at a rate of 0.124 Gy/s. Luminescence was stimulated with blue light (470±30 nm) from a diode array and measured with an EMI model 9235QA PMT in the UV emission range (5 mm Hoya U-340). OSL single aliquot regeneration (SAR) data collection procedures of Murray and Wintle (2000) were used with the minor modification of maintaining uniform cut-heat and preheat treatment of 160°C for 10s as employed by Lepper et al. (2000; 2007). Four regeneration doses were used as well as a "check dose" (D_c) to assess the fidelity of dose recovery from individual aliquots (Lepper et al., 2000). Dose response calibration was conducted for every aliquot and equivalent doses (D_e) were interpolated by linear local slope approximation. Between 142 and 144 individual aliquots were analyzed from each field sample in this investigation (**Table 4.2.**).

4.4.1.4. Data filtering

In order to ensure data integrity, three criteria were applied to exclude invalid D_e data. First, aliquots with background-subtracted natural signals less than or equal to zero at any point in the regeneration process were removed from the dataset. Second, aliquots with negatively sloped regeneration curves were excluded. Lastly, aliquots with δD_c (an assessment of dose recovery following regeneration) values greater than 100% were excluded (Lepper et al. 2003).

4.4.1.5. OSL data analysis

An OSL age (t_{OSL}) can be summarized as the total ionizing radiation dose recorded by a sediment sample (D_e) divided by the rate at which it is being irradiated in-situ, the environmental dose rate (D'):

$$t_{OSL} = \frac{De}{D\prime} \qquad (4.1.)$$

D_e is determined by laboratory measurement made directly on sediment grains. Modern data collection techniques produce numerous independent dose determinations for any given field

sample. This produces a distribution of doses, such that D_e is a parameter that represents the significant or representative value determined from the equivalent dose dataset.

The appropriate method for calculating age is determined based on the degree of asymmetry of the data distribution using a simple ratio of the mean to median. Provided the data is sufficiently symmetric ($M/m \leq 1.05$), the mean ionizing radiation dose recorded by a sediment sample (D_{mean}) can be used to calculate the age. However, alluvial fan deposits often exhibit higher degrees of asymmetry ($M/m > 1.05$), in which case D_{mean} does not provide an accurate sample age. In these cases, the "leading edge" method of Lepper & McKeever (2002; see also the supplement to Lepper et al., 2007 for greater detail) can be employed to use only the data along the rising limb of the data set; i.e. the leading edge dose (D_{LE}). The resulting age is more accurate than if D_{mean} were used but, due to the smaller sample size, the "leading edge" age has increased error relative to ages based on D_{mean}. Because there have been few applications of OSL dating to Antarctic samples and none specifically applied to fan deposits in Antarctica, the mode of the dose distribution (D_{mode}) was also evaluated for asymmetric samples in this study.

4.4.2. OSL results

Results of dosimetric analysis of six dated samples are reported in **Table 4.1.** Luminescence data are summarized in **Table 4.2.** and the calculated age of fan deposits are reported in **Table 4.3.** The age of the fan sediments from the Jason Fan were reported by Lewis et al. (2010) but have not been published. They are reproduced in **Table 4.4.** OSL signals from the sample from the Northern Bull Fan were generally at the measurement noise threshold and therefore yielded a small number of D_e values after the data filtering described above. For this reason, an age was not calculated for the Northern Bull Fan.

4.4.3. Interpretation of OSL results

The Aeolus Fan experienced the most recent deposition, between 1.4 to 2.3 ka ago **(Table 4.3.**). The most recent deposition on the Upper Wright Fan occurred ~ 2.6 ± 0.3 ka ago. The Southern Bull Fan experienced deposition between 2.3 to 2.8 ka ago (**Table 4.3.**). The ages of the stacked melt-packages represented in samples FZ1134A (upper melt- package) and FZ1134B (lower melt-package) from the Aeolus Fan indicate that, at a minimum, 1000 years passed between periods of fan aggradation, at this particular location, with the lower melt-package being deposited ~ 3.3 ± 0.4 ka ago and the upper melt-package being deposited between 1.4 and 2.3 ka ago.

Table 4.1. Concentration of dosimetrically relevant elements From INAA.

Sample	**[K] (ppm)**	**± [K] (ppm)**	**[Rb] (ppm)**	**± [Rb] (ppm)**	**[Th] (ppm)**	**± [Th] (ppm)**	**[U] (ppm)**	**± [U] (ppm)**
FZ1134A	7093	522	32.63	5.11	4.179	0.334	1.134	0.236
FZ1134B	5315	416	27.25	5.23	3.132	0.262	0.806	0.271
FZ1142	7092	628	33.22	5.31	6.245	0.485	1.790	0.221
FZ1148A	9315	820	36.46	6.69	2.911	0.258	0.597	0.284
FZ1158A	10649	984	57.50	7.82	7.116	0.557	0.768	0.238
FZ1162	5526	452	33.82	5.78	3.703	0.310	2.183	0.278

INAA irradiations completed at the Ohio State University RES-Reactor; Data Reduction by Joe Talnagi.

Table 4.2. Results of OSL analysis.

Sample	**N[1]**	**M/m[2]**	**δD_c[3]**	**Dose Rate (J/kg/ka)**	**D_{mean} (J/kg)**	**D_{mode} (J/kg)**	**D_{LE} (J/kg)**
FZ1134A	134/144	1.08	97%	1.388	-	3.289	2.038
FZ1134B	132/142	1.00	89%	1.024	3.542	-	-
FZ1142	84/144	1.11	87%	1.657	-	3.021	1.833
FZ1148A	29/143	4.15	80%		-	-	-
FZ1158A	55/143	1.39	99%	1.825	-	5.296	4.258
FZ1162	122/143	1.03	80%	1.286	3.754	-	-

[1] Number of aliquots used for OSL D_e calculation / number of aliquots from which OSL data was collected
[2] Mean/median ratio; a measure of dose distribution symmetry (see supplement to Lepper et al., 2007)
[3] Dose recovery fidelity (refer to check dose in Lepper et al., 2000)

Table 4.3. Ages of the most recent alluvial fan deposits on the sampled fans.

Sample	Fan	"Leading Edge" Age (ka)	Mode Age (ka)	Mean Age (ka)
FZ1134A	Aeolus	1.4 ± 0.2	2.3 ± 0.2	- - -
FZ1134B	Aeolus	- - -	- - -	3.3 ± 0.4
FZ1142	Aeolus	1.1 ± 0.1	1.8 ± 0.2	- - -
FZ1148A*	North Bull	- - -	- - -	- - -
FZ1158A	South Bull	2.3 ± 0.4	2.8 ± 0.2	- - -
FZ1162	Upper Wright	- - -	- - -	2.6 ± 0.3

* An age was not calculated for sample FZ1148A due to very poor signal to noise ratios.

Table 4.4. Ages of recent deposits on the Jason Fan.

Sample ID	N	M/m	Dose Rate (J/kg/ka)	Mean Age (ka)	Mode Age (ka)	"Leading Edge" Age (ka)
ALE0861	107/111	1.04	1.405 ± 0.106	9.7 ± 0.8	- - -	- - -
ALE0860D	102/111	1.11	1.419 ± 0.113	- - -	10.4 ± 0.9	8.1 ± 1.0
ALE0860C	75/96	1.19	1.280 ± 0.101	- - -	10.3 ± 1.0	6.1 ± 1.6
ALE0860B	92/107	1.26	1.290 ± 0.105	- - -	19.0 ± 1.6	14.1 ± 1.7
ALE0860A*	68/92	1.00	2.084 ± 0.146	63.8 ± 5.0	- - -	- - -

* Sample was collected from a sand wedge within the till and did not extend upward into alluvium.
Lewis et al. (2010)

Comparison of these data to other dated climate records shows that deposition of the lower melt-package in the Aeolus Fan took place near the end of the last optimum between 6.0 ka and 3.0 ka ago, as identified in water isotope records preserved in ice cores (Masson et al., 2000). Conditions conducive to fan formation on the Aeolus, Southern Bull, and Upper Wright Fans were most recently present several centuries after this last optimum. Conditions conducive to fan formation on the Aeolus (upper melt-package), Southern Bull, and Upper Wright Fans were most recently present several centuries after this last optimum. Interestingly, the time of recent activity on the Southern Bull and Upper Wright Fans corresponds to a period of global cooling between 3,500 and 2,500 yr B.P. identified by Mayewski et al. (2004) based on ^{14}C and ^{10}Be residual proxies that indicate subdued solar radiation.

During the preliminary study on the Jason Fan by Lewis et al. (2010), an excavation revealed a sand wedge within till that did not extend up into alluvium (**Figure 4.6.**). The sand wedge and the overlying alluvium were sampled for OSL dating (ALE0860A). Results show that the fan was not present as recently as 63.8 ka ago, near the end of the Pleistocene. Furthermore, ~50 ka passed between the development of this wedge and the deposition of the fan. Deposition of the Jason Fan corresponds to the retreat of the Ross Ice Shelf at the end of the LGM, ~10.1 ka (Dunbar et al., 2007; McKay et al., 2008). Meltwater production on the Jason Fan has been insufficient to produce fan-building flows since the early Holocene, which corresponds to the Antarctic early Holocene optimum (Masson et al., 2000).

Figure 4.6. Image of OSL sampled sand wedge on Jason Fan. Planar-bedded alluvial sediments above the sand wedge are separated by till pavements. Note that the wedge does not extend up into alluvium indicating the wedge is a relict feature formed before deposition of alluvium.

4.5. Fan chronology

The different geomorphic age indicators and age constraints they impose for the five study fans are summarized in **Table 4.5**. Results from OSL analyses are provided in the table for comparison. The time constraints provided by stratigraphic relationships, desert pavements, and polygonal ground permit a simple chronology to be described regarding fan evolution in the Dry Valleys. The superposition of fans over mid-Miocene aged tills indicates that they are younger than 14 Ma. Buried desert pavements separating tills from alluvium are evidence that, at minimum, centuries to millennia passed between till deposition and fan deposition. The buried desert pavement separating alluvial beds on the Aeolus Fan indicate at least two episodes of fan aggradation, with a long hiatus in between. Pavements on fan surfaces suggest deposition has not taken place on any of the fans for centuries to millennia. Comparisons of patterned ground development and sand wedges on the fan surfaces show that deposition occurred most recently on the North Bull, South Bull, and Upper Wright fans. Sharp boundaries between polygonal patterned ground of different maturities on the South Bull fan reaffirm that multiple episodes of fan aggradation have occurred on some fans with long hiatuses in between.

OSL results suggest that fan activation does not occur simultaneously in the Dry Valleys. This may be a result of local variation in snow pack, permafrost depth, and cloud cover over time, allowing one fan to actively aggrade while another does not. Optimal conditions for fan aggradation appear to occur over century to millennial timescales. These results do not show fan activation correlating exclusively to global warming or cooling events. The dated fan deposits are no older than early Holocene, and at one location no fan was present during the late Pleistocene. Fans may have only begun developing since the end of the LGM.

Table 4.5. Summary of age constraints based on stratigraphic and geomorphic observations and OSL dating of the youngest deposits.

Fan	Stratigraphy	Desert Pavement	Polygon Ground	OSL
Jason	< 13.85 Ma	$\geq 10^2$ - 10^3 yrs	$\geq 10^3$ yrs	8.1 ± 1.0 ka
Aeolus	< 13.85 Ma	$\geq 10^2$ - 10^3 yrs	$\geq 10^3$ yrs	1.1 ± 0.1 ka
North Bull	< 13.85 Ma	$\geq 10^2$ - 10^3 yrs	$\geq 10^2$ yrs	n/a
South Bull	< 13.85 Ma	$\geq 10^2$ - 10^3 yrs	$\geq 10^2$ - 10^3 yrs	2.3 ± 0.4 ka
Upper Wright	< 13.85 Ma	$\geq 10^2$ - 10^3 yrs	$\geq 10^2$ yrs	2.6 ± 0.3 ka

CHAPTER 5. CONCLUSIONS

- High-elevation alluvial fans in the McMurdo Dry Valleys are evidence of past climatic warmth along the margins of the EAIS. They are a sedimentary archive recording meltwater production from high-elevation glaciers and snowbanks that under modern conditions produce little to no meltwater. The sedimentary record preserved in alluvial fans could be used to address unknowns regarding surface melting along margins of the EAIS, which is a key shortcoming in models of future sea-level rise.
- Fans in the Dry Valleys are comprised of beds of poorly sorted, planar-bedded gravelly sand only centimeters to tens of centimeters deep. Based on texture, sediment color, and stratigraphic contacts individual beds or sets of beds can be distinguished that correspond to a discrete period of melting. Sediments deposited during a period of melting constitute a melt-package. Some fans are comprised of a single melt-package, whereas others, such as the Aeolus Fan, are comprised of as many as four.
- High-elevation fans in the Dry Valleys aggrade from sheet flooding. Sheet flooding occurs when meltwater emerges from channels and spreads over fan surfaces. Paleohydraulic reconstruction based on the maximum size of clasts within the fan deposits suggests that these flows are slow and shallow during fan aggradation. Only one bed on a single fan was deposited from a debris flow. This is in sharp contrast to fans in other regions, which primarily aggrade from debris flows generated during storm events.
- GIS analysis suggests that the distance of the meltwater source from the Ross Sea is the most important variable explaining variation in fan size, which is used as a proxy for fan activity. The location of meltwater sources between the Ross Sea and the EAIS influences the balance between sublimation and melting. Because fans are smaller nearer to the EAIS where

sublimation is much more common than melting, meltwater generation at high-elevation glaciers must coincide with a period of decreased sublimation and increased melting. This change could be from a reduction in sublimation (in favor of melting), an increase in precipitation (creating more snowbanks susceptible to solar heating) or an increase in temperatures. All of these could represent a westward shifting of the climatic gradients present in the Dry Valleys.

- The study fans immediately overlie Miocene-aged tills and erosion surfaces that characterize much of the landscape, making alluvial fans some of the youngest landscape features in high-elevation regions of the Dry Valleys. The boundary between till and alluvium is sharply marked by a buried desert pavement that extends to surfaces around the fan, indicating a prolonged period of surface stability prior to fan deposition.
- Well-developed gravel pavements over the study fans suggest deposition has not occurred, at a minimum, for centuries to millennia. The interlocking of pavement clasts and preferential varnishing on their northern faces suggests these pavements have been stable since their development. Buried pavements identical to those on fan surfaces separate melt-packages on the Aeolus Fan, indicating a centuries- to millennia-long hiatus between periods of fan aggradation.
- Polygonally patterned ground covers the surface of all studied fans. Polygons on the Northern Bull, Southern Bull, and Upper Wright Fans are the largest and have the least relief, suggesting these fans have aggraded as recently as decades to centuries ago. The Jason and Aeolus Fans have smaller polygons with higher relief, which suggests that they have not aggraded for at least millennia. The presence of polygonal ground of different ages on the Southern Bull Fan reaffirms that long hiatuses pass between periods of fan aggradation.

- OSL dating of near-surface sediments shows that fan deposits are no older than the early Holocene. Optimal conditions for meltwater generation at high-elevation glaciers and snowbanks appear to occur over century to millennial timescales. Dating of a buried sand wedge in till beneath the Jason Fan revealed that the fan was not present as recently as the late Pleistocene. Differing OSL ages from four fans can be interpreted to suggest that fan activation does not occur simultaneously in the Dry Valleys. This may be due to regional variations in snowpack or cloud cover that restrict melting at some locations. However, only a small number of OSL samples have been processed as part of this thesis. Further dating of multiple melt-packages could show that activation sometimes does occur simultaneously.

REFERENCES

Bacon, S.N., McDonald, E.V., Caldwell, T.G., Dalldorf, G.K., 2010. Timing and distribution of alluvial fan sedimentation in response to strengthening of late Holocene ENSO variability in the Sonoran Desert, southwestern Arizona, USA. Quaternary Research 73(3), 425-438.

Black, R.F., Berg, T.E., 1963. Patterned ground in Antarctica, *in* Proceeding: Permafrost International Conference, Publ. 1287, National Academy of Science, Research Council. Washington D.C. pp. 121-128.

Blair, T.C. McPherson, J.G., 1994. Alluvial fans and their natural distinction from rivers based on morphology, hydraulic processes, sedimentary processes, and facies assemblages. Journal of Sedimentary Research 64 (3), 450-489.

Blair, T.C., 1987. Sedimentary Processes, Vertical Stratification Sequences, and Geomorphology of the Roaring River Alluvial Fan, Rocky Mountain National Park, Colorado. Journal of Sedimentary Petrology 57 (1), 1-18.

Bockheim, J.G., 2010. Evolution of desert pavements and the vesicular layer in soils of the Transantarctic Mountains. Geomorphology 118, 433-443.

Bomblies, A., 1998. Climatic controls on streamflow generation from Antarctic glaciers. M.S. Thesis, University of Colorado, Boulder, CO.

Broecker, W.S., 1991. The Great Ocean Conveyor. Oceanography 4(2). 79-89.

Bromley, A.M., 1985. Weather Observations: Wright Valley, Antarctica. Wellington (New Zealona): New Zealand Meteorological Service. Information Publication 11.

Bull, C., Carnein, C.R., 1970. The mass balance of a cold glacier: Meserve Glacier, south Victoria Land, Antarctica, *in*: Gow, A.J. et al. (Eds.), International Symposium on Antarctic Glaciological Exploration, Publication 86., International Association of Hydrological Sciences, pp. 429-446.

Bull, W.B., 1962. Relation of textural (CM) patterns to depositional environment of alluvia-fan deposits. Journal of Sedimentary Petrology 32(2), 211-216.

Bull, W.B., 1963. Alluvial-Fan Deposits in Western Fresno County, California. Journal of Geology 71, 243-251.

Bull, W.B., 1977. The alluvial fan environment. Progress in Physical Geography 1, 222-270.

Calkin, P.E., 1964. Geomorphology and Glacial Geology of the Victoria Valley System, Southern Victoria Land, Antarctica. Institute of Polar Studies: Report No. 10. National Science Foundation. Washington, D.C.

Chinn, T.J., 1981. Hydrology and climate in the Ross Sea area. Journal of the Royal Society of New Zealand 11, 373-386.

Chinn, T.J.H., 1987. Accelerated ablation at a glacier ice-cliff margin, Dry Valleys, Antarctica. Arctic and Alpine Research 19(1), 71-80.

Church, M, Ryder, J.M., 1972. Paraglacial Sedimentation: A Consideration of Fluvial Processes Conditioned by Glaciation. Geological Society of America Bulletin 83, 3059-3072.

Clow, G.D., McKay, C.P., Simmons, G.M., Wharton, R.A., 1988. Climatological observations and predicted sublimation rates at Lake Hoare, Antarctica. Journal of Climatology 1(7), 715-728.

Conovitz, P.A., McKnight, D.M., MacDonald, L.H., Fountain, A.G., House, H.R., 1998. Hydrologic processes influencing streamflow variation in Frycell Basin, Antarctica. *in* Priscu, J.C. (Ed.). Ecosystem dynamics in a polar desert: the McMurdo Dry Valleys, Antarctica. American Geophysical Union. Washington, D.C. pp. 93-108.

Cooke, R.U., 1970. Stone Pavements in Deserts. Annals of the Association of American Geographers 60(3), 560-577.

Costa, J.E., 1983. Paleohydraulic reconstruction of flash-flood peaks from boulder deposits in the Colorado Front Range. Geological Society of America Bulletin 94(8), 986-1004.

Cummings, D.I., Gorrell, G., Guilbault, J.P., Hunter, J.A., Logan, C., Ponomarenko, D., Andre, J.M.P, Pullan, S.E., Russell, H.A.J., Sharpe, D.R., 2010. Sequence stratigraphy of a glaciated basin fill, with focus on esker sedimentation. Geological Society of America Bulletin 123(7-8), 986-1004.

Delong, S.B., Arnold, L.J., 2007. Dating alluvial deposits with optically stimulated luminescence, AMS ^{14}C and cosmogenic techniques, western Transverse Ranges, California, USA. Quaternary Geochronology 2, 129-136.

Dana, D.L., Wharton, R.A., Dubayah, R., 1998. Solar radiation in the McMurdo Dry Valleys, Antarctica. *in:* Priscu, J.C. (Ed.), Ecosystems dynamics in a polar desert: The McMurdo Dry Valleys, Antarctica. American Geophysical Union, Washington, D.C. pp. 39-64

Dickson, J.L., Head, J.W., Marchant, D.R., Morgan, G.A., Levy, J.S., 2007. Recent gully activity on Mars: clues from late-stage water flow in gully systems and channels in the Antarctic Dry Valleys. Lunar and Planetary Science 38. Abstract 1678.

Doran, P.T., McKay, C.P., Clow, G.D., Dana, G.L, Fountain, A.G., Nylen, T., Lyons, W.B., 2002. Valley floor climate observation from the McMurdo dry valleys, Antarcica, 1986-2000. Journal of Geophysical Research 107(D24), 4772.

Doran, P.T., McKay, C.P., Fountain, A.G., Nylen, T., McKnight, D.M., Jaros, C., Barrett, J.E., 2008. Hydrologic response to extreme warm and cold summers in the McMurdo Dry Valleys, East Antarctica. Antarctic Science 20(5), 499-509.

Dorn, R.I., 2009. The Role of Climatic Change in Alluvial Fan Development, *in* Parsons, A.J., Abrahams, A.D. (Eds.), Geomorphology of Desert Environments, 2nd edition. Springer Science+Business Media.

Dunbar, G., Niessen F., Vogel, S., & 18 others. 2007. Late Pleistocene to Holocene Strata from Soft-Sediment Coring at the AND-1B Site, ANDRILL McMurdo Ice Shelf Project, Antarctica. Terra Antartica 14(3), 141-154.

Ebnet, A.F., Fountain, A.G., Nylen, T.H., McKnight, D.M., Jaros, C.L., 2005. A temperature-index model of stream flow at below-freezing temperatures in Taylor Valley, Antarctica. Annals of Glaciology 40, 76-82.

Elliot, D.E., Fleming, T.H., 2004. Occurrence and dispersal of magmas in the Jurrasic Ferrar large igneous province, Antarctica. Gondwana Research 7(1), 223-237.

Elvidge, C.D., Iverson, R.M., 1983. Regeneration of desert pavement and varnish, *in* Webb, R.H. and Wilshire, H.G., (Eds.), Environmental effects of off-road vehicles. Springer-Verlag, New York, pp. 225-243.

Folk, R.L., 1974. Petrology of Sedimentary Rocks. Hemphill Publishing Company. Austin, TX.

Fountain, A.G., Vaughn, B.H., Dana, G.L., 1994. McMurdo LTER: Glacier mass balances of Taylor Valley, Antarctica. Antarctic Journal of the United States – Review 1994 29(5), 226-228.

Fountain, A.G., Dana, G.L., Lewis, K.J., Vaughn, B.H., McKnight, D., 1998. Glaciers of the McMurdo Dry Valleys, Southern Victoria Land, Antarctica. *in*: Priscu, J.C. (Ed.), Ecosystems dynamics in a polar desert: The McMurdo Dry Valleys, Antarctica. American Geophysical Union, Washington, D.C., pp. 65-75.

Fountain, A.G., Lewis, K.J., Dana, G.L., 1999. McMurdo Dry Valleys LTER: Spatial variation of glacier mass balance in Taylor Valley, Antarctica. Antarctic Journal of the United States – 1996 Review Issue (NSF 98-28) 31(2), 194-195.

Fountain, A.G., Lewis, K.J., Doran, P.T., 1999. Spatial climatic variation and its control on glacier equilibrium line altitude in Taylor Valley, Antarctica. Global and Planetary Change 22, 1-10.

Fountain, A.G., Lyons, W.B., Burkins, M.N. & 9 others, 1999. Physical Controls on the Taylor Valley Ecosystem, Antarctica. Bioscience 49(12), 961-971.

Fountain, A.G., Nylen, T.H., Monoghan, A., Basagic, H.J., Bromwich, D., 2010. Snow in the McMurdo Dry Valleys. International Journal of Climatology 30(5), 633-789.

Fuchs, M., Lang, A., 2009. Luminescence dating of hillslope deposits – A review. Geomorphology 109, 17-26.

Fuchs, M., Fischer, M., Reverman, R., 2010. Colluvial and alluvial sediment archives temporally resolved by OSL dating: Implication for reconstructing soil erosion. Quaternary Geochronology 5, 269-273.

Hall, B.L., Denton, G.H., Lux, D.R., Bockheim, J.G., 1993. Later Tertiary paleoclimate and ice-sheet dynamics inferred from surficial deposits in Wright Valley, Antarctica. Geografiska Annaler 75(4), 239-268.

Hall, B.L., Denton, G.H., 2000. Radiocarbon Chronology of Ross Sea Drift, Eastern Taylor Valley, Antarctica: Evidence for a Grounded Ice Sheet in the Ross Sea at the Last Glacial Maximum. Geografiska Annaler 82(2-3), 305-336.

Hall, B.L., Denton, G.H., Fountain, A.G., Hendy, C.H., Henderson, G.M., Bender, M.L., 2010. Antarctic lakes suggest millennial reorganizations of Southern Hemisphere atmospheric and oceanic circulation. Proceedings of the National Academy of Sciences of the United States of America 107(50), 21355-21359.

Harvey, A.M., 1984. Aggradation and Dissection Sequences on Spanish Alluvial Fans: Influence on Morphological Development. Catena 11, 289-304.

Haug, E.W., Kraal, E.R., Sewall, J.O., Dijk, M.V., Diaz, G.C., 2010. Climatic and Geomorphic Interactions on Alluvial Fans in the Atacama Desert, Chile. Geomorphology 121, 184-196.

Head, J.W., Marchant, D.R., Dickson, J.L., Levy, J.S, Morgan, G.A., 2007. Mars gully analogs in the Antarctic Dry Valleys: Geological setting and processes. Lunar and Planetary Science 38. Abstract 1617.

Hoffman, M.J., Fountain, A.G., Liston, G.E., 2008. Surface energy balance and melt thresholds over 11 years at Taylor Glacier, Antarctica. Journal of Geophysical Research 113, F04014.

IPCC AR4 WG1, 2007. *in* Solomon, S., Qin, M., Manning, M., Chen, Z., Marquis, M., Averyt., K.B., Tignor., M., Miller, .L. (Eds.), Climate Change 2007: The Physical Science Basis. Contribution of Working Group I to the Fourth Assessment Report of the Intergovernmental Panel on Climate Change. Cambridge University Press, Cambridge, United Kingdon and New York, NY, USA.

Isaac, M.J., Chinn, T.J., Edbrook, S., Forsyth, J., 1996. Geology of the Olympus Range area, southern Victoria Land, Antarctica. Institute of Geological and Nuclear Sciences. 60. Wellington, NZ.

Keys, J.R., 1980. Air Temperature, Wind, Precipitation and Atmospheric Humidity in the McMudo Region. Victoria University, Geology Department, Wellington, NZ.

Leonard, K., Fountain, A., Cook, J., 1998. Methods of estimating average glacier equilibrium line altitude. EOS supplement 79, F227.

Lepper, K., Wilson, C., Gardner, J., Reneau, S., Lavine, A., 2003. Comparison of SAR techniques for luminescence dating of sediments derived from volcanic tuff. Quaternary Science Reviews 22, 1131-1138.

Lepper, K., Fischer, T.G., Hajdas, I., Lowell, T.V., 2007. Ages for the Big Stone Moraine and the oldest beaches of glacial Lake Agassiz: Implications for deglaciation chronology. Geology 35(7), 667-670.

Lepper, K., Crowell, K., Wilson, C., 2011. Chronology of colluvial apron deposition within Canada del Buey, Pajarito Plateau, New Mexico. New Mexico Geology 33(1), 3-

Levy, J.S., Head, J.W., Marchant, D.R. 2008. The Role of Thermal Contraction Crack Polygons in Cold-Desert Fluvial System. Antarctic Science 20 (6). 565-579.

Levy, J.S., Head, J.W., Marchant, D.R., Dickson, J.L., Morgan, G.A., 2009. Geologically recent gully-polygon relationships on Mars: Insights from the Antarctic Dry Valleys on the roles of permafrost, microclimates, and water sources for surface flow. Icarus 201, 113-126.

Lewis, A.R., Marchant, D.R., Kowalewski, D.E., Baldwin, S.L., Webb, L.E., 2006. The age and origin of the Labyrinth, western Dry Valleys, Antarctica: Evidence for extensive middle Miocene subglacial floods and freshwater discharge to the Southern Ocean. Geological Society of America Bulletin 34(7), 513-516.

Lewis, A.R., Ashworth, A.R., Marchant, D.R., Hemming, S.R., Machlus, M.L., 2007. Major middle Miocene global climate change: Evidence from East Antarctica and the Transantarctic Mountains. Geological Society of America Bulletin 119(11-12), 1449-1461.

Lewis, A.R., Marchant, D.R., Ashworth, A.C., Hedenas, L., Hemming, S.R., Johnson, J.V., Leng, M.J., Machlus, M.L., Newton, A.E., Raine, J.I., Willenbring, J.K., Wolfe, A.P., 2008. Mid-Miocene colling and the extinction of tundra in continental Antarctica. Proceedings of the National Academy of Sciences of the United States of America 105(31), 10676-10680.

Lewis, A.R., Willenbring, J.K., Lepper, K., 2010. Collaborative Research: Activation of high-elevation alluvial fans in the Transantarctic Mountains – a proxy for Plio-Pleistocene warmth along East Antarctic ice margins. National Science Foundation: Division of Polar Programs. Washington, D.C., ANT-1043601.

Lewis, K.G., Dana, G., Fountain, A., Tyler, S., 1995. The surface energy balance of the Canada Glacier, Taylor Valley. Antarctic Journal of the United States 30, 280-282.

Lewis, K.J., Fountain, A.G., Dana, G.L., 1998. Surface energy balance and meltwater production for a Dry Valley glacier, Taylor Valley, Antarctica. Annals of Glaciology 27, 603-609.

Lewis, K.J., Fountain, A.G., Dana, G.L, 1999. How important is terminus cliff melt?: a study of the Canada Glacier terminus, Taylor Valley, Antarctica. Global Planetary Change 22(1-4), 105-115.

Maizels, J.K., 1987. Large-scale flood deposits associated with the formation of coarse-grained, braided terrace sequences. *in* Ethridge F.C., Flores, R.M., Harvey, M.D. (Eds.) Recent Developments in Fluvial Sedimentology 39, pp. 135-148.

Marchant, D.R., Denton, G.H., Sugden, D.E., 1993. Miocene glacial stratigraphy and landscape evolution of the western Asgard Range, Antarctica. Geografiska Annaler 75A, 303-330.

Marchant, D.R., Head, J.W., 2007. Antarctic dry valleys: Microclimate zonation, variable geomorphic processes, and implications for assessing climate change on Mars. Icarus 192, 187-222.

Margerison, H.R., Phillips, W.M., Stuart, F.M., Sugden, D.E., 2005. Cosmogenic ^{3}He concentration in ancient flood deposits from the Coombs Hills, northern Dry Valleys, East Antarctica: interpreting exposure ages and erosion rates. Earth and Planetary Science Letters 230, 163-175.

Masson, V., Vimeux, F., Jouzel, J., Morgan, V., Delmotte, M., Ciais, P., Hammer, C., Johnsen, S., Lipenkov, V.Y., Mosley-Thompson, E., Petit, J.R., Steig, E.J., Stievenard, M., Vaikmae, R. 2000. Holocene Climate Variability in Antarctica Based on 11 Ice-Core Isotopic Records. Quaternary Research 54, 348-358.

Mather, A.E., Hartley, A.E., 2005. Flow Events on a Hyper-Arid Alluvial Fan: Quebrada Tambores, Salar de Atacama, Northern Chile. *in:* Harvey, A.M., Mather, A.E., Stokes, M. (Eds.). Alluvial Fans: Gemorphology, Sedimentology, Dynamics. Geological Society of London, Bath, UK., pp. 9-29.

Mayewski, P.A., Rohling, E.E., Stager, J.C., Karlen, W., Maasch, K.A., Meeker, L.D., Meyerson, E.A., Gasse, F., van Kreveld, S., Holmgren, K., Lee-Thorp, J., Rosqvist, G., Rack, F., Staubwasser, M., Schneider, R.R., Steig, E.J., 2004. Holocene climate variability. Quaternary Research 62, 243-255.

McKay, R.M., Dunbar, G.B., Naish, T.R., Barrett, P.J., Carter, L., Harper, M., 2008. Retreat history of the Ross Ice Sheet (Shelf) since the Last Glacial Maximum from deep-basin sediment cores around Ross Island. Paleogeography, Paleoclimatology, Paleoecology 260, 245-261.

McKnight, D.M. Gooseff, M.N., Vincent, W.F., Peterson, B.J., (2008). High-latitude River and Streams. *In:* Vincent, W.F., Laybourn-Parry, J. (Eds.). Polar Lakes and Rivers: Limnology of Arctic and Antarctic Aquatic Ecosystems. Oxford University Press, New York. pp. 83-102.

Moorhead, D.L., McKnight, D.M., 1998. McMurdo Dry Valleys LTER: Stream discharge as a function of ambient temperature and incoming shortwave radiation in Taylor Valley, Antarctica. Antarctic Journal of the United States – 1996 Review Issue (NSF 98-28) 31(2), 196-197.

Naish, T., Powell, R., Levy, R. & 53 others, 2009. Obliquity-paced Pliocene West Antarctic ice sheet oscillations. Nature 458. 322-328.

Parish, T.R., Bromwich, D.H., 1987. The surface windfield over the Antarctic ice sheets. Nature 328, 51-54.

Porter, S.C., 1975. Equilibrium-line altitudes of Late Quaternary glaciers in the Southern Alps, New Zealand. Quaternary Research 5, 27-97.

Quade, J., 2001. Desert pavements and associated rock varnish in the Mojave Desert: How old can they be? Geology 29(9), 855-858.

Ragotzkie, R.A., Likens, G.E., 1964. The heat balance of two Antarctic lakes. Limnology and Oceanography 9, 412-425.

Rignot, E., Velicogna, I., van den Broeke, M.R., Monaghan, A., Lenaerts, J.T.M., 2011. Acceleration of the contribution of the Greenland and Antarctic ice sheets to sea level rise. Geophysical Research Letters 38(5),

Robinson, R.A.J., Spencer, J.Q.G., Strecker, M.R., Richter, A., Alonso, R.N., 2005. Luminescence dating of alluvial fans in intramontane basins of NW Argentica, *in* Harvey, A.M., Mather, A.E., Stokes, M., (Eds.) Alluvial Fans: Geomorphology, Sedimentology, Dynamics. Geological Society of London. Bath, UK. pp. 95-115.

Roberts, S.J., Hodgson, D.A., Bentley, M.J., Sanderson, D.C.W., Milne, G., Smith, J.A., Verleyen, E., Balbo. A., 2009. Holocene relative sea-level change and deglaciation on Alexander Island Antarctic Peninsula, from elevated lake deltas. Geomorphology 112, 122-184.

Schafer, J.M., Ivy-Ochs, S., Wieler, R., Leya, I., Baur, H., Denton, G.H., Schluchter, C., 1999. Comsogenic noble gas studies in the oldest landscape on earth: surface exposure ages of the Dry Valleys, Antarctica. Earth and Planetary Science Letters 167, 215-226.

Silva, P.G., Harvey, A.M., Zazo, C., Goy, J.L., 1992. Geomorphology, depositional styles and morphometric relationships of Quaternary alluvial fans in the Guadalentin depression (Murcia, southeast Spain): Zeitschrift Fur Geomorphologies. N.F. 36, 325-341.

Sletten, R.S., Hallet, B., Fletcher, R.C., 2003. Resurfacing time of terrestrial surfaces by the formation and maturation of polygonal patterned ground. Journal of Geophysical Research. 108(E4), 8044.

Strand, R.I., 1973. Sedimentation. *in* Design of small dams. U.S. Bureau of Reclamation, Washington, D.C., pp. 767-796.

Sugden, D.E., Summerfield, M.A., Denton, G.H., Wilch, T.I., McIntosh, W.C., Marchant, D.R., Rutford, R.H. ,1999. Landscape development in the Royal Society Range, southern Victoria Land, Antarctica: stability since the mid-Miocene. Geomorphology 28, 181-200.

Summerfield, M.A., Stuart, F.M., Cockburn, H.A.P., Sugden, D.E., Denton, G.H., Dunai, T., Marchant, D.R., 1999. Long-term rates of denudation in the Dry Valleys, Transantarctic Mountains, southern Victoria Land, Antarctica based on in-situ produce cosmogenic ^{21}Ne. Geomorphology 27, 113-129.

Williams, R.S., Hall, D.K., 1993. Glaciers, *in* Gurney, R.J., Foster, J.L., Parkinson, C.L., (Eds.). Atlas of Satellite observations related to global change: Cambridge, U.K. Cambridge University Press. pp. 401-422.

Wells, S.G., Harvey, A.M., 1987. Sedimentologic and Geomorphic Variations in Storm-Generated Alluvial Fans, Howgill Fells, Northwest England. Geological Society of America Bulletin 98, 182-198.

Wells, S.G., McFadden, L.D., Poths, J., Olinger, C.T., 1995. Cosmogenic ^{3}He surface-exposure dating of stone pavements: Implications for landscape evolution in deserts. Geology 23, 613-616.

von Guerard, P., McKnight, D.M., Harnish, R.A., Gartner, J.W., Andrews, E.D., 1994. Streamflow, water temperature, and specific conductance data for selected streams draining into Lake Fryxell, Lower Taylor Valley, Victoria Land, Antarctica. U.S. Geological Survey. Open-file Report 94-545. 65.

APPENDIX A. EXCAVATION LOCATIONS

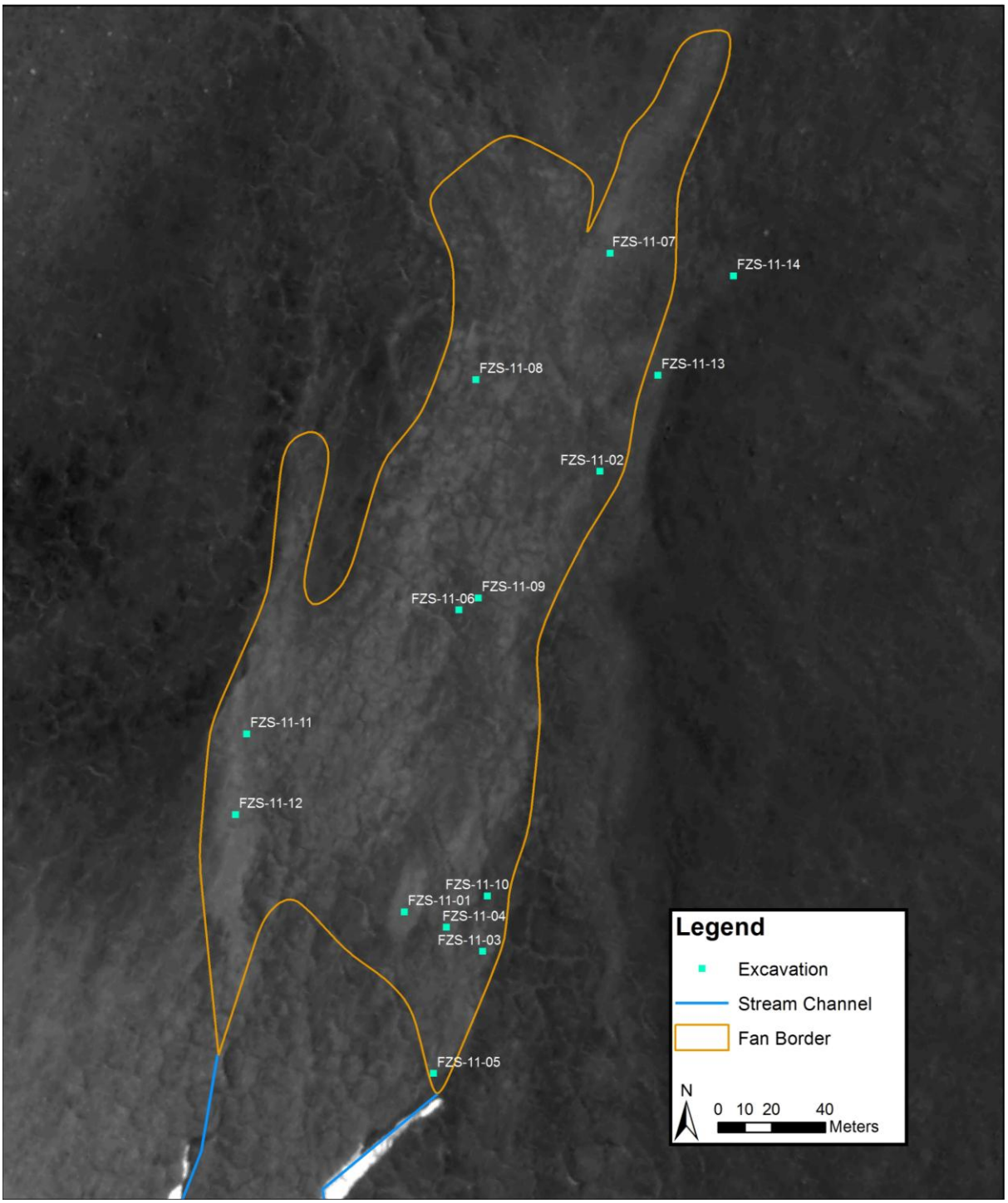

Figure A.1. Jason Fan excavation locations.

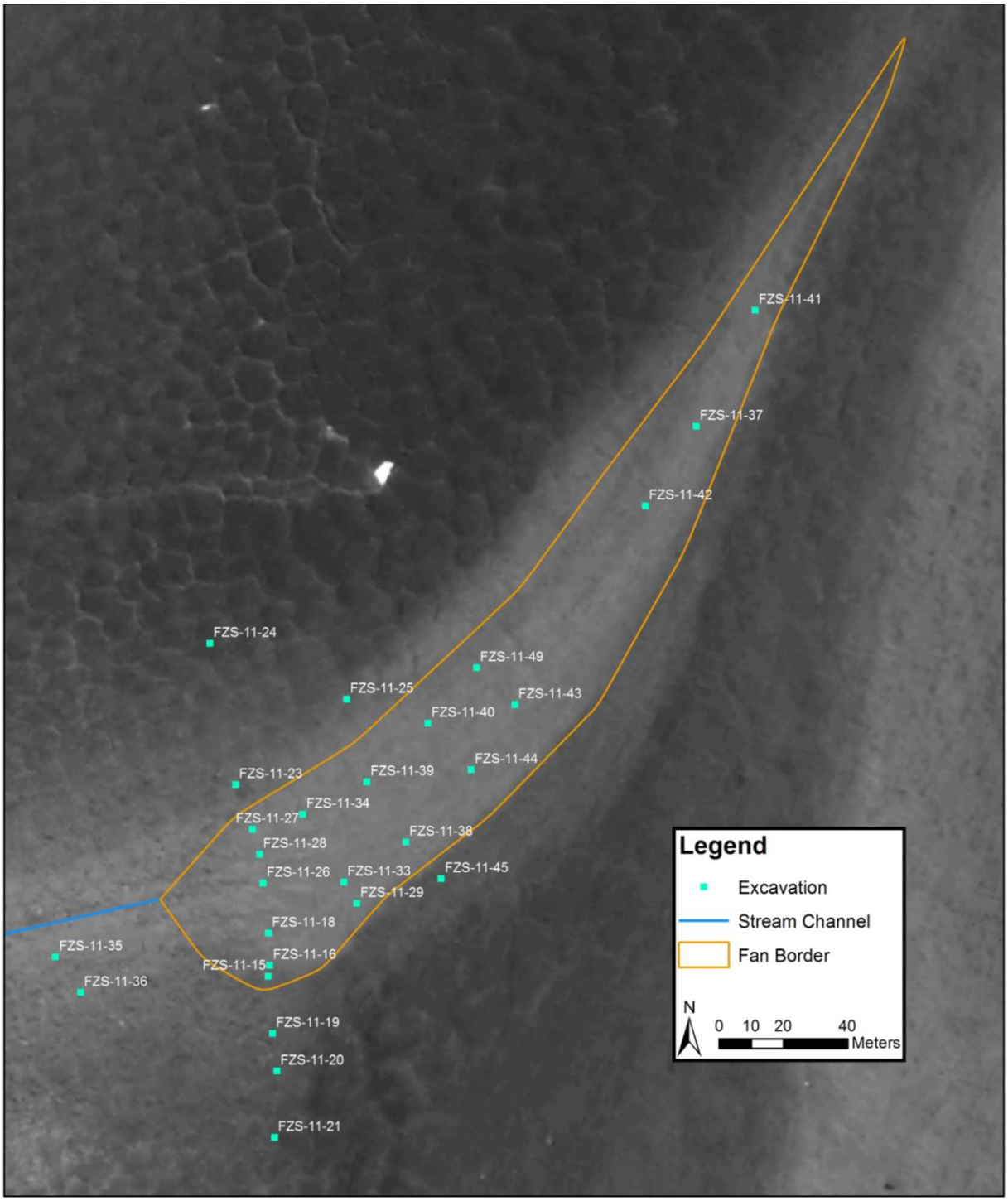

Figure A.2. Aeolus Fan excavation locations.

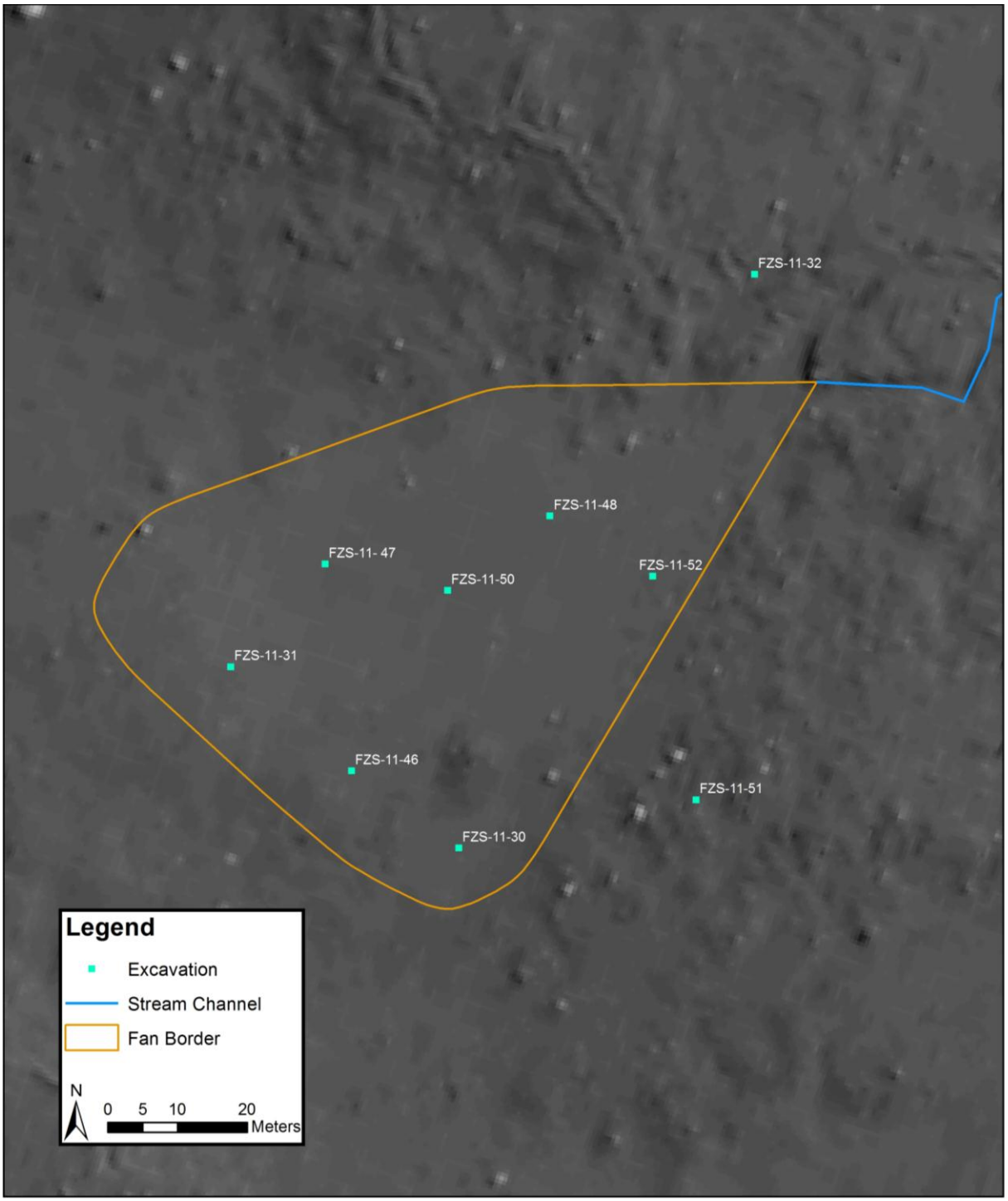

Figure A.3. Northern Bull Pass Fan excavation locations.

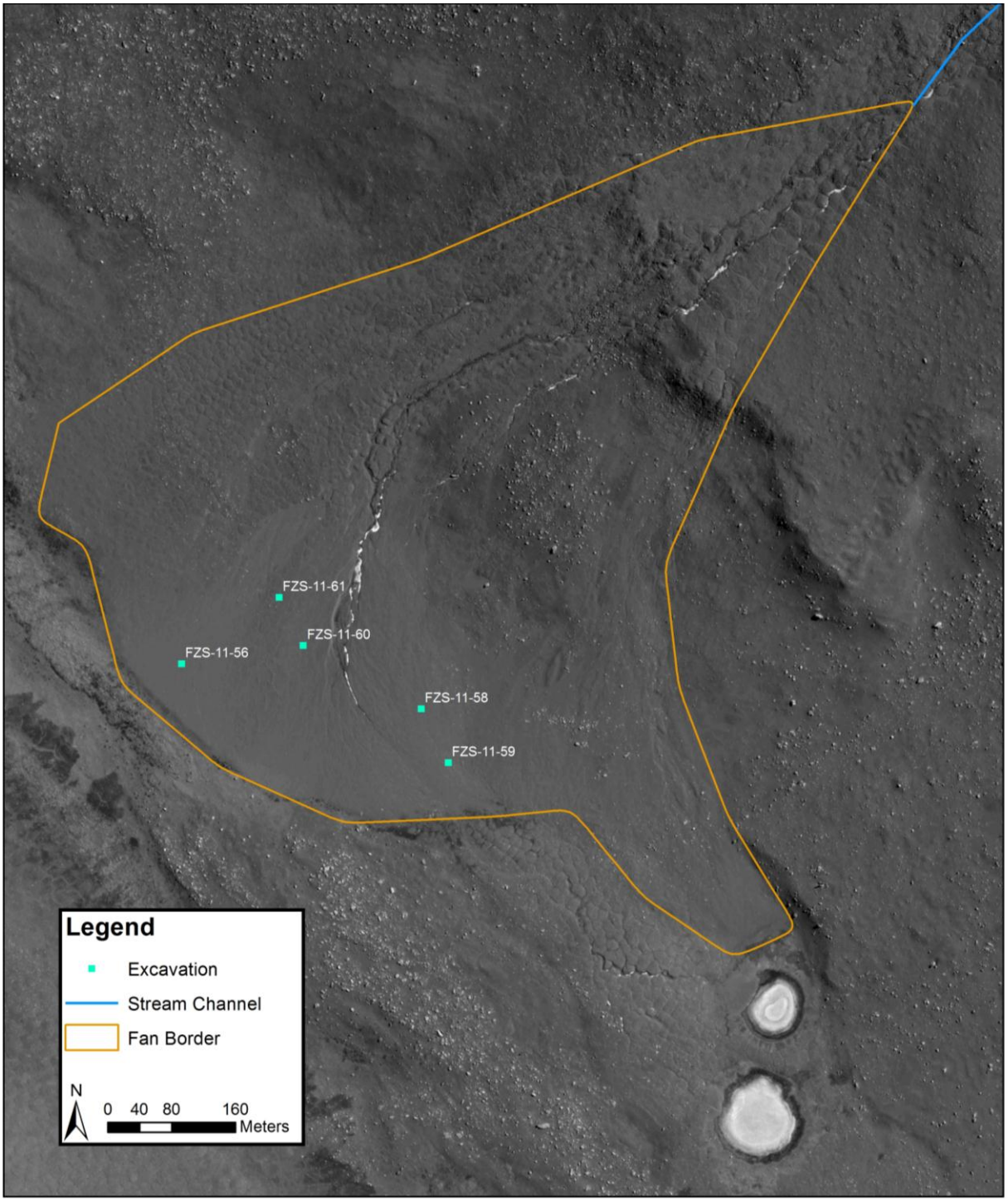

Figure A.4. Southern Bull Pass Fan excavation locations.

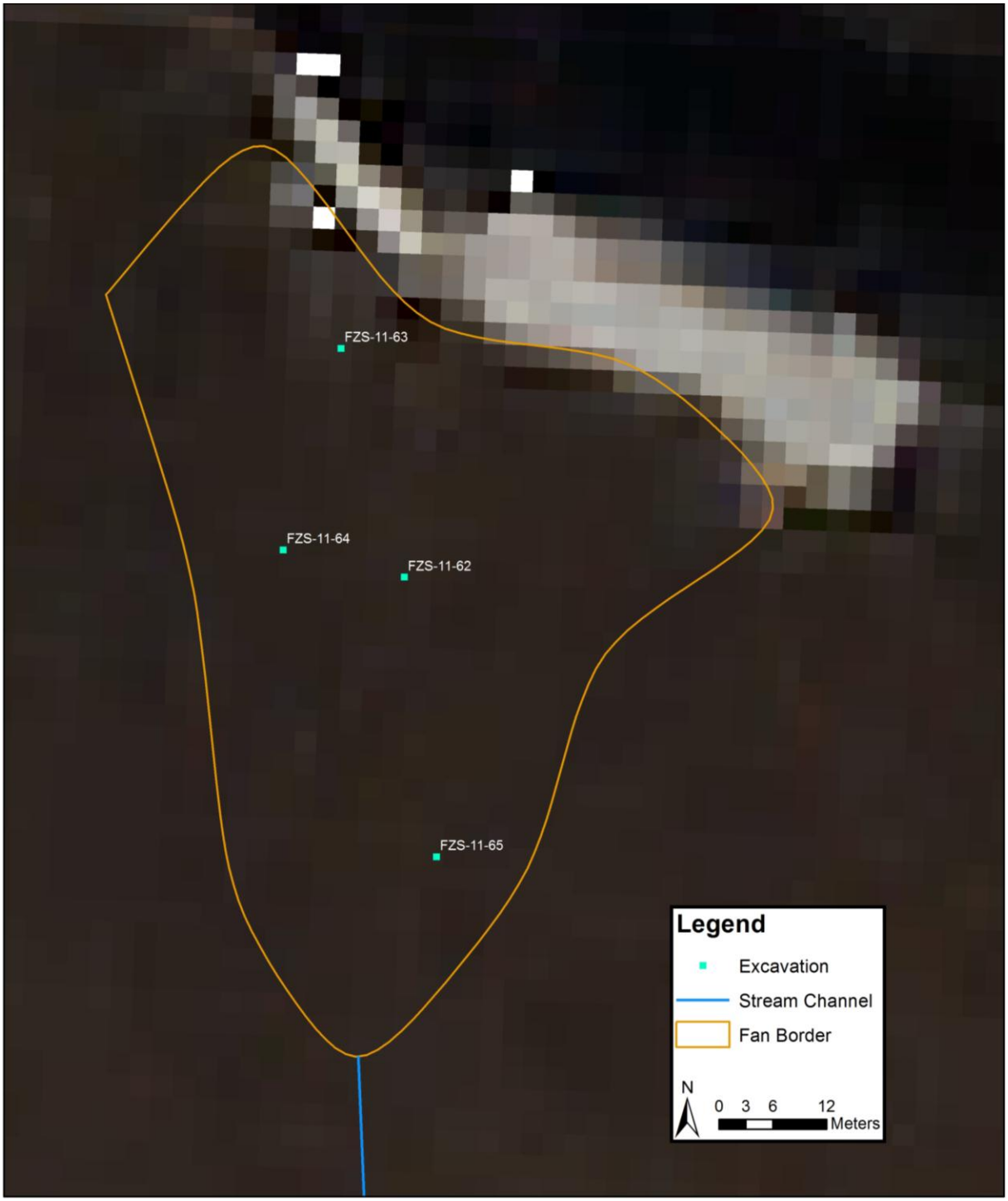

Figure A.5. Upper Wright Fan excavation locations.

APPENDIX B. EXCAVATION DIAGRAMS

B.1. Jason Fan

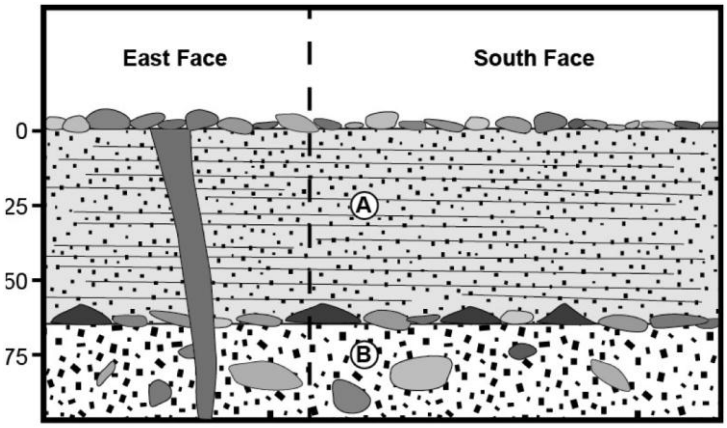

-77.4551° 161.51559°
OSL: A=25 cm, B=75 cm

- Planar bedded sands with thin pebble layers; capped by sandstone pavement; ~20 cm to ice cement

- till; massive with cobbles set within a muddy sand-matrix; capped by heavily ventifacted cobble pavement

Figure B.1. Diagram of excavation FZE-11-01.

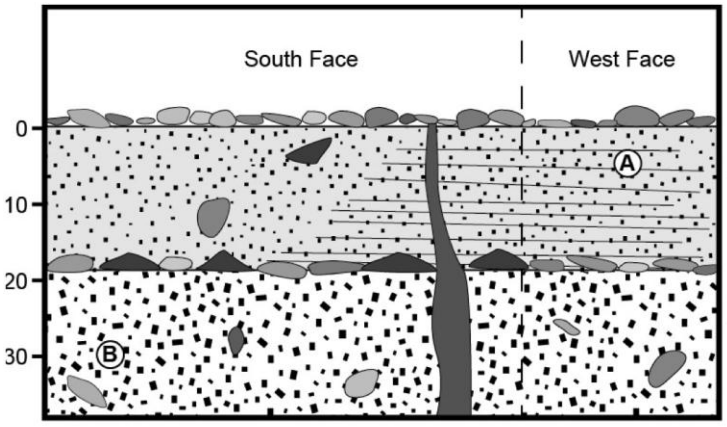

-77.45354° 161.51933°
OSL: A=5 cm

- western portions of pit are planar bedded sands; eastern portion is poorly bedded sands with a couple of cobbles; capped by sandstone and siltstone pavement
- massive till of muddy sand with a few cobbles; heavily ventifacted cobbley pavement separates till and

Figure B.2. Diagram of excavation FZE-11-02.

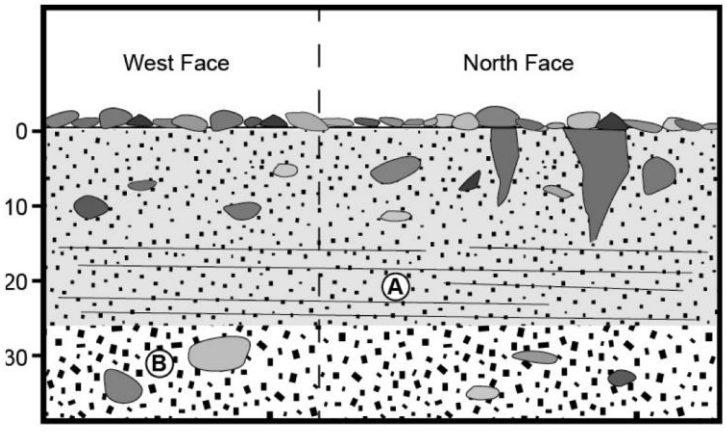

-77.45515° 161.51671°
OSL: A=20 cm, B=30 cm

- Planar bedded sands, coarsening upwards to poorly bedded cobbles, gravel and sand; capped by sandstone, dolerite, and siltstone pavement

- massive till of a light tan muddy sand with a few cobbles

Figure B.3. Diagram of excavation FZE-11-03.

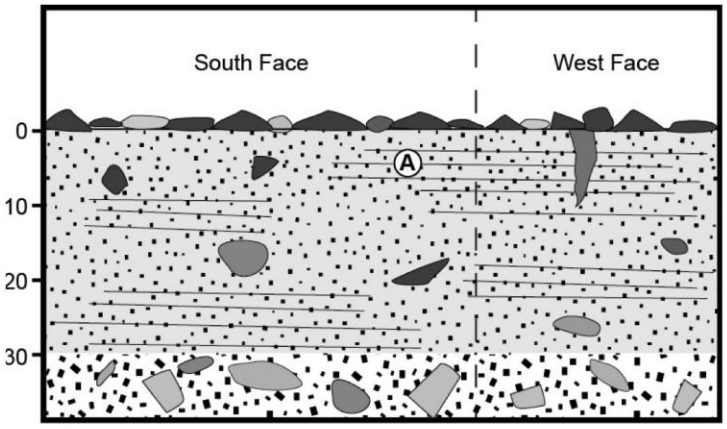

-77.45523° 161.51765°
OSL: A=5 cm

- Poorly bedded gravelly sands; coarsens upward; sand wedge; capped by heavily ventifacted pavement of siltstone cobbles

- till; massive with angular clasts

Figure B.4. Diagram of excavation FZE-11-04.

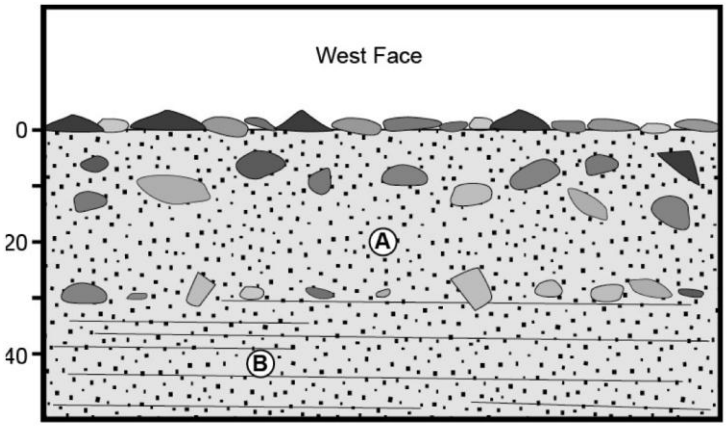

-77.45588° 161.51476°
OSL: A=20 cm, B=40 cm

- Poorly bedded gravelly sands; capped by sandstone and siltsone pavement

- Planar bedded sands; Possibly capped by pavement

Figure B.5. Diagram of excavation FZE-11-05.

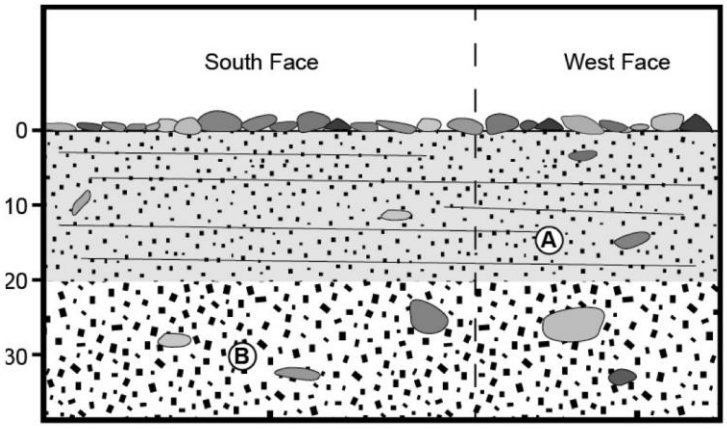

-77.454° 161.51714°
OSL: A=15 cm, B=30 cm

- planar bedded gravelly sands; capped by sandstone pavement

- Till; massive with cobbles set within a muddy sand matrix

Figure B.6. Diagram of excavation FZE-11-06.

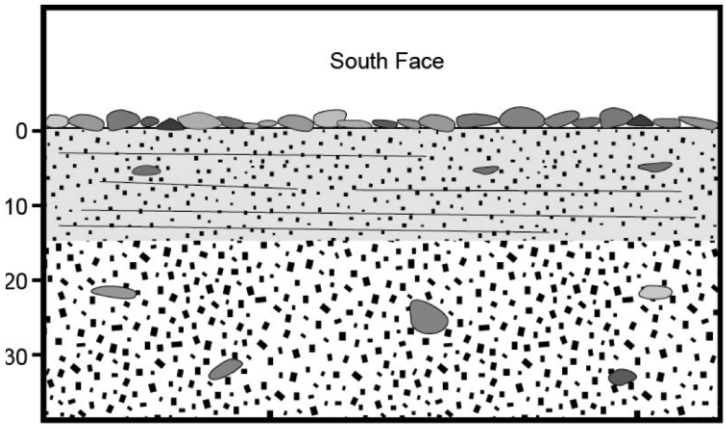

-77.4528° 161.51889°

- Planar bedded gravelly sands; capped by sandstonen and dolerite pavement

- Till; massive with cobbles; possibly capped by distrubed pavement

Figure B.7. Diagram of excavation FZE-11-07.

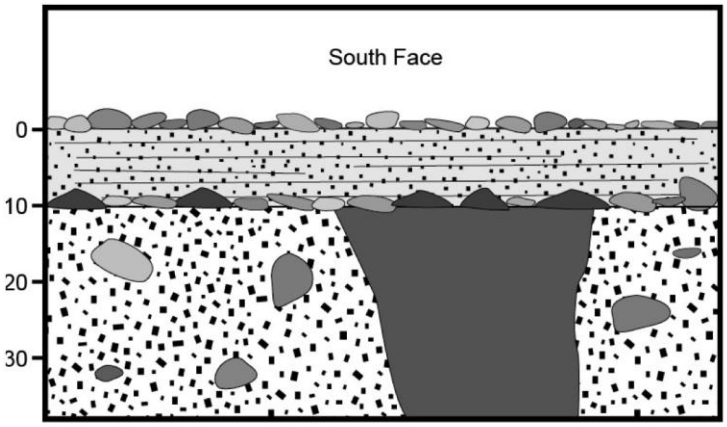

-77.45436° 161.513°

- planar bedded sands; capped by sandstone pavement
- Till; massive with intermixed cobbles; large sand wedge that does not extend up into the alluvium; capped by well developed cobble pavement

Figure B.8. Diagram of excavation FZE-11-11.

B.2. Aeolus Fan

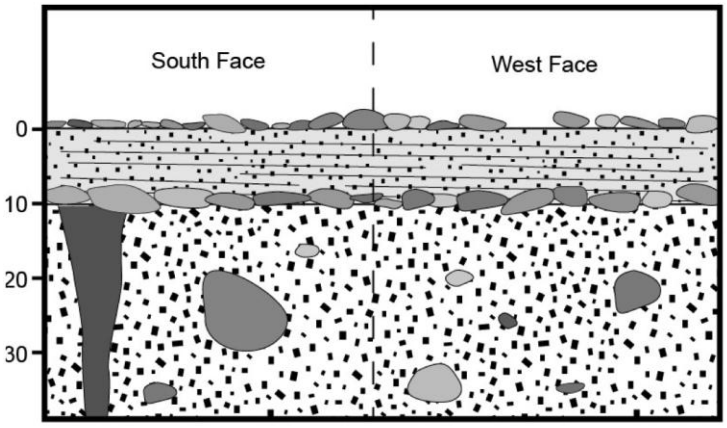

-77.46487° 161.34674°

- planar bedded sands; pebble couplets; capped by sandstone pavement
- Till; massive with intermixed cobbles; sandwedge that does not extend up into alluvium; capped by intensely varnished pavement of sandstone and dolerite cobbles

Figure B.9. Diagram of excavation FZE-11-15.

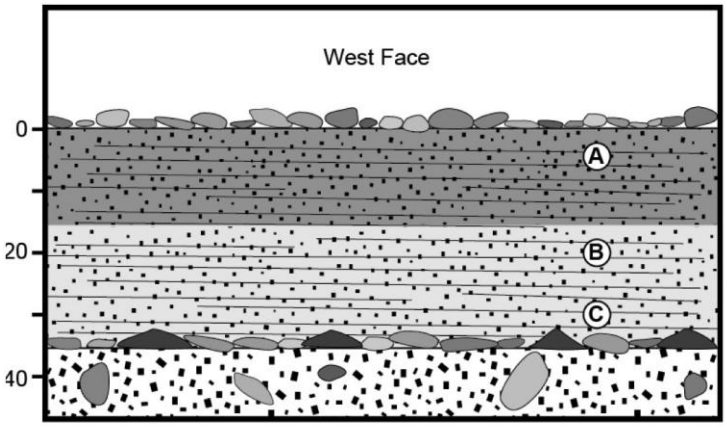

-77.46484° 161.34676°
OSL: A=5 cm, B=20 cm, C=30 cm

- planar bedded sands; pebble couplets; two melt-packages differentiated based on color; capped by sandstone pavement;

- till; massive with intermixed cobbles; capped by well-developed sandstone and dolerite pavement

Figure B.10. Diagram of excavation FZE-11-16.

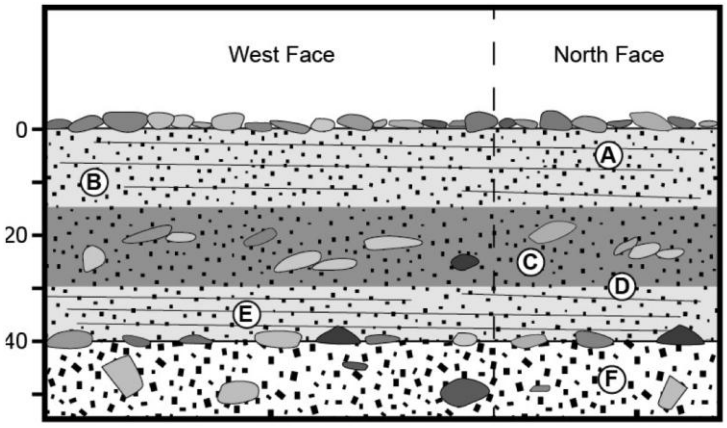

-77.46475° 161.34675°
OSL: A=5 cm, B=10 cm, C=25 cm, D=30 cm, E=35 cm, F=45 cm
- planar bedded sands; capped by pavement; upper melt-package
- massive sands with imbricated cobbles; middle melt-package
- planar bedded sands; fining upwards; lower melt-package
- till; massive with intermixed cobbles; capped by well-developed pavement

Figure B.11. Diagram of excavation FZE-11-17.

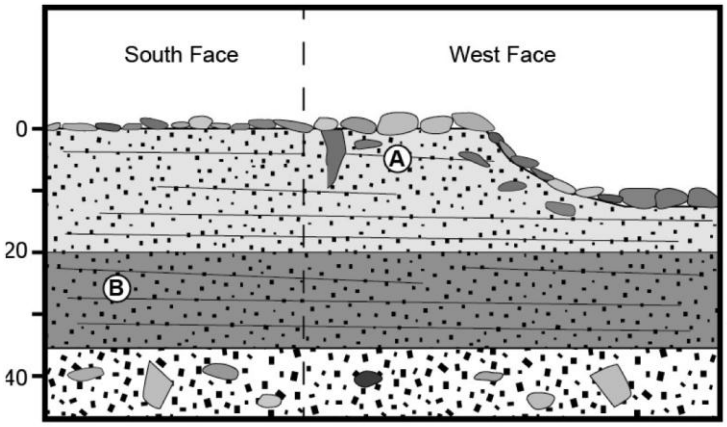

-77.46461° 161.34669°
OSL: A=5 cm, B=25 cm

- planar bedded sands; upper melt-package; adjacent to modern channel; sand wedges; capped by pavement
- planar bedded sands; lower melt-package
- Till; massive with cobbles intermixed

Figure B.12. Diagram of excavation FZE-11-26.

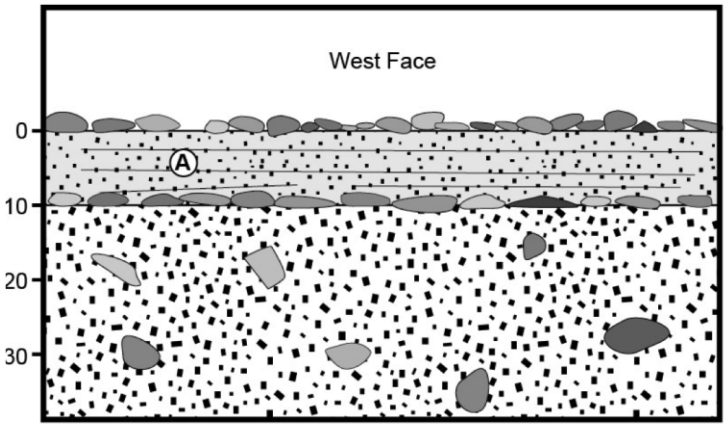

-77.46446° 161.34656°
OSL: A=5 cm

- planar bedded sands; capped by sandstone pavement
- Till; massive with intermixed cobbles; capped by well-developed pavement of sandstone and dolerite cobbles

Figure B.13. Diagram of excavation FZE-11-27.

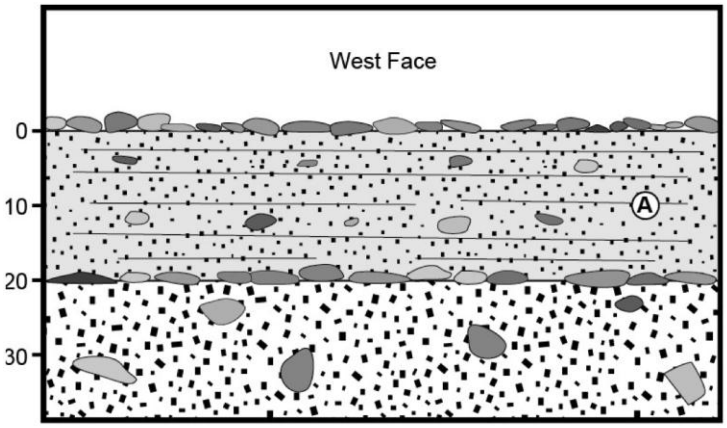

-77.46453° 161.34665°
OSL: A=10 cm

- planar bedded gravelly sands; capped by sandstone pavement

- till; massive with intermixed cobbles; capped by well-developed pavement of sandstone and dolerite cobbles

Figure B.14. Diagram of excavation FZE-11-28.

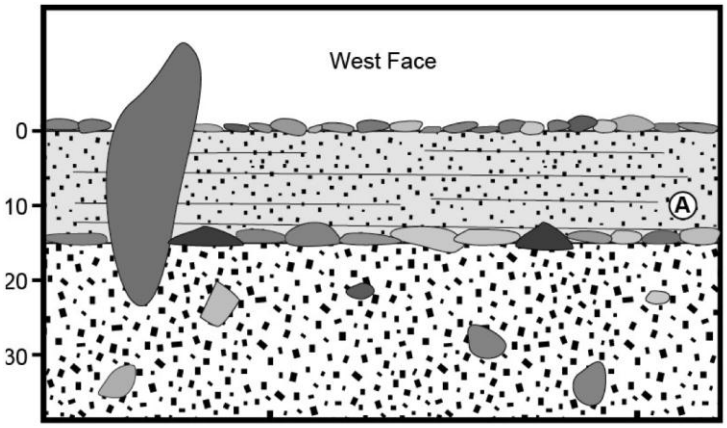

-77.46467° 161.34789°
OSL: A=10 cm

- planar bedded sands; capped by sandstone pavement; adjacent to southern boundary of fan
- till; massive with intermixed cobbles; capped by well developed pavement of sandstone and dolerite cobbles

Figure B.15. Diagram of excavation FZE-11-29.

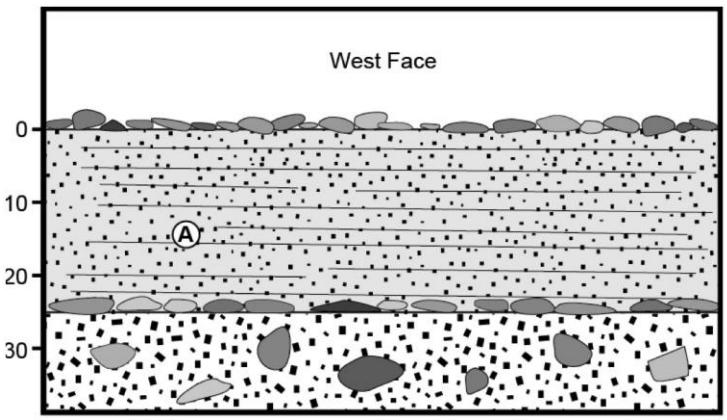

-77.46461° 161.34773°
OSL: A=15 cm

- Planar bedded sands; some gravel lenses; color lightens upwards; capped by pavement

- till; massive with intermixed cobbles; capped by well-pavement

Figure B.16. Diagram of excavation FZE-11-33.

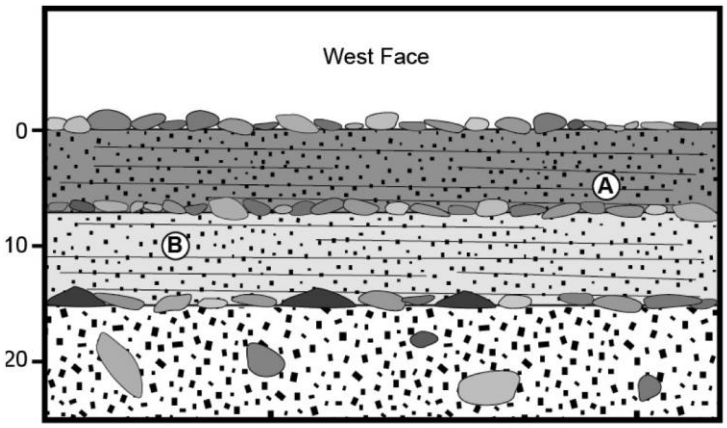

-77.46442° 161.34721°
OSL: A=5 cm, B=10 cm

- planar bedded sands; upper melt-package; capped by pavement
- planar bedded sands; lower melt-package; capped by pavement
- till; massive with intermixed cobbles; capped by well-developed pavement of sandstone and dolerite cobbles

Figure B.17. Diagram of excavation FZE-11-34.

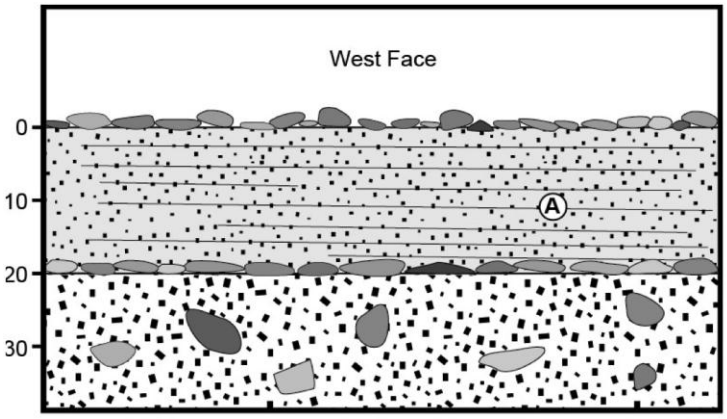

-77.46481° 161.34401°
OSL: A=10 cm

- planar bedded sands; some pebble couplets; capped by sandstone pavement

till; massive with intermixed cobbles; capped by well-developed pavement of sandstone and dolerite cobbles

Figure B.18. Diagram of excavation FZE-11-35.

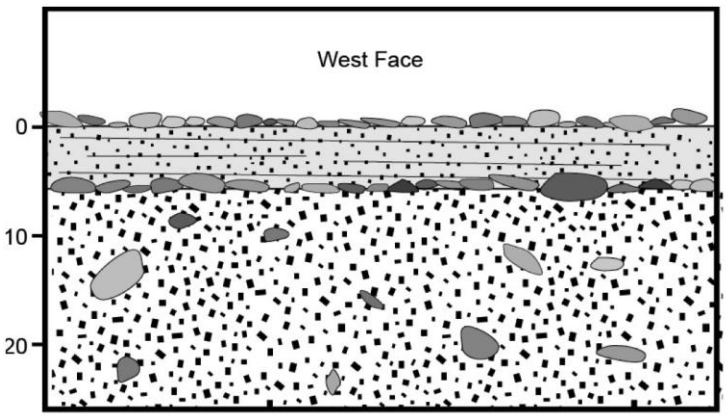

-77.46491° 161.34433°

- planar bedded sands; capped by sandstone pavement
- till; massive with intermixed cobbles; capped by well-developed pavement of sandstone and dolerite cobbles

Figure B.19. Diagram of excavation FZE-11-36.

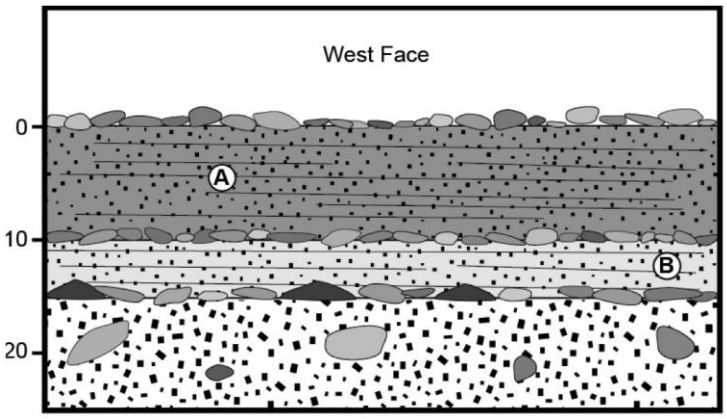

-77.46313° 161.35217°
OSL: A=5 cm, B=12 cm

- planar bedded sands; capped by sandstone pavement; upper melt-

- planar bedded sands; capped by gravel pavement; lower melt-package
- till; massive with intermixed cobbles; capped by well-developed pavement of sandstone and dolerite cobbles

Figure B.20. Diagram of excavation FZE-11-37.

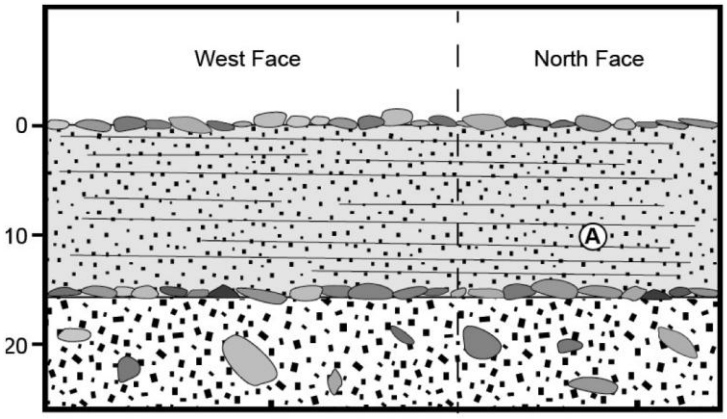

-77.4645° 161.34853°
OSL: A=10 cm

- planar bedded gravelly sands; capped by sandstone pavement

- till; massive with intermixed cobbles; capped by well developed pavement of sandstone and dolerite cobbles

Figure B.21. Diagram of excavation FZE-11-38.

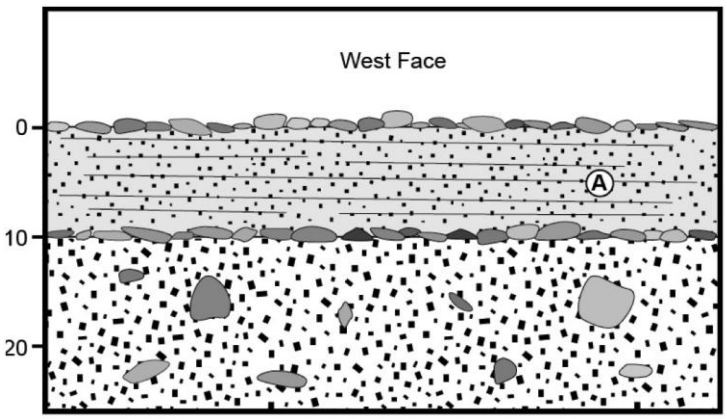

-77.46427° 161.3476°
OSL: A=5 cm

- planar bedded sands; capped by sandstone pavement

- till; cobbles intermixed; capped by well-developed pavement of sandstone and dolerite cobbles

Figure B.22. Diagram of excavation FZE-11-39.

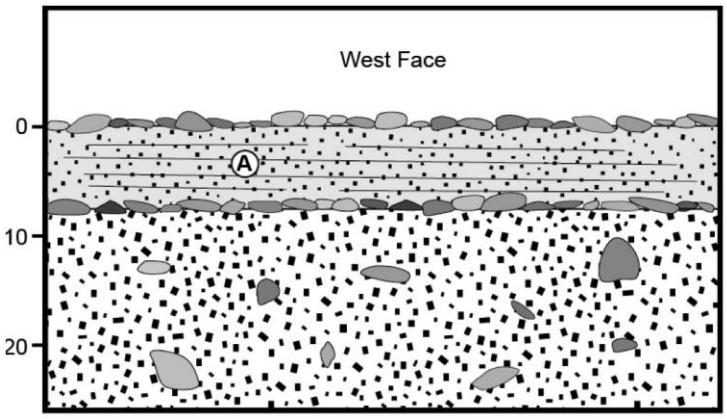

-77.46413° 161.34869°
OSL: A=5 cm

- planar bedded sands; capped by sandstone pavement
- till; capped by well-developed pavement of sandstone and dolerite cobbles

Figure B.23. Diagram of excavation FZE-11-40.

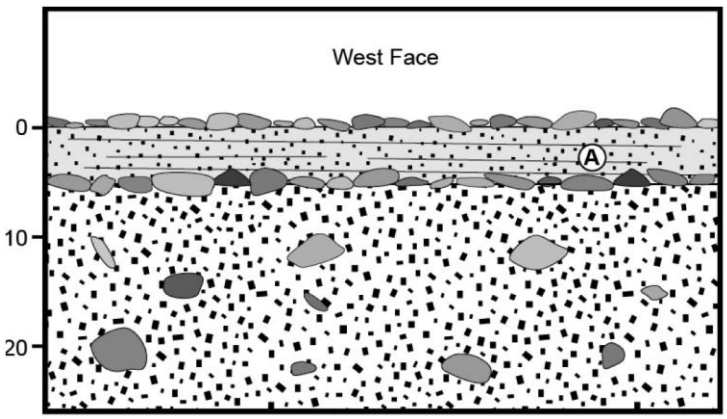

-77.46295° 161.35262°
OSL: A=4 cm

- planar bedded sands; capped by sandstone pavement
- till; capped by well-developed pavement of sandstone and dolerite cobbles

Figure B.24. Diagram of excavation FZE-11-41.

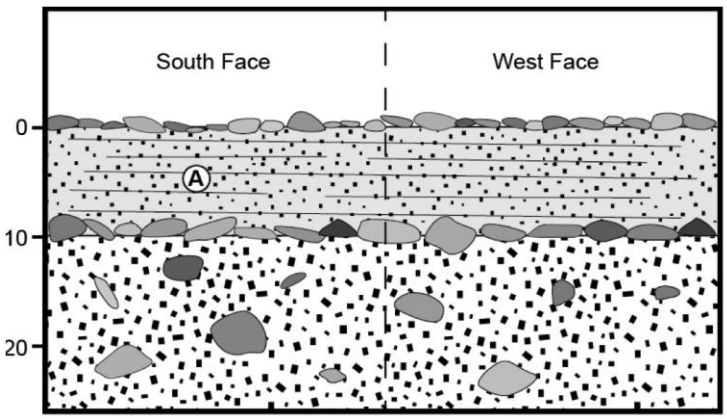

-77.46336° 161.35182°
OSL: A=5 cm

- planar bedded sands; capped by sandstone pavement

- till; capped by well developed pavement of sandstone and dolerite cobbles

Figure B.25. Diagram of excavation FZE-11-42.

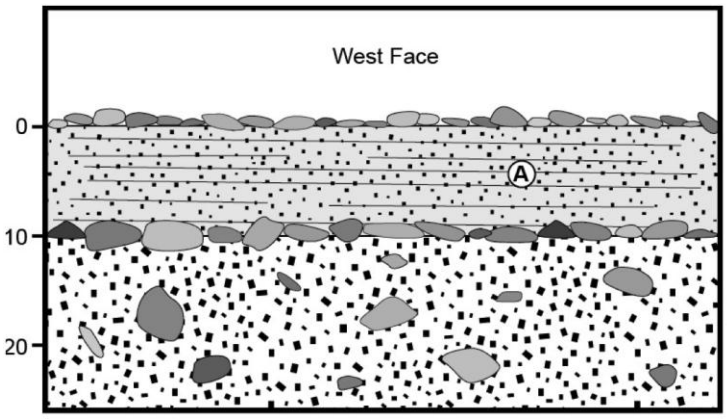

-77.46412° 161.34995°
OSL: A=5 cm

- planar bedded sands; capped by sandstone pavement

- till; capped by well-developed gravel pavement of sandstone and dolerite cobbles

Figure B.26. Diagram of excavation FZE-11-43.

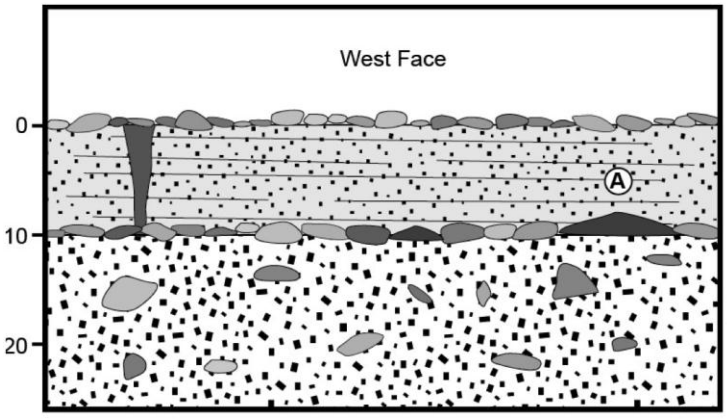

-77.4643° 161.34938°
OSL: A=5 cm

planar bedded sands; capped by sandstone pavement; ~ 2 cm wide relict sand wedge
- till; capped by well-developed gravel pavement of sandstone and dolerite cobbles

Figure B.27. Diagram of excavation FZE-11-44.

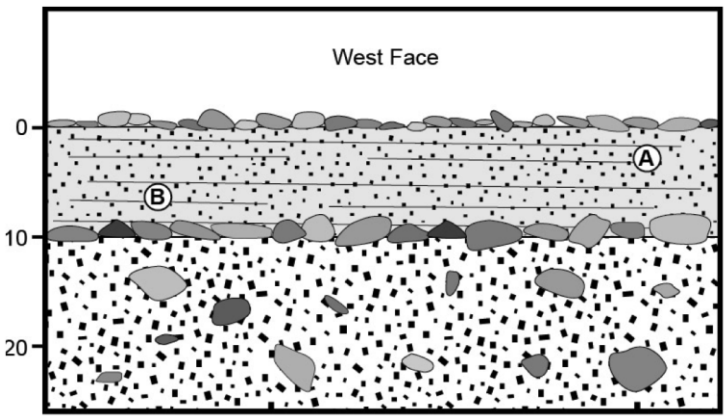

-77.46409° 161.34912°
OSL: A=4 cm, B=8 cm

- planar bedded sands; capped by sandstone pavement

- till; capped by well-developed pavement of sandstone and dolerite cobbles

Figure B.28. Diagram of excavation FZE-11-49.

B.3. Northern Bull Pass Fan

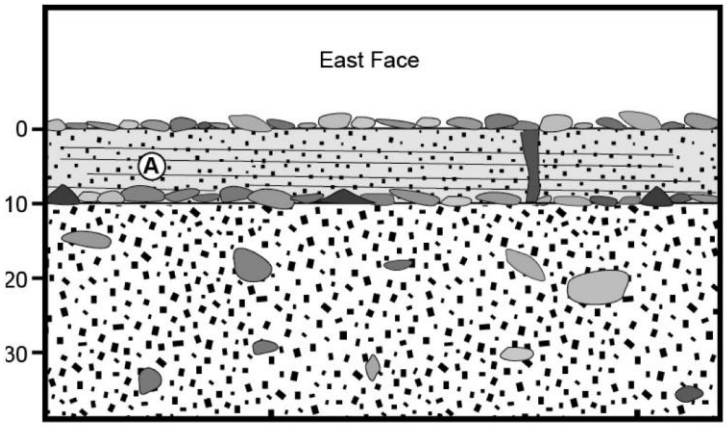

-77.44901° 161.70665°
OSL: A= 5 cm

- planar bedded sands; thin sand wedge; capped by granite pavement
- till; massive with intermixed cobbles; capped by granite cobble pavement

Figure B.29. Diagram of excavation FZE-11-30.

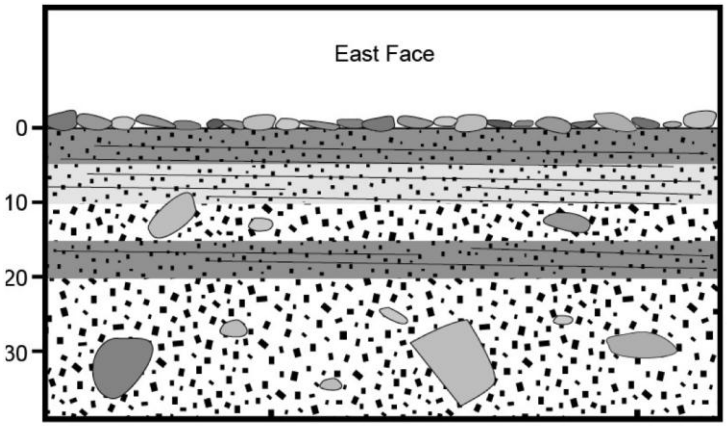

-77.44884° 161.70561°

- Thin beds of planar sands differentiated by color; capped by granite pavement; underlain by thin mud bed identical to lowest layer; thin planar bedded sands; lower bed of massive silty sands with cobbles (likely a till)

Figure B.30. Diagram of excavation FZE-11-31.

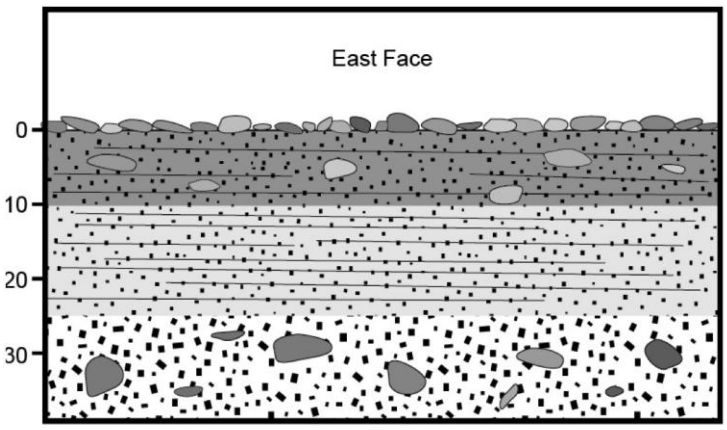

-77.44804° 161.70969°

- planar bedded gravelly sands; upper bed of melt-package; differentiated by color; capped by granite pavement
- planar bedded sands; lower bed of melt-package
- till; massive sands with cobbles

Figure B.31. Diagram of excavation FZE-11-32.

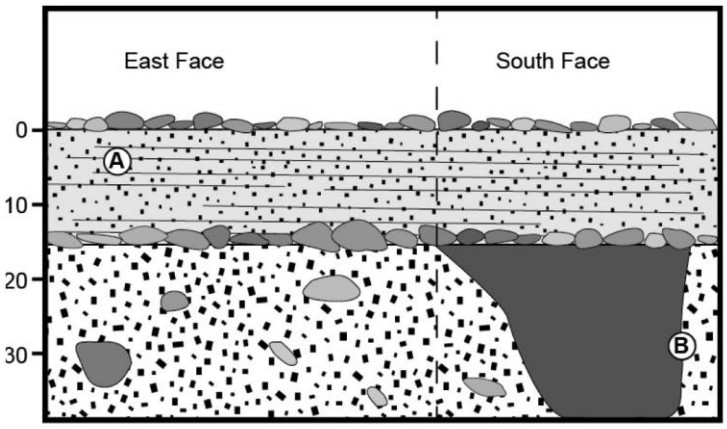

-77.44888° 161.70612°
OSL: A=5 cm, B=30 cm

- planar bedded sands; capped by granite pavement

- till; massive with cobbles intermixed; thick sand wedge that does not extend up into alluvium; capped by granite cobble pavement

Figure B.32. Diagram of excavation FZE-11-46.

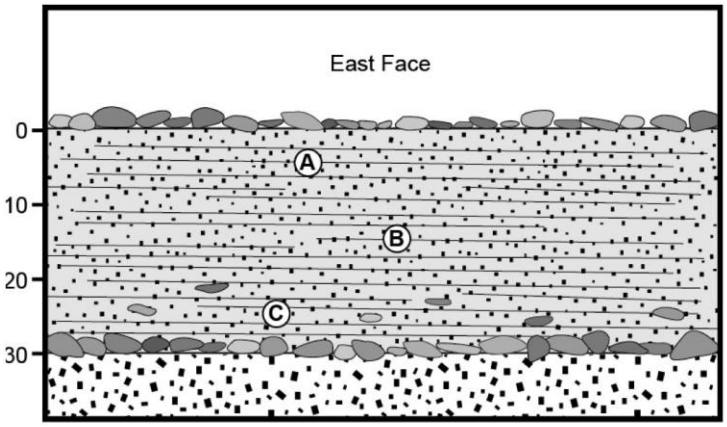

-77.44863° 161.70609°
OSL: A=5 cm, B=15 cm, C=25 cm

- planar bedded sands; coarsens upwards; capped by granite pavement

- massive sands; capped by granite cobble pavement

Figure B.33. Diagram of excavation FZE-11-47.

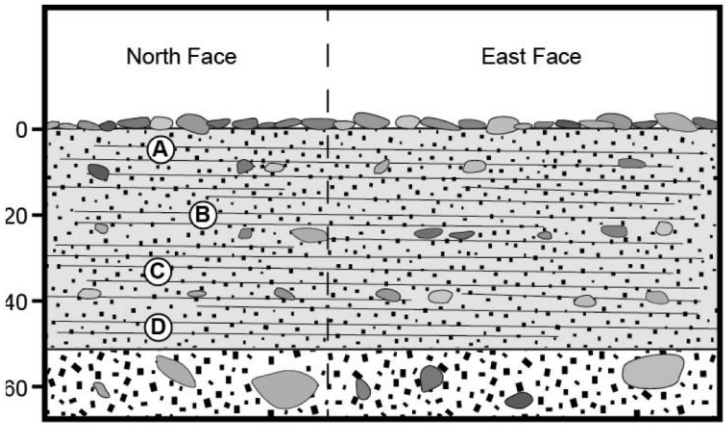

-77.44858° 161.70769°
OSL: A=5 cm, B=20 cm, C=35 cm, D=45 cm
- planar bedded gravelly sands; gravel couplets; capped by granite pavement

- massive sands with cobbles intermixed

Figure B.34. Diagram of excavation FZE-11-48.

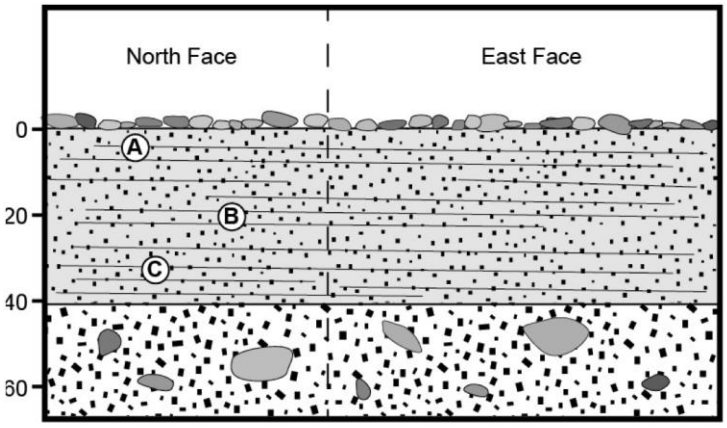

-77.44878° 161.70721°
OSL: A=5 cm, B=20 cm, C=35 cm

- planar bedded sands; capped by granite pavement

- massive sands with cobbles intermixed

Figure B.35. Diagram of excavation FZE-11-50.

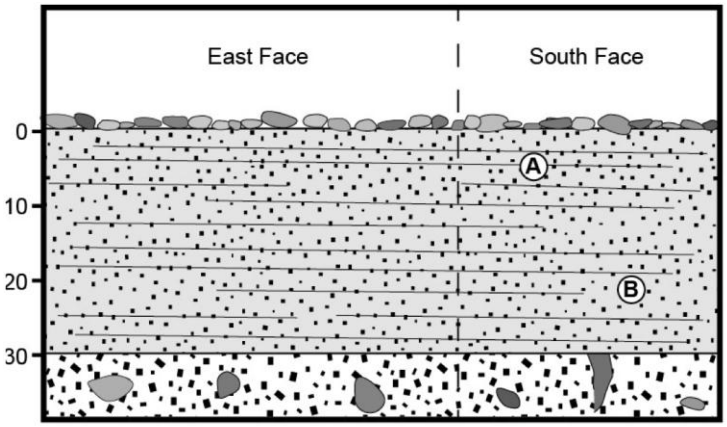

-77.44873° 161.70784°
OSL: A=5 cm, B=20 cm

- planar bedded sands; capped by grantie pavement

- massive sands with cobbles intermixed; thin sands wedge that does not extend up into alluvium

Figure B.36. Diagram of excavation FZE-11-52.

B.4. Southern Bull Pass Fan

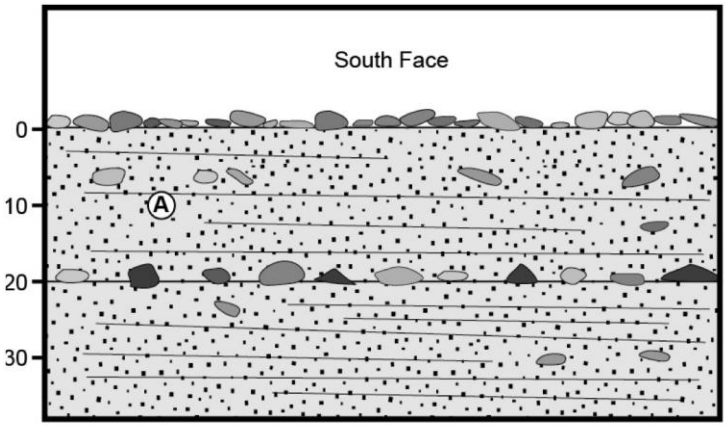

-77.47305° 161.77986°
OSL: A=10 cm

- planar bedded gravelly sands; unconsolidated; capped by granite pavement; upper melt-package

- planar bedded gravelly sands; capped by granite and siltstone pavement; lower melt-package

Figure B.37. Diagram of excavation FZE-11-56.

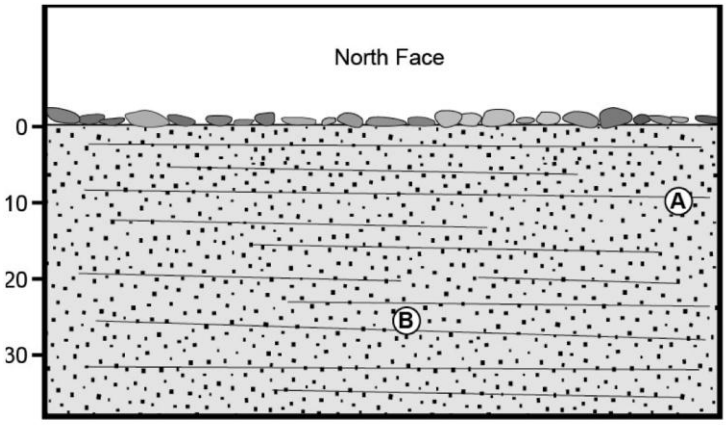

-77.47438° 161.79672°
OSL: A=10 cm, B=25 cm

- planar bedded gravelly sand; coarsens upwards; capped by granite pavement

Figure B.38. Diagram of excavation FZE-11-58.

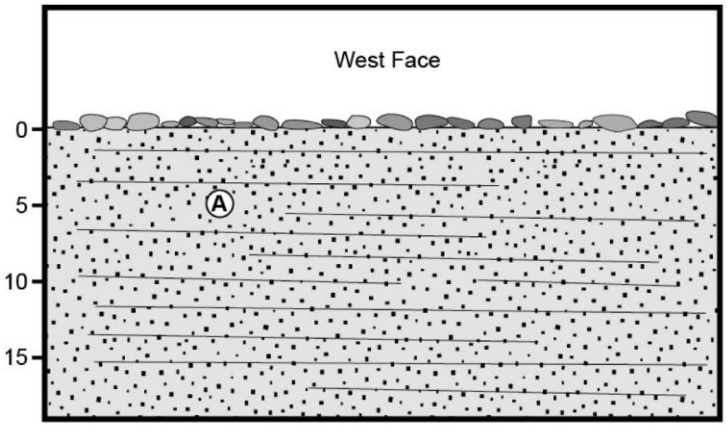

-77.47437° 161.79222°
OSL: A=5 cm

- planar bedded gravelly sands; unconsolidated; capped by granite pavement

Figure B.39. Diagram of excavation FZE-11-59.

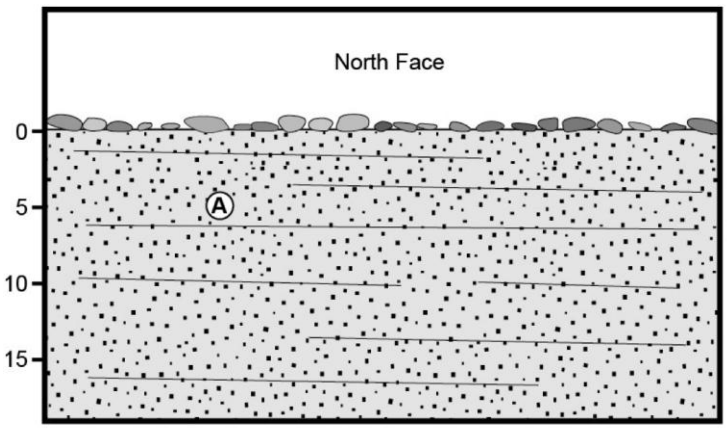

-77.47326° 161.78902°
OSL: A=5 cm

- planar bedded sands; uncondsolidated; capped by granite pavement

Figure B.40. Diagram of excavation FZE-11-60.

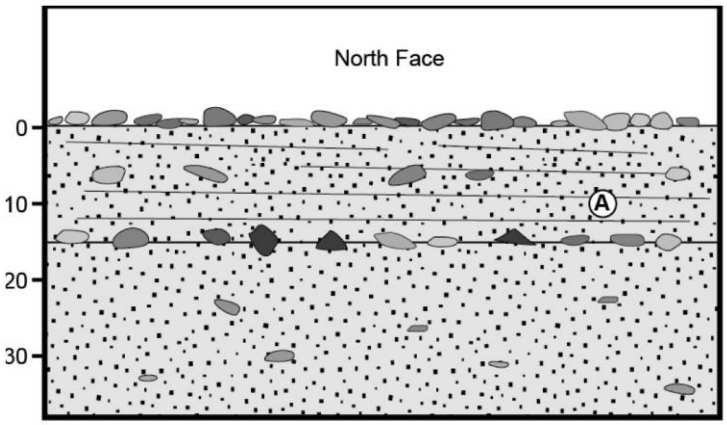

-77.46200° 161.78662°
OSL: A=10 cm

- planar bedded gravelly sands; gravel couplets; uppper-melt package; capped by granite pavement
- massive sands with gravel intermixed; capped by buried granite and siltstone pavement

Figure B.41. Diagram of excavation FZE-11-61.

B.5. Upper Wright Fan

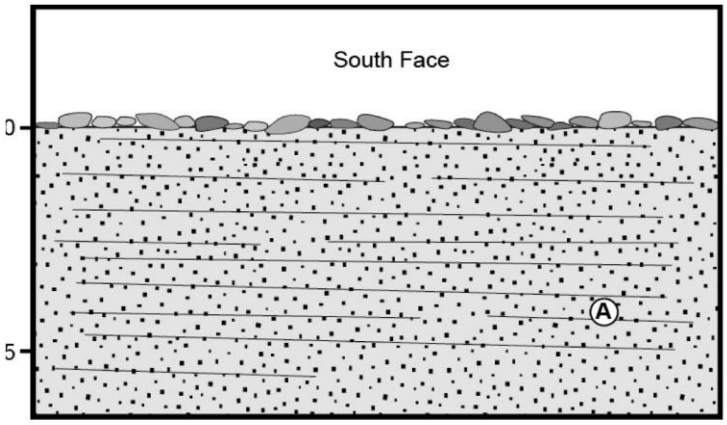

-77.57015° 160.69638°
OSL: A=4 cm

- planar bedded sands; capped by sandstone pavement; ice-cement encountered at ~5 cm

Figure B.42. Diagram of excavation FZE-11-62.

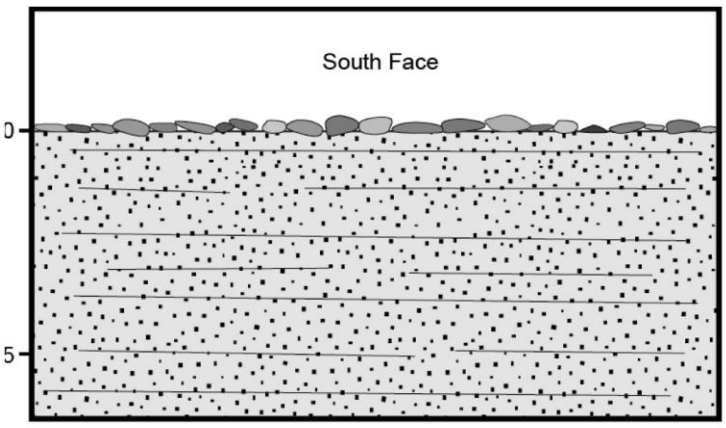

-77.56992° 160.69611°

- planar bedded sands; capped by sandstone pavement; ice-cement encountered at ~5 cm

Figure B.43. Diagram of excavation FZE-11-63.

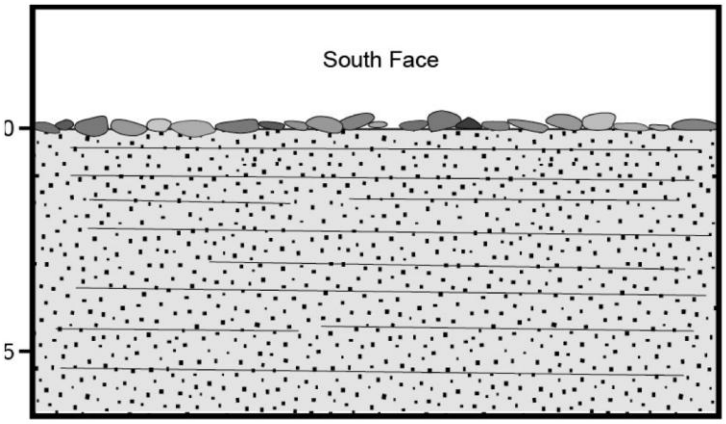

-77.57012° 160.69582°

- planar bedded sands; capped by sandstone pavement; ice-cement encountered at ~5 cm

Figure B.44. Diagram of excavation FZE-11-64.

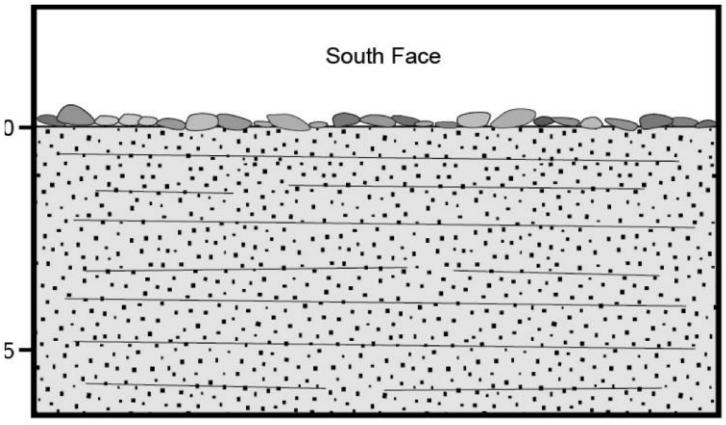

-77.57043° 160.69650°

- planar bedded sands; capped by sandstone pavement; ice-cement encountered at ~5 cm

Figure B.45. Diagram of excavation FZE-11-65.

APPENDIX C. GRAIN SIZE ANALYSIS

Table C.1. Cumulative percentage values of grain size distribution of sediment samples.

Sample	Clasts/ pan	>-4Φ	>-3Φ	>-2Φ	>-1Φ	>0Φ	>1 Φ	>2 Φ	>3 Φ	>4 Φ	> Silt & Clay	σ_I	M_Z (Φ)
Jason													
FZS-11-01A	0	0.2%	0.8%	2.5%	6.0%	13.5%	36.9%	69.6%	94.8%	98.2%	99.6%	1.24	1.33
FZS-11-02A	4	0.0%	2.6%	7.4%	13.3%	21.4%	45.5%	76.6%	94.5%	96.7%	99.8%	1.52	0.97
FZS-11-03A	10	0.0%	10.9%	20.5%	28.6%	36.2%	54.8%	78.2%	94.6%	97.9%	100.1%	2.08	0.03
FZS-11-04	1	0.0%	0.4%	1.9%	4.3%	11.4%	38.3%	71.7%	94.1%	97.6%	99.8%	1.12	1.33
FZS-11-05A	34	0.0%	12.5%	20.8%	28.3%	37.4%	61.0%	85.1%	96.4%	98.2%	100.0%	2.09	-0.03
FZS-11-05B	5	0.0%	1.5%	4.7%	7.8%	12.9%	31.3%	67.3%	91.6%	94.6%	100.1%	1.48	1.47
FZS-11-06A	29	0.0%	3.5%	11.0%	19.8%	30.3%	54.7%	81.8%	96.6%	98.7%	99.9%	1.72	0.50
FZS-11-07A	3	0.0%	8.4%	13.6%	19.1%	26.3%	45.4%	75.3%	94.2%	97.2%	99.8%	1.96	0.70
FZS-11-08	-	0.0%	0.0%	0.2%	11.8%	42.4%	85.6%	98.2%	99.6%	99.8%	99.9%	0.88	0.10
FZS-11-09	-	0.0%	0.2%	0.6%	4.4%	21.0%	62.0%	89.1%	98.1%	98.9%	99.9%	0.99	0.73
FZS-11-10	-	0.0%	0.0%	0.4%	4.6%	19.1%	54.1%	85.5%	98.0%	99.1%	100.0%	1.05	0.90
FZS-11-11	0	0.7%	2.6%	3.8%	6.0%	12.5%	31.1%	60.2%	91.0%	98.0%	100.0%	1.28	1.57
Aeolus													
FZS-11-16A	4	0.0%	7.8%	17.0%	23.2%	32.0%	47.1%	76.6%	94.2%	97.3%	99.9%	2.08	0.43
FZS-11-16B	2	0.0%	6.0%	14.3%	22.0%	31.3%	46.4%	77.8%	95.5%	98.2%	99.9%	1.95	0.53
FZS-11-16C	1	0.0%	3.4%	17.0%	27.4%	41.0%	57.0%	81.9%	95.1%	97.9%	100.3%	1.93	0.20
FZS-11-18A	15	0.0%	4.7%	7.7%	11.8%	18.6%	34.4%	71.8%	94.8%	98.0%	99.9%	1.61	1.23
FZS-11-18B	14	0.4%	9.4%	20.0%	28.1%	36.4%	50.2%	77.3%	94.3%	96.7%	100.0%	2.18	0.30
FZS-11-18C	-	4.9%	14.2%	21.7%	29.4%	39.3%	52.9%	79.3%	95.7%	98.1%	99.9%	2.30	0.10
FZS-11-18D	-	0.0%	3.6%	9.0%	15.5%	27.3%	48.1%	83.1%	97.3%	98.9%	100.0%	1.54	0.73
FZS-11-26A	15	0.0%	4.5%	8.7%	12.2%	18.0%	32.0%	70.8%	95.2%	98.2%	99.9%	1.55	1.27
FZS-11-26B	6	0.0%	6.5%	15.8%	25.3%	36.6%	51.7%	79.5%	95.8%	98.1%	100.0%	1.97	0.37
FZS-11-27		0.0%	4.1%	11.3%	19.9%	33.8%	53.0%	83.6%	97.6%	99.1%	100.0%	1.68	0.50
FZS-11-28	20	0.0%	7.8%	14.7%	21.3%	30.2%	46.1%	77.4%	95.6%	98.0%	100.2%	1.98	0.53
FZS-11-29	16	0.0%	9.3%	16.9%	24.8%	36.5%	51.7%	77.2%	92.9%	95.8%	100.0%	2.19	0.40
FZS-11-33	15	0.0%	6.1%	12.5%	19.1%	30.5%	48.7%	79.4%	95.0%	97.4%	100.1%	1.84	0.63
FZS-11-34A	1	0.0%	5.3%	13.4%	22.6%	38.8%	60.7%	86.1%	95.9%	97.2%	100.1%	1.78	0.23
FZS-11-34B	5	0.0%	7.4%	13.1%	19.2%	30.6%	46.4%	78.6%	93.7%	95.6%	99.9%	1.98	0.70
FZS-11-35	23	0.9%	15.1%	21.7%	28.9%	40.1%	55.0%	81.8%	96.5%	98.4%	99.9%	2.23	-0.03
FZS-11-36	5	0.0%	7.9%	13.6%	19.5%	28.5%	43.9%	73.0%	92.2%	95.4%	100.0%	2.13	0.70
FZS-11-37A	0	0.0%	4.9%	9.6%	13.6%	22.9%	48.3%	90.3%	98.6%	99.3%	99.9%	1.10	1.17

(continued)

Table C.1. Cumulative percentage values of grain size distribution of all sediment samples. (continued)

Sample	Clasts/ pan	>-4Φ	>-3Φ	>-2Φ	>-1Φ	>0Φ	>1 Φ	>2 Φ	>3 Φ	>4 Φ	> Silt & Clay	σ_I	M_Z (Φ)
FZS-11-37B	1	0.0%	6.6%	14.0%	23.8%	45.1%	71.0%	90.5%	96.4%	97.5%	100.0%	1.70	0.03
FZS-11-38	-	0.0%	6.3%	11.0%	17.0%	27.8%	46.9%	81.0%	96.0%	97.8%	99.9%	1.72	0.70
FZS-11-39	0	0.0%	2.2%	9.8%	17.6%	28.2%	46.5%	79.2%	95.4%	98.1%	100.0%	1.70	0.70
FZS-11-40	5	0.0%	2.7%	9.0%	14.2%	24.2%	45.2%	80.9%	96.0%	98.5%	99.9%	1.16	1.33
FZS-11-41	1	0.0%	2.6%	10.9%	25.5%	50.7%	76.6%	94.3%	97.5%	98.0%	100.0%	1.44	-0.10
FZS-11-42	7	0.0%	11.8%	19.7%	26.5%	39.4%	58.1%	83.9%	96.0%	97.9%	99.9%	2.11	0.03
FZS-11-43	2	0.0%	2.4%	5.6%	9.0%	19.8%	45.3%	85.5%	97.7%	98.8%	100.0%	1.25	0.93
FZS-11-44	4	0.5%	11.0%	15.1%	20.3%	29.4%	45.2%	77.8%	93.6%	95.7%	99.8%	2.07	0.57
FZS-11-49A		0.0%	5.9%	11.2%	16.5%	26.6%	48.0%	85.0%	97.2%	98.8%	99.9%	1.60	0.67
FZS-11-49B		0.6%	7.8%	12.6%	17.9%	28.0%	46.8%	78.8%	92.9%	94.9%	100.0%	2.02	0.70
Northern Bull Pass													
FZS-11-30	-	0.0%	2.3%	11.0%	24.9%	49.8%	75.2%	88.6%	93.8%	95.4%	100.0%	1.75	0.00
FZS-11-31A	-	0.0%	0.4%	5.1%	17.8%	35.2%	56.1%	82.9%	94.8%	96.5%	100.0%	1.56	0.57
FZS-11-32A	-	0.0%	11.4%	22.8%	33.6%	50.8%	66.6%	86.7%	96.1%	97.2%	99.0%	1.78	0.00
FZS-11-32B	-	0.0%	3.6%	8.4%	12.0%	23.2%	53.3%	88.7%	96.8%	98.4%	100.0%	1.56	0.57
FZS-11-46A	0	0.0%	5.5%	17.7%	27.4%	44.0%	65.7%	82.6%	90.7%	95.2%	99.9%	2.05	-0.27
FZS-11-46B	-	0.0%	0.0%	0.3%	0.7%	6.8%	37.4%	84.0%	97.2%	98.3%	100.0%	1.38	0.73
FZS-11-47A	0	0.0%	1.6%	9.8%	19.3%	38.1%	63.1%	87.4%	97.0%	98.5%	100.0%	2.13	0.10
FZS-11-47B	-	0.0%	0.8%	4.5%	11.9%	27.0%	58.2%	85.7%	92.0%	94.8%	99.9%	0.82	1.23
FZS-11- 47C	-	0.0%	0.0%	2.3%	7.4%	19.1%	44.1%	81.7%	97.0%	98.1%	99.9%	1.56	0.33
FZS-11-48A	7	0.0%	2.5%	3.7%	4.9%	8.6%	29.6%	79.4%	97.5%	99.1%	100.0%	1.52	0.67
FZS-11-48B	-	5.7%	9.7%	11.5%	13.3%	18.4%	36.1%	77.0%	95.7%	98.7%	99.9%	1.20	1.03
FZS-11-48C	-	2.5%	4.7%	8.0%	12.6%	24.5%	57.0%	86.9%	95.4%	97.4%	100.0%	0.95	1.33
FZS-11-48D	-	2.5%	2.9%	5.8%	8.9%	15.8%	37.3%	74.3%	91.4%	95.4%	100.1%	1.70	1.10
FZS-11-50A	-	0.0%	4.0%	7.6%	10.2%	19.3%	47.7%	87.2%	97.4%	98.8%	99.9%	1.52	0.70
FZS-11-50B	-	1.0%	4.0%	6.2%	8.4%	14.1%	34.4%	75.9%	92.8%	97.2%	99.9%	1.55	1.27
FZS-11-50C	-	1.1%	4.8%	6.5%	8.3%	17.0%	44.6%	81.7%	93.4%	96.7%	99.9%	1.33	0.93
FZS-11-52A	9	0.0%	3.4%	5.1%	7.4%	14.3%	37.5%	76.7%	93.7%	97.4%	100.0%	1.43	1.27
FZS-11-52B	-	0.0%	1.9%	3.1%	4.2%	7.0%	22.8%	68.3%	91.5%	96.4%	100.0%	1.50	1.03
Southern Bull Pass													
FZS-11-56	14	0.0%	6.1%	14.2%	23.4%	34.3%	53.9%	87.2%	98.8%	99.8%	100.1%	1.79	0.30
FZS-11-58	3	0.0%	4.0%	7.3%	10.8%	17.4%	40.8%	82.5%	96.5%	97.9%	100.1%	1.38	1.07
FZS-11-59	1	0.0%	1.5%	2.7%	5.1%	9.3%	28.0%	76.4%	98.0%	99.2%	99.8%	1.03	1.43
FZS-11-60	2	0.0%	0.7%	2.2%	3.5%	5.2%	17.1%	69.3%	98.0%	99.5%	99.8%	0.80	1.60

(continued)

Table C.1. Cumulative percentage values of grain size distribution of all sediment samples. (continued)

Sample	Clasts/ pan	>-4Φ	>-3Φ	>-2Φ	>-1Φ	>0Φ	>1 Φ	>2 Φ	>3 Φ	>4 Φ	> Silt & Clay	σ_I	M_Z (Φ)
FZS-11-61	7	0.0%	1.4%	4.6%	8.7%	15.8%	35.8%	80.3%	95.1%	97.0%	100.0%	1.28	1.13
Upper Wright													
FZS-11-62	4	0.0%	5.6%	9.5%	12.4%	17.9%	36.1%	69.8%	91.5%	97.3%	100.0%	1.68	1.27
FZS-11-63	0	0.0%	2.9%	5.4%	8.0%	12.3%	28.5%	67.0%	93.4%	98.5%	100.2%	1.35	1.50
FZS-11-64	10	0.0%	9.9%	15.6%	21.1%	30.5%	50.4%	76.6%	93.4%	97.7%	99.9%	2.12	0.47
FZS-11-65	15	0.0%	9.4%	15.7%	21.1%	29.1%	46.5%	75.6%	94.2%	98.1%	99.8%	2.10	0.50

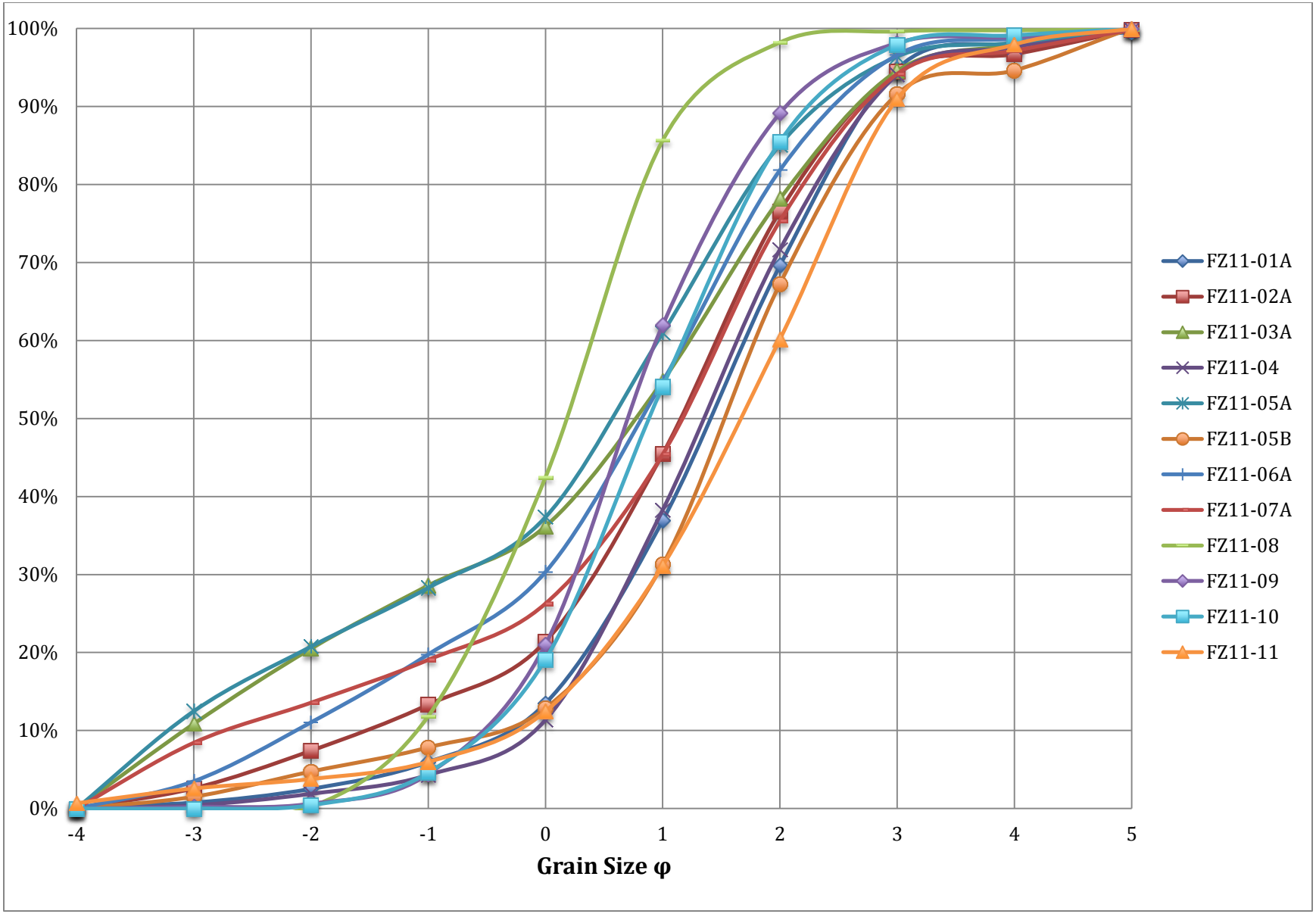

Figure C.1. Cumulative percentage curves of grain size distribution of Jason Fan sediment samples.

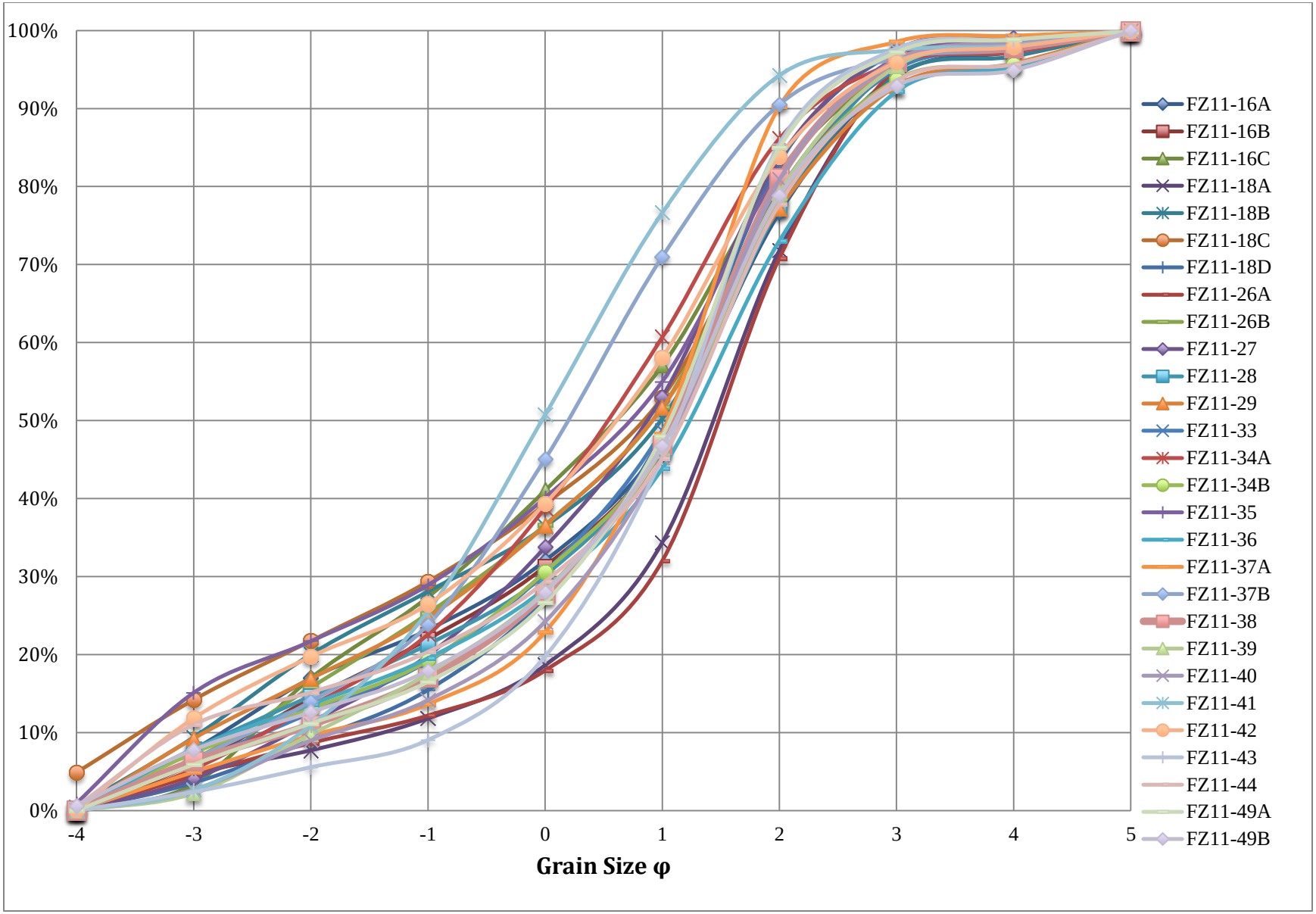

Figure C.2. Cumulative percentage curves of grain size distribution of Aeolus Fan sediment samples.

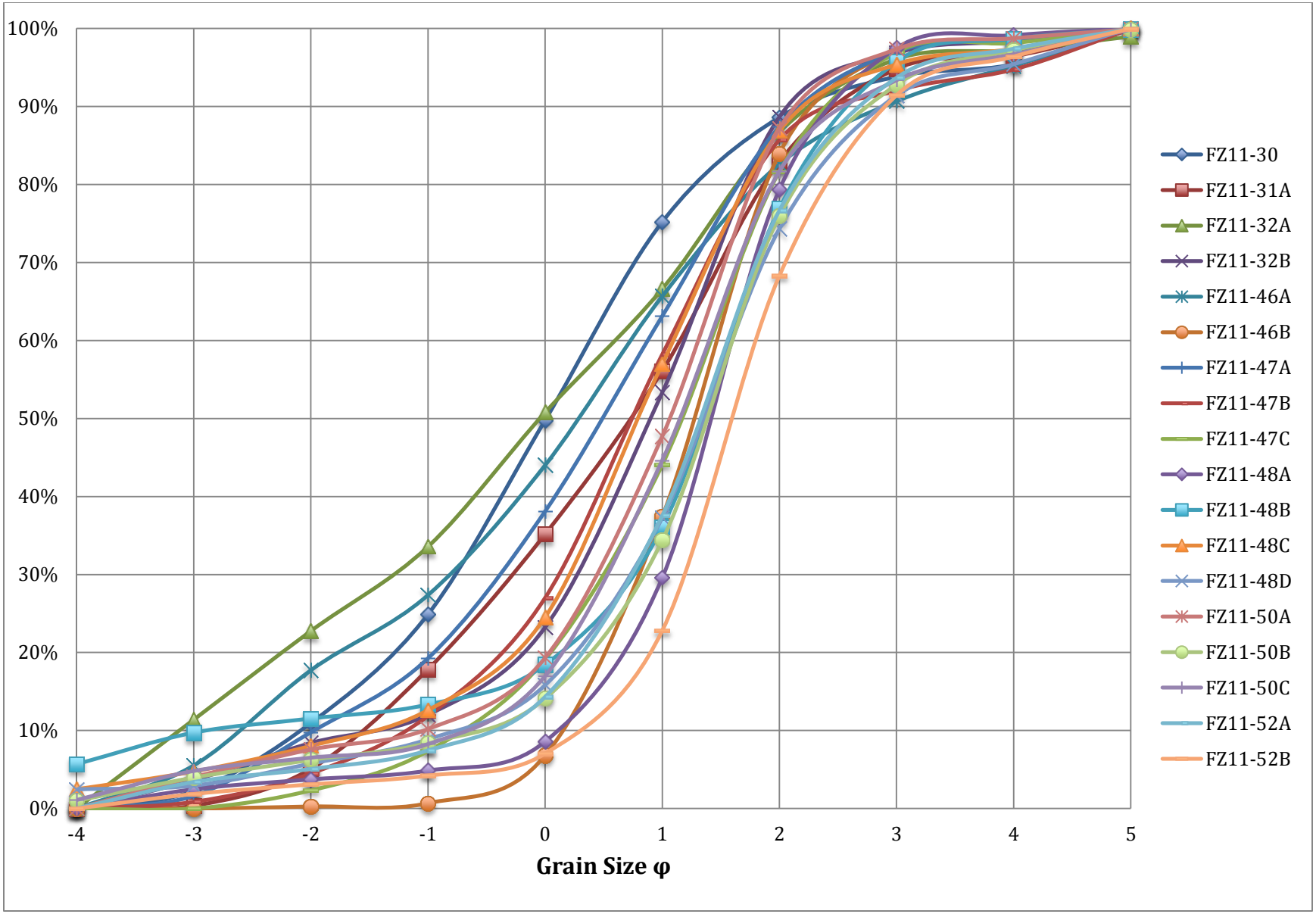

Figure C.3. Cumulative percentage curves of grain size distribution of Northern Bull Pass Fan sediment samples.

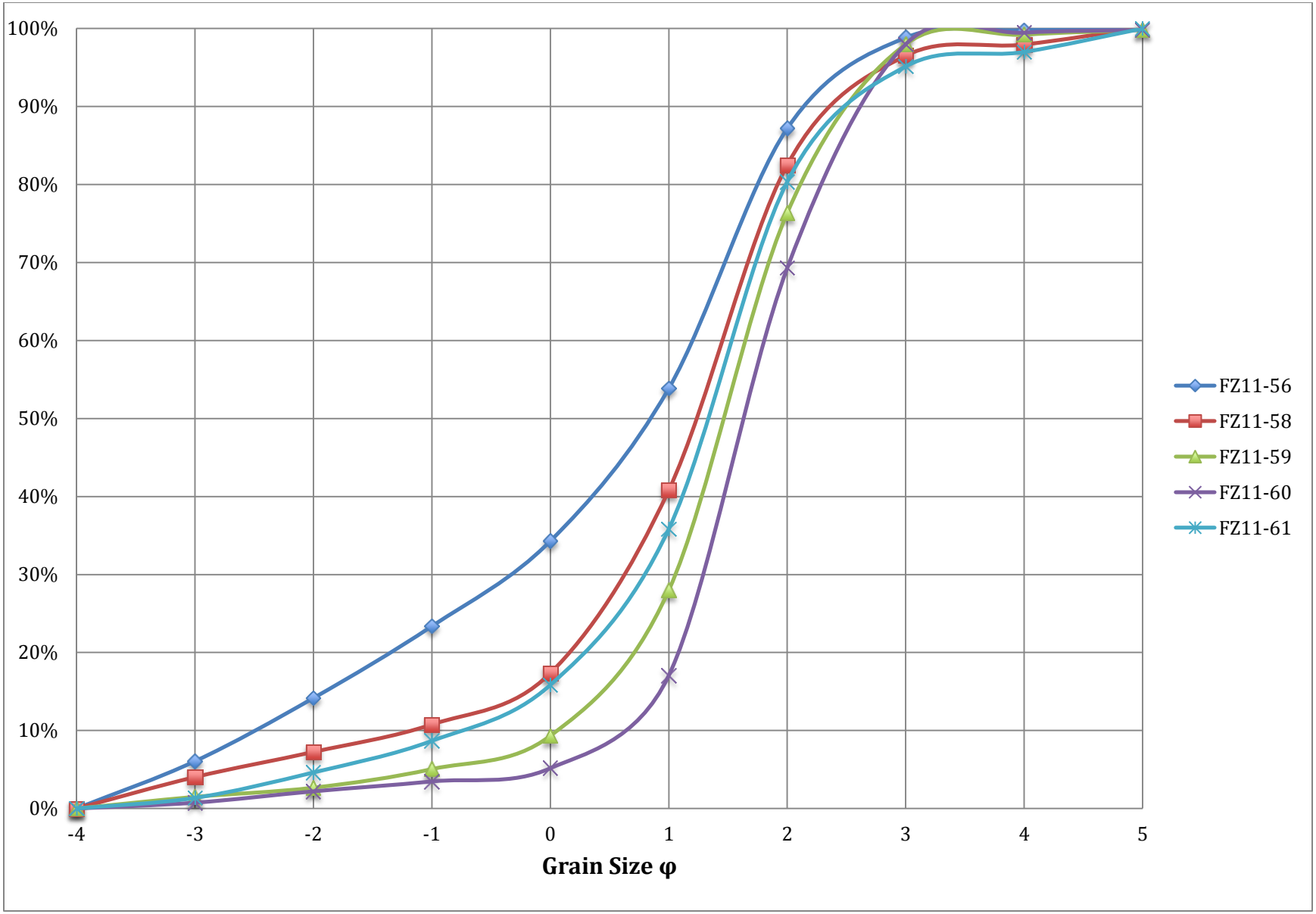

Figure C.4. Cumulative percentage curves of grain size distribution of Southern Bull Pass Fan sediment samples.

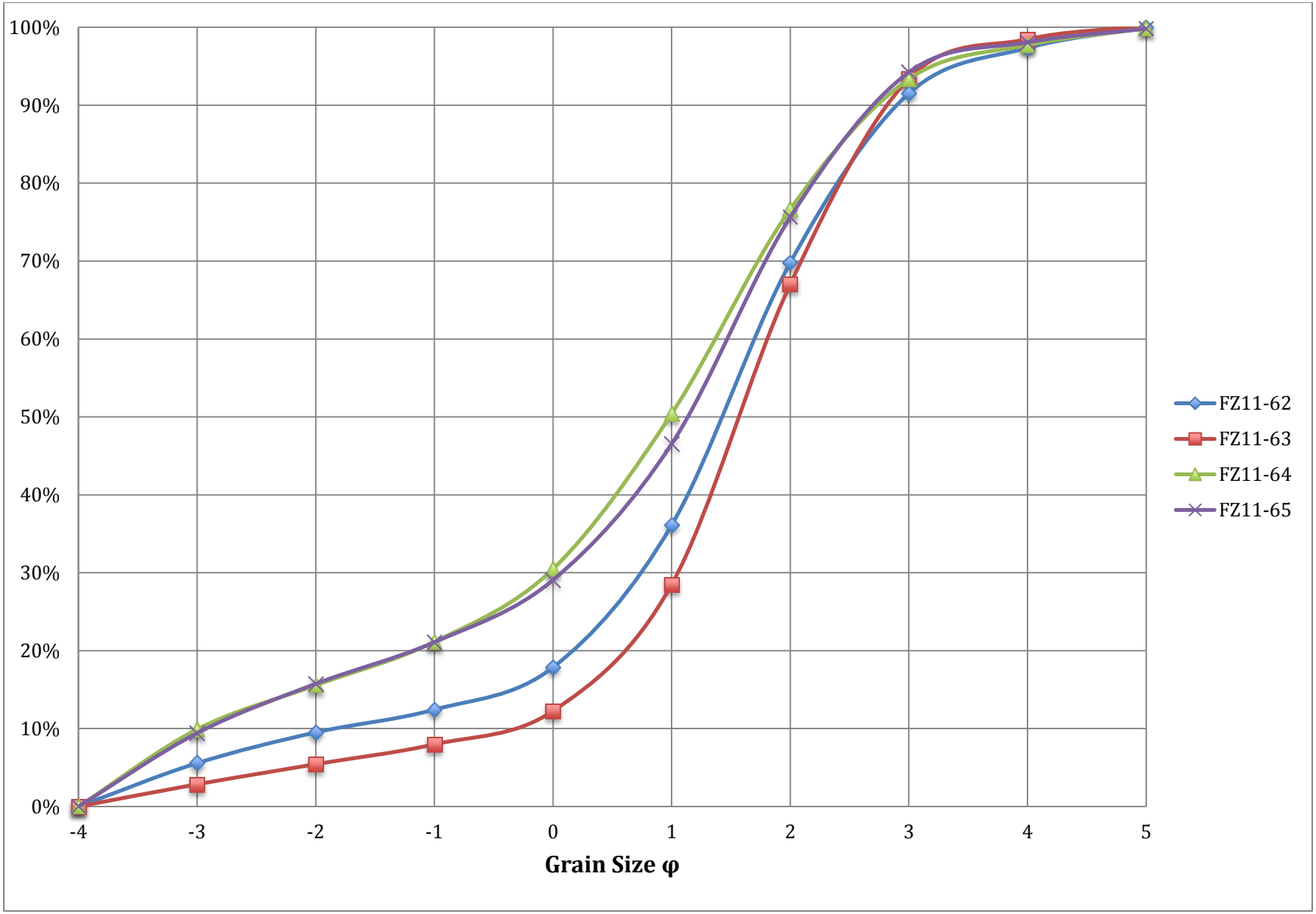

Figure C.5. Cumulative percentage curves of grain size distribution of Upper Wright Fan sediment samples.

APPENDIX D. RESULTS OF PALEOHYDRAULIC RECONSTRUCTION

Sample	Max d_I (mm)					Avg. d_I	v (Costa 1983)	v (Costa's Regression)	v_b (Strand 1973)	v (Strand)	Avg. v	Manning's D (m)
Jason ($\bar{S}$ = 0.11)												
FZ1101	69.04	61.15	53.42	68.86	51.79	60.85	1.30	1.33	1.46	1.75	1.46	0.107
FZ1103	66.50	47.27	46.81	49.82	47.94	51.67	1.20	1.23	1.34	1.61	1.35	0.095
FZ1105A	73.05	52.28	42.80	42.27	44.68	51.02	1.20	1.22	1.33	1.60	1.34	0.094
FZ1106	41.34	37.08	37.75	34.38	32.57	36.62	1.03	1.04	1.13	1.35	1.14	0.074
Aeolus ($\bar{S}$ = .424)												
FZ1116	41.49	42.38	31.11	37.96	29.12	36.41	1.03	1.04	1.13	1.35	1.14	0.026
FZ1118A	35.84	34.71	36.70	28.42	44.89	36.11	1.02	1.03	1.12	1.35	1.13	0.026
FZ1118B	42.96	37.95	36.71	25.64	25.16	33.68	0.99	1.00	1.08	1.30	1.10	0.024
FZ1118C	45.00	39.33	37.84	33.65	62.81	43.73	1.12	1.13	1.23	1.48	1.24	0.029
FZ1126A	51.17	41.05	37.30	38.06	32.57	40.03	1.07	1.09	1.18	1.42	1.19	0.028
FZ1128	68.42	42.43	57.62	55.90	36.97	52.27	1.21	1.24	1.35	1.62	1.35	0.034
FZ1129	38.00	35.83	37.02	34.43	41.94	37.44	1.04	1.05	1.14	1.37	1.15	0.026
FZ1133	44.29	43.99	47.82	42.32	38.13	43.31	1.11	1.13	1.23	1.47	1.24	0.029
FZ1134B	37.26	30.79	37.12	29.14	28.61	32.58	0.98	0.98	1.07	1.28	1.08	0.024
FZ1135	41.54	36.69	42.08	41.16	34.24	39.14	1.06	1.07	1.17	1.40	1.18	0.027
FZ1136	38.41	35.40	30.96	36.25	27.44	33.69	0.99	1.00	1.08	1.30	1.10	0.024
FZ1138	30.49	31.66	31.62	31.09	32.33	31.44	0.96	0.97	1.05	1.26	1.06	0.023
FZ1140	57.86	47.64	33.32	32.82	35.54	41.44	1.09	1.10	1.20	1.44	1.21	0.028
FZ1142	33.00	30.03	28.01	27.96	29.83	29.77	0.94	0.94	1.02	1.22	1.03	0.022
FZ1144	28.73	31.96	29.98	27.34	27.06	29.01	0.93	0.93	1.00	1.21	1.02	0.022
FZ1149A	33.08	29.05	31.93	33.16	28.17	31.08	0.96	0.96	1.04	1.25	1.05	0.023
Northern Bull Pass ($\bar{S}$ = 0.28)												
FZ1148A	33.12	42.03	35.12	30.17	31.33	34.35	1.00	0.029	1.09	1.31	1.11	0.034
FZ1152	32.22	34.99	33.13	30.96	35.92	33.44	0.99	0.028	1.08	1.29	1.09	0.033

(continued)

Sample	Max d_I (mm)					Avg. d_I	v (Costa 1983)	v (Costa's Regression)	v_b (Strand 1973)	v (Strand)	Avg. v	Manning's D (m)
Southern Bull Pass ($\bar{S}$ = 0.13)												
FZ1156	36.53	33.92	34.44	30.39	30.79	33.21	0.98	0.99	1.08	1.29	1.09	0.058
FZ1158	50.57	50.24	38.84	36.54	36.08	42.45	1.10	1.12	1.22	1.46	1.23	0.069
FZ1159	43.30	34.78	30.94	36.02	30.47	35.10	1.01	1.02	1.11	1.33	1.12	0.060
FZ1160	55.94	58.71	55.84	61.24	53.68	57.08	1.26	1.29	1.41	1.69	1.41	0.086
FZ1161	53.29	41.48	41.34	39.10	50.92	45.23	1.13	1.15	1.25	1.51	1.26	0.073
Upper Wright ($\bar{S}$ = 0.30)												
FZ1162	30.67	30.52	30.11	31.11	29.69	30.42	0.95	0.95	1.03	1.23	1.04	0.029
FZ1163	31.55	27.92	30.64	29.20	27.74	29.41	0.93	0.93	1.01	1.21	1.03	0.029
FZ1164	30.33	27.30	25.59	27.77	25.66	27.33	0.90	0.90	0.98	1.17	0.99	0.027
FZ1165	32.56	40.18	48.32	34.88	31.65	37.52	1.04	1.05	1.14	1.37	1.15	0.034

APPENDIX E. GEOGRAPHIC ATTRIBUTES OF FANS USED IN GEOSPATIAL ANALYSIS

Fan	Fan Area (m^2)	Source Type	Source Area (m^2)	Channel Length (m)	Max. Channel Slope	Min. Channel Slope	Dist. Sea (km)	Min. Elev. (m)	Mean Elev. (m)	Mean. Drct. Rad. (WH/m^2)	Net Direct Rad. (WH)
North Bull	5430	Glacier	186288	1798	30	15.7	43.59	1171	1299	109006	22564300
Aeolus	10716	Glacier	15975	660	30	23.0	53.72	1492	1506	142147	2416500
Little Harker	20412	Glacier	37353	2838	24	11.8	37.74	965	999	99862	3994470
Jason	40988	Glacier	650729	1949	9	6.0	49.14	1280	1383	150940	108677000
Sykes	68392	Glacier	214335	1960	31	23.2	48.24	1189	1490	173417	41793500
Marsh Cirque	101110	Glacier	306363	3020	36	19.3	49.71	1172	1235	122352	41966900
Sponsors NE	162726	Glacier	101388	2177	30	19.0	50.82	1227	1356	164869	18465400
Pearse	197122	Glacier	2479979	6262	40	16.9	44.29	1190	1392	129409	356263008
Jason South	285428	Glacier	172844	868	33	26.6	46.25	793	1274	83646	16227300
Meserve	362031	Glacier	3415104	2240	23	15.1	27.72	832	1292	144473	547553984
South Bull	591649	Glacier	234745	4721	20	7.5	40.96	1059	1130	99613	26397300
Theseus	792376	Glacier	358636	2362	43	23.4	33.15	1103	1186	119142	47537500
Wrenn	906369	Glacier	265073	6394	36	13.3	37.15	1184	1232	112173	33203200
Mt. Harker	3331661	Glacier	1829391	9454	19	6.5	37.66	842	1042	116005	235490000
Insel S.	1298	Snow	1080	278	19	13.1	51.80	1000	1000	92479	92479
Upper Wright	4297	Snow	79671	584	26	16.7	67.65	1074	1189	172150	14977100
Barwick	22504	Snow	11522	1033	37	17.7	57.86	963	1005	144164	2018290
Apocalypse	26630	Snow	7364	827	37	31.2	63.96	1456	1562	175445	1754450
Insel W.	73693	Snow	22597	1810	37	20.0	52.36	1218	1262	163899	4097480
Sponsors SE	92099	Snow	591824	6519	19	6.1	50.71	1025	1183	105121	68644304
Sponsors SW	156532	Snow	564196	7486	17	5.9	53.10	947	1151	132543	82707000
Sponsors C	184807	Snow	11011	1440	28	23.5	49.73	1142	1169	156816	2038600
Don Juan	244907	Snow	67376	4562	33	21.9	53.45	1056	1287	172832	12962400
Insel C.	251943	Snow	13912	1483	35	24.0	51.59	1244	1289	163851	2621610
Boreas	253177	Snow	18943	767	26	22.6	57.56	1432	1444	165795	3647500
Goldich	316006	Snow	56823	1014	37	30.1	44.50	1174	1413	55904	3577850
Insel E.	484602	Snow	33144	1011	31	20.4	50.36	1194	1211	152682	5496570